NONLINEAR ANALYSIS OF A SPACE-CHARGE-WAVE AMPLIFIER

By

RONALD CARL HOUTS

A DISSERTATION PRESENTED TO THE GRADUATE COUNCIL OF
THE UNIVERSITY OF FLORIDA
IN PARTIAL FULFILLMENT OF THE REQUIREMENTS FOR THE
DEGREE OF DOCTOR OF PHILOSOPHY

UNIVERSITY OF FLORIDA
August, 1963

ACKNOWLEDGMENTS

The author wishes to express his sincere appreciation to Dr. A.D. Sutherland for his counsel and guidance during the course of this research. He also would like to acknowledge the guidance given him throughout his graduate program by his supervisory committee and in particular to Dr. W.E. Lear, who was his chairman but is now on a year's leave of absence, and to Dr. W.W. Peterson who is his new chairman.

The author also wishes to thank the Department of Health, Education, and Welfare without whose support he would not have been able to study for the degree of Doctor of Philosophy. The use of computer time, provided by the University of Florida Computing Center, is gratefully acknowledged.

The author's special thanks go to his wife, Marilyn, who has been in many ways an important partner in this venture.

TABLE OF CONTENTS

Page

ACKNOWLEDGMENTS ii

LIST OF ILLUSTRATIONS v

CHAPTER

1. INTRODUCTION 1

    Amplification by a Modulated Electron Beam 1
    Small-Signal Analysis 3
    Space-Charge-Wave Amplifiers 3
    Finite Beam Considerations 5
    Extensions to Small-Signal Theory 6
        Extension of Webster's theory 6
        Electron disk approach 9
        Paschke's successive approximation 10
    Scope of the Present Investigation 12

2. SMALL-SIGNAL ANALYSIS OF A SPACE-CHARGE-WAVE AMPLIFIER 14

    Synopsis 14
    Small-Signal Equations 14
    Initial Conditions 15
    Small-Signal Analysis 19
    Conclusions Based on Small-Signal Theory 26

3. DERIVATION OF SPACE-CHARGE-WAVE EQUATIONS USING THE METHOD OF SUCCESSIVE APPROXIMATIONS 27

    Synopsis 27
    Assumptions 27
    Derivation of the Space-Charge-Wave Equations 28
    Method of Successive Approximations 32

4. GENERAL SOLUTIONS FOR THE SPACE-CHARGE-WAVE EQUATIONS 37

    Synopsis 37
    First-Order Solutions 37
    Second-Order Solutions 40
    Third-Order Solutions 43

TABLE OF CONTENTS--Continued

CHAPTER Page

5. PARTICULAR SOLUTIONS FOR REGION OF FIRST DRIFT TUBE 48

  Synopsis 48
  Boundary Conditions 48
    Continuity of current 49
    Conservation of energy 50
  First-Order Solutions 52
  Second-Order Solutions 53
  Third-Order Solutions 55
  Results 59
    Saturation of fundamental current 60
    Locations of velocity and current maxima and minima 60
    Phase shift 64
    Second harmonic generation 67

6. PARTICULAR SOLUTIONS FOR REGION OF SECOND DRIFT TUBE 69

  Synopsis 69
  Boundary Conditions 70
  First-Order Solutions 73
  Second-Order Solutions 75
  Third-Order Solutions 80
  Transition Near a Velocity Maximum 84
  Transition Near a Velocity Minimum 91

7. SUMMARY AND CONCLUSIONS 99

APPENDICES

A. LIST OF PRINCIPLE SYMBOLS 103

B. LIST OF PARAMETERS USED IN EQUATIONS 106

C. DISCUSSION OF ELECTRON OVERTAKING 114

D. METHOD FOR OBTAINING SOLUTIONS FOR THE CONSTANTS OF INTEGRATION IN REGION B 118

LIST OF REFERENCES 124

BIOGRAPHY 127

LIST OF ILLUSTRATIONS

Figure Page

2.1 Space-charge reduction factors for cylindrical beams in cylindrical drift tubes 16

2.2 Model of a space-charge-wave amplifier using three drift-tube sections 18

2.3 Space-charge-wave amplification with the first transition at a current maximum 22

2.4 Space-charge-wave amplification with the first transition at a velocity maximum 25

3.1 Current flow in an infinitesimal beam element 30

5.1 Fundamental frequency current vs. position 61

5.2 Fundamental frequency velocity vs. position 62

5.3 Maximum fundamental frequency current as a function of α 63

5.4 Location of current and velocity maxima and minima as a function of α 65

5.5 Phase shift at the point of maximum current as a function of α 66

5.6 Second harmonic current vs. position 68

6.1 Current in Region B as a function of drift-tube radius 86

6.2 Current in Region B as a function of drift-tube voltage 87

6.3 Maximum current in Region B as a function of the location of the first transition 89

6.4 Velocity in Region B as a function of the drift-tube voltage 92

LIST OF ILLUSTRATIONS--Continued

Figure | Page
6.5 Velocity in Region B as a function of the drift-tube radius 94
6.6 Maximum velocity in Region B as a function of α 96
6.7 Location of the first transition for maximum velocity in Region B 97
6.8 Location of the maximum velocity in Region B 97
6.9 Effect of drift-tube lengths upon the velocity amplification 98

CHAPTER 1

INTRODUCTION

Amplification by a Modulated Electron Beam

The ability of a modulated electron beam to propagate space-charge waves was first investigated by Hahn [1] and Ramo [2]. Passing a beam of electrons through a gap, across which an r-f electric field is applied, causes the electrons to be decelerated or accelerated depending on the phase of the electric field at the time of passage. The accelerated electrons tend to catch up with the electrons which left the gap at an earlier time, but were decelerated by the applied electric field. This grouping of electrons is referred to as bunching. It is assumed that the charge density of an unmodulated electron beam is zero, as there are equal numbers of electrons and positive ions. The positive ions result from the ionization of the residual gases by the electron beam. In the modulated electron beam, the charge density in the region where the electrons are bunched is negative; whereas, in the region between bunches, the charge density is positive. Because of this difference in charge density, the space-charge forces between the electrons move electrons from the region of high density into the region of low density. Since regions of lower electron density appear both ahead of and behind a region of high density, some electrons are accelerated with respect to the average beam velocity while others are decelerated. To a stationary observer, there would appear to be two waves propagating with velocities slightly higher and lower than the average beam velocity. As the bunches of electrons spread apart in the axial direction under the influence of space-charge repulsion, new bunches of electrons form from the decelerated electrons of one bunch, and the accelerated electrons of the following bunch formed by the r-f field a short time later. A second gap is positioned at some point along the beam where a new bunch of electrons has formed. This large grouping or bunching of electrons means a sizeable component of r-f current is present in the beam. This current will induce a similar component of r-f current in the output cavity, provided the cavity is tuned to the r-f frequency at which the beam is excited. The cavity may be tuned instead to a harmonic of the fundamental frequency, in which case the device is considered a frequency multiplier rather than an amplifier. The resultant voltage produced in the output cavity is an amplified version of the input excitation. The analyses of Hahn and Ramo shows that the optimum position for the output gap is one-fourth of a plasma wavelength, where the plasma frequency is the frequency at which the bunched electrons oscillate under the effect of space-charge forces. The bunching process takes place without further influence by external fields if the beam is enclosed in the region between cavities by a conducting cylinder called a drift tube. The two cavities with the drift tube separating them are the essential elements of the microwave device called the klystron. Because of the use of tuned resonant cavities, the klystron has an inherent bandwidth limitation, and another device called the traveling-wave tube has been developed. Essentially the drift tube is replaced by a helix, which supports an electromagnetic wave which propagates with an axial velocity less than the speed of light. Thus the electromagnetic wave can interact with the space-charge wave on the beam in a continuous fashion. This helix eliminates the need for the tuned output cavity, which has a limited bandwidth, since the amplified signal is taken from the helix directly.

Small-Signal Analysis

The action of the electron beam may be described by specifying how the velocity v(z,t) and current i(z,t) modulations fluctuate. A first approximation for the solutions of velocity and current may be obtained by a process referred to as small-signal analysis. Essentially the equations are derived by utilizing the equations for the space-charge force on an electron; the continuity of current; the relations between velocity, current, and charge density; and Maxwell's equations. In this approach it is assumed that the time variation is sinusoidal, and the equations are linearized by discarding the product of a-c terms. The separation of a-c and d-c terms then yields equations which are functions of position (z) alone, since the variation with time ($e^{j\omega t}$) cancels in the a-c equation.

Space-Charge-Wave Amplifiers

Tien and Field [3] reëxamined the principles of klystron operation, and found that further amplification could be obtained if the drift tube was divided into sections of appropriate length, each having a d-c potential different from the adjacent sections. Additional energy is available for increasing the amplitude of velocity modulation over that which would occur in a single section of drift tube. This device, called the velocity-jump amplifier, was the first of a series of devices classified as space-charge-wave amplifiers. Others in this class are the rippled-wall amplifier, where the sections of the drift tube take on different diameters without changing potentials, and the rippled-stream amplifier, where the drift tube is unchanged, but the beam diameter fluctuates. The former device was investigated by Birdsall and Whinnery [4], and the latter by Birdsall [5] and Mihran [6]. A general analysis of a space-charge-wave amplifier which incorporates all these possible alternatives has been performed by Peter, Bloom and Ruetz [7] using small-signal theory. It was found that maximum amplification resulted if the drift-tube potential and the drift-tube diameter were increased while the beam cross section was decreased at the point where the a-c velocity was minimum. At a velocity maximum all parameters were then returned to their original values. One interesting approach for investigating the operation of space-charge-wave amplifiers is a construction by Bloom and Peter [8] of a transmission-line analog which has a standing-wave pattern that represents the amplitude pattern of the space-charge wave. The approach is based on the small-signal analysis which predicts that the maximum current and velocity amplitudes interchange every quarter plasma wavelength. A general discussion of the linearized small-signal analysis as applied to the various microwave amplifiers is presented in books by Beck [9], Harman [10], and Hutter [11]. The small-signal theory is presented in Chapter 2, and the nonlinear analysis is the subject of the following chapters.

Finite Beam Considerations

Since beams are of finite diameter and located close to metallic conductors, i.e., the walls of the drift tube, it is apparent that the space-charge forces, which cause the bunching and debunching of the beam, will be reduced because of the fringe effect of the electric field. This fringe effect increases as the beam radius (b) approaches that of the drift tube (a), and is more prominent in beams having a small normalized beam radius ($\beta_e b$). The effect of reducing the space-charge force is a reduction in the plasma frequency (ω_p), i.e., the frequency at which the beam bunching takes place. This modification is obtained by multiplying the plasma frequency by a parameter called the plasma reduction factor (R_1). Hahn made the first analysis of finite beams in his original report, and discovered that an infinite number of modes of space-charge-wave propagation can exist. Ramo suggested that for a reasonable approximation only the fundamental mode need be considered. More rigorous summation techniques demonstrate that the effect of the higher order modes is most pronounced in beams which effectively fill the drift tube and have high $\beta_e b$ values. Branch and Mihran [12] have solved the transcendental equations which result from the Hahn-Ramo theory for the radial propagation constant needed to determine the reduction factor. Curves are presented with R_1 plotted against either $\beta_e b$ or b/a, with the remaining variable as a parameter, for several beam geometries. The plasma reduction factor affects the wavelengths of the standing-wave envelopes of the velocity and current modulations, and the amplitude of the current is also inversely proportional to the reduction factor. The plasma reduction factor is derived under the assumptions of small-signal theory, and one of the problems involved in large-signal analysis has been the applicability of the reduction factor to large-signal situations. Mihran [13] has demonstrated experimentally that replacement of ω_p by $R_1\omega_p$ in the extrapolated small-signal theory leads to errors in both magnitude and location of current maxima.

Extensions to Small-Signal Theory

The small-signal theory correctly predicts the fundamental operation of these microwave devices for small ratios of buncher voltage (V_m) to beam voltage (V_0). As the signal level is raised, experimentally observed phenomena such as harmonic generation, saturation of the fundamental current, phase shift, and growth of the second harmonic component are not even predicted, much less analyzed, by the small-signal approach. Several approaches have been conceived to extend the linear analysis into the nonlinear region of operation. These schemes are discussed in the following sections.

Extension of Webster's theory

One of the earliest analyses of klystron operation was performed by Webster [14]. The Webster solution for the fundamental component of current is

$$I_f = 2I_o J_1(X_o), \tag{1.1}$$

where

X_o = ballistic bunching parameter $\mu(\alpha/2)\beta_e z$,

I_o = d-c beam current,

J_1 = Bessel function of 1st order and 1st kind,

μ = gap coupling coefficient,

α = voltage modulation index (V_m/V_0),

V_m = amplitude of signal voltage applied to buncher,

V_0 = d-c beam voltage,

β_e = ω/v_o.

This solution is based on the assumption of no space-charge interaction, and hence is a ballistic analysis. The Webster theory has been modified to account for space-charge effects by comparing (1.1) with the solution derived by the small-signal space-charge wave theory,

$$I_f = I_o(\alpha/2)\mu\beta_e z \sin(\beta_p z)/(\beta_p z), \tag{1.2}$$

where $\beta_p = \omega_p/v_o$. The solutions given by (1.1) and (1.2) yield identical results for small values of α. The Bessel function may be replaced by one-half of its argument for small values of the argument. Calling the argument X, and comparing (1.1) and (1.2) under the assumption that X is small gives

$$X = \mu(\alpha/2)\beta_e z \sin(\beta_p z)/(\beta_p z). \tag{1.3}$$

This solution for the bunching parameter when space-charge effects are accounted for is substituted into (1.1), and used as the solution for I_f regardless of the value of X. There is no mathematical justification for this substitution, and it is used simply because an extrapolated solution is better than no solution at all. Comparison of the ballistic bunching parameter (X_o) defined in (1.1) with the solution obtained in (1.3) shows that the bunching parameter including space-charge effects is related to X_o by the relation

$$X = X_o \sin(\beta_p z)/(\beta_p z). \tag{1.4}$$

The term $\sin(\beta_p z)/(\beta_p z)$ is called the debunching factor. As α increases the modified Webster theory indicates that the current does not increase proportionally, i.e., the fundamental component of current saturates. Although the modified solution has been extrapolated past the point of electron crossover, the predicted ballistic paths of the electrons are incorrect. The modified theory fails to account for a change in the direction of the space-charge force past crossover, and for a change in the magnitude of the force. Moreover, the theory is one-dimensional, i.e., the fringing effect of the finite beam is neglected. Mihran [13] traces the development of a further modification to Webster's theory for predicting the electron paths past crossover. This theory, developed by Roe, corrects the first two errors of the extrapolated theory; however, the analysis is still one-dimensional. In order to approximate the effect of the fringe field, the plasma reduction factor is introduced into the equations by replacing β_p by $R_1\beta_p$. Mihran demonstrates that klystron design based on this approximation results in significantly less than optimum efficiency. He cites a typical large-signal case where the efficiency is 20 per cent less than an empirical optimum.

Electron disk approach

Tien, Walker, and Wolontis [15] devised the idea of replacing the electron beam by a set of charged disks which have radii equal to the beam radius, and are evenly distributed along the axis of the beam. They applied this electron disk approach to the traveling-wave tube for small values of the gain parameter (C), and later Tien [16] extended the analysis to larger values of C. Webber [17, 18] applied the disk model to the klystron, and Rowe [19] applied it to the traveling-wave tube using a space-charge field based on an electron distribution in time rather than in space. Although the disk approach includes the effect of space charge in an approximate manner, the idea of replacing a plasma of electrons by 16 or 24 charged disks is questionable. Webber's klystron computations do not fit Mihran's [13] experimentally derived values of "peel-off" angle anywhere over a wide range of $\beta_e b$ values. The "peel-off" angle is that normalized distance of the drift tube for which the normalized r-f current is one-half db below its ballistic maximum. This model does, however, predict the growth of the second harmonic which Mihran [20] verified experimentally.

Paschke's successive approximation

An alternative approach has been applied by Paschke [21], who considered the electron beam as a fluid just as was done for the linear case by Hahn and Ramo. Maxwell's equations are applied to the model, and the resulting nonlinear partial differential equation is solved without discarding products of a-c terms or assuming $e^{j\omega t}$ variation in time as the small-signal analysis does. The technique for solving the nonlinear equation is referred to as the method of successive approximations. It is assumed that the dependent variable may be expressed as a power series in the voltage modulation coefficient (α). The space-charge-wave equation is then grouped into terms according to degree. The first-order solution, which is proportional to α, is obtained by retaining only the first-degree terms. This solution is then used to obtain the second-order solution which is proportional to α^2, and is found by retaining terms in the general equation which are proportional to α^2. This process is repeated until it is assumed that the additional terms have a negligible contribution, i.e., the power series is convergent. In the approach used by Paschke, a third-order theory was considered to be sufficient to investigate the phenomena of saturation, phase shift, and second harmonic generation. Thus the solution is of the form

$$i = \sum_{n=1}^{3} i_n , \tag{1.5}$$

where i_n is proportional to α^n. The approach has a fundamental assumption, which is shared with the disk model, that the electric field does not vary over the cross section of the beam. It has been shown by Olving [22] and Mihran [13] that this assumption is valid for thin beams ($\beta_e b \lesssim 1$). The main limitation to the theory is the fact that it is only valid for velocities which are single-valued functions of space, i.e., no electron overtaking is permitted. In succeeding reports, Paschke considered finite beams with fringe fields in order to evaluate the second harmonic component [23], saturation of the fundamental and third harmonic generation [24], and phase shift of the fundamental [25]. The phase-shift problem has also been investigated by Engler [26] without using some of the approximations utilized by Paschke [25]. Olving [22, 27] applied the method of successive approximations to a velocity-modulated electron beam and obtained an infinite series solution. The results included the effect of higher order modes, whereas Paschke had assumed that only the fundamental mode was generated. Olving demonstrated that Paschke's intuitive idea of using plasma reduction factors in the nonlinear region is justified for thin beams where higher order modes of the harmonics may be neglected. Since this restriction also applies to the approximation of constant electric field over the beam cross section, the method of successive approximations introduces no new restrictions other than the one of no electron overtaking. Although this method does not consider overtaking, Paschke [24] showed that his method fits the experimental values of "peel-off" angle defined by Mihran [13] very well in the region where $\beta_e b \lesssim 1$, i.e., in the region where the model is valid. With the method of successive approximations it is possible to investigate right up to the point of electron overtaking with some assurance that the results can be verified by experiments.

Scope of the Present Investigation

Paschke's method of analysis is applied to the space-charge waves propagating in a space-charge-wave amplifier which combines the features of the velocity-jump and rippled-wall amplifiers.[1] Beam diameter changes are not considered as it is relatively difficult to produce this variation physically, whereas the other two changes can be done with comparative ease. Some of the phenomena investigated in the first region include the saturation of the fundamental current as the bunching voltage is increased, phase shift, second harmonic generation, and the shift in locations of the velocity and current maxima and minima from the predicted small-signal locations. Investigation in the second region includes the effect of different ratios of drift-tube potentials, the effect of changing the drift-tube radius between sections, and the location of the transition between the two regions in order to cause maximum current or velocity variations for fixed sets of beam potentials and drift-tube geometries. These changes will be investigated with the thought in mind of how the current excited in an output cavity can best be increased for some fixed value of α by properly utilizing the velocity-jump and rippled-wall principles in combination. The proper lengths of the drift tube sections in order to optimize the output current will also be examined, as will the saturation effect which limits the output current as α increases.

---

[1] McIsaac [28] applied this nonlinear analysis to a device with an alternate series of gaps and drift tubes; however, no provision was made for applying d-c potentials across the gaps, or modifying the drift-tube diameters.

All symbols utilized in this paper are defined in Appendix A, and all constants defined in the derivation of the space-charge-wave equation are evaluated in Appendix B.

CHAPTER 2

SMALL-SIGNAL ANALYSIS OF A SPACE-CHARGE-WAVE AMPLIFIER

Synopsis

The small-signal solutions of the Hahn-Ramo theory are applied to a space-charge-wave amplifier composed of three drift-tube sections. The first and the third sections have identical properties, while the middle section possesses both a different potential and a different drift-tube radius. Investigation includes both increasing and decreasing the potential and radius of the second drift tube, relative to the values of these parameters in the first region. The gain is found to be proportional to the ratio of the plasma reduction factors and the three-fourths power of the voltage ratio. Maximum gain results if the lengths of the drift tubes are some multiple of one-quarter of a reduced plasma wavelength.

Small-Signal Equations

The small-signal equations developed by Hahn and Ramo, as given by Hutter [11], are

$$i = [i_i \cos(\beta_q z) - j(\omega/\omega_q)\,(i_o/v_o)\,v_i \sin(\beta_q z)]\, e^{j(\omega t - \beta_e z)} \tag{2.1}$$

$$v = [v_i \cos(\beta_q z) - j(\omega_q/\omega)\,(v_o/I_o)\; i_i \sin(\beta_q z)]\; e^{j(\omega t - \beta_e z)}, \tag{2.2}$$

where the i subscript indicates an initial value at the entrance to the region described by the equations, and $j = \sqrt{-1}$. The other variables were defined in connection with (1.1) and (1.2), and are tabulated for easy reference in Appendix A. These equations are derived on the assumptions that the variation with time is given by $e^{j\omega t}$, that a-c terms are small compared with d-c quantities, and that the theory, which is derived for a beam of infinite cross section, can be applied to beams of finite diameter by use of the plasma reduction factor as tabulated by Branch and Mihran [12]. A plasma reduction factor curve for a beam of radius (b) inside a drift tube of radius (a) is shown in Fig. 2.1. A list of the properties required of the plasma, in order to derive the small-signal equations, is stated in Chapter 3 in connection with the derivation of the nonlinear space-charge-wave equations. Equations (2.1) and (2.2) are valid for any region in which the d-c velocity (v_o) is constant, such as inside a section of drift tube.

Initial Conditions

The velocity-jump amplifier, developed by Tien and Field [3], utilizes a change in d-c potential between drift-tube sections to further amplify the current and velocity modulation. In order to use (2.1) and (2.2) to describe the amplification process, it is

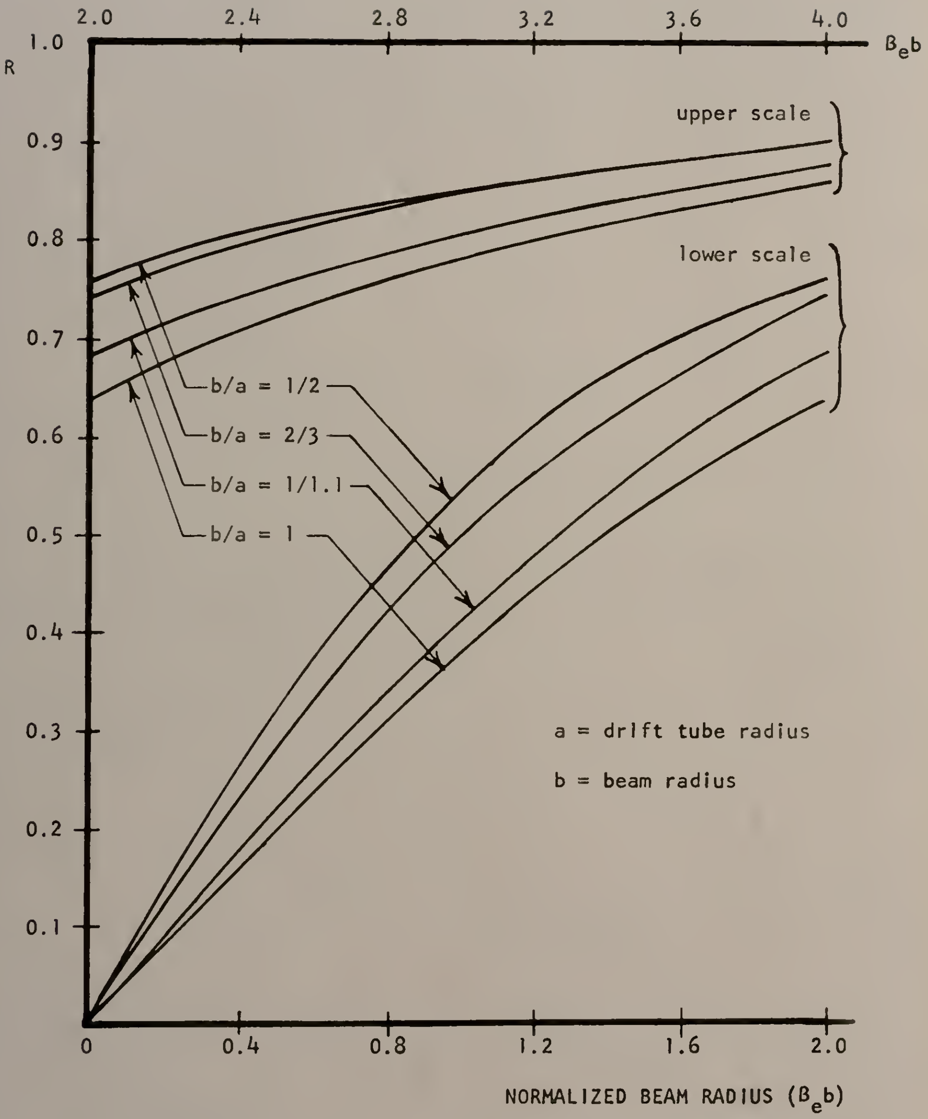

Fig. 2.1 - Space-charge reduction factors for cylindrical beams in cylindrical drift tubes.

necessary to determine what happens to the magnitude of the a-c current and velocity as the beam passes through the transition point. Hutter develops a proof, using the Lorentz force equation, which demonstrates that the a-c current is continuous, whereas, the a-c velocity undergoes a transition proportional to the ratio of the d-c velocities in the two regions.

$$i_b(z_t) = i_a(z_t) \tag{2.3}$$

$$v_b(z_t) = (V_a/V_b)^{\frac{1}{2}}\ v_a(z_t), \tag{2.4}$$

where the subscripts a and b refer to the first and second regions respectively, and z_t is the position at which the transition is located. A model of the amplifier is shown in Fig. 2.2.

Before the beam enters the input cavity, located at z_o, there is no a-c excitation. A signal voltage $V_m \cos(\omega t)$ velocity modulates the beam at the input cavity. The initial values of a-c current and velocity are derived in Chapter 3 in connection with the nonlinear analysis. The small-signal solutions are

$$i_i(z_o) = 0 \tag{2.5a}$$

$$v_i(z_o) = (\alpha/2)\ v_{oa}, \tag{2.5b}$$

where α is the ratio of signal voltage (V_m) to d-c beam voltage (V_o). The equations for the first drift-tube region are found by substituting

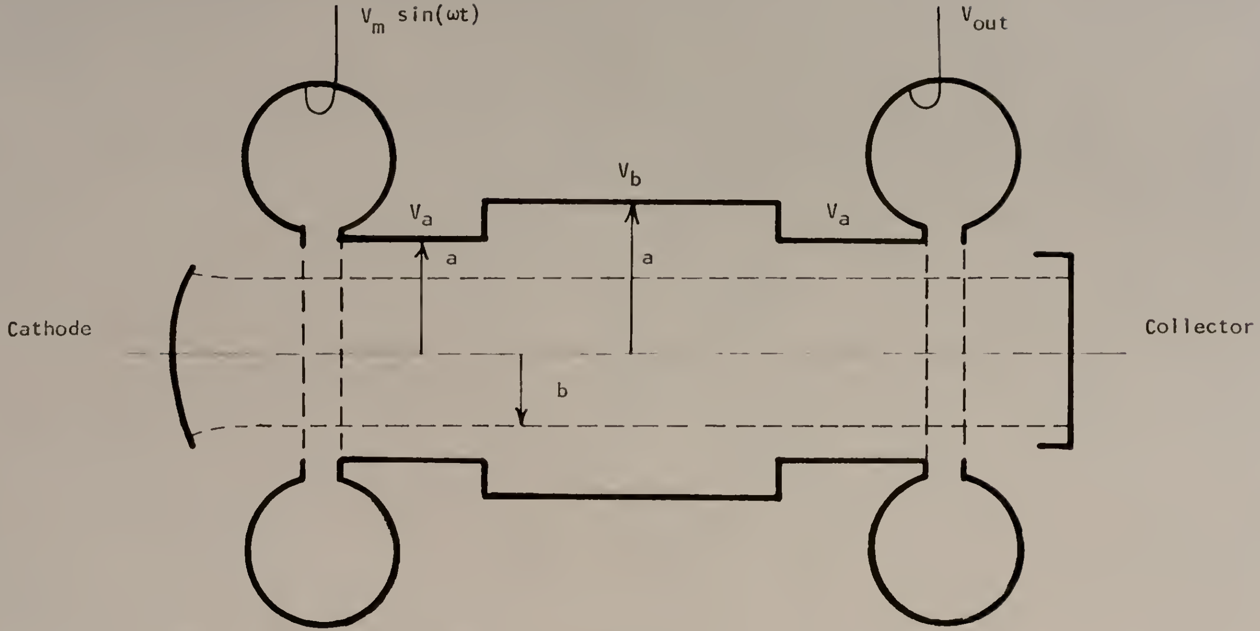

Fig. 2.2 - Model of a space-charge-wave amplifier using three drift-tube sections.

(2.5) into (2.1) and (2.2).

$$i_a = - j(\alpha/2)\ (\omega/\omega_{qa})\ i_o \sin(\beta_{qa}z) \qquad (2.6)$$

$$v_a = (\alpha/2)\ v_{oa} \cos(\beta_{qa}z) \qquad (2.7)$$

The exponential term, which carries only phase shift information, has been omitted from (2.6) and (2.7), and is also omitted in the rest of the equations in this chapter. To derive any instantaneous solution, it is necessary to insert the exponential term, and take the real portion of the product. Only envelope magnitudes are considered, therefore this exponential term may be omitted.

Small-Signal Analysis

If the first drift tube is one-fourth of a reduced plasma wavelength long ($\beta_{qa}z_a = 90^o$), then the magnitude of the a-c variations at z_a are

$$i_a(z_a) = (\alpha/2)\ (\omega/\omega_{qa})\ i_o \qquad (2.8a)$$

$$v_a(z_a) = 0. \qquad (2.8b)$$

Equations (2.8) are utilized to obtain entrance conditions for the second drift-tube region. Solutions for the second region are obtained by substituting (2.8) into (2.1) and (2.2).

$$i_b = (\alpha/2)\ (\omega/\omega_{qa})\ i_o \cos(\beta_{qb}z) \tag{2.9a}$$

$$v_b = -\,j\ (\alpha/2)\ (\omega_{qb}/\omega_{qa})\ v_{ob} \sin(\beta_{qb}z) \tag{2.9b}$$

If the length of the second drift tube is $\beta_{qb}z_b = 90^\circ$, then

$$i_b(z_b) = 0 \tag{2.10a}$$

$$v_b(z_b) = (\alpha/2)\ (\omega_{qb}/\omega_{qa})\ v_{ob}. \tag{2.10b}$$

The entrance conditions for the third section are obtained by comparing (2.10) and the requirement given by (2.4).

$$i_i(z_b) = 0 \tag{2.11a}$$

$$v_i(z_b) = (V_b/V_a)^{\frac{1}{2}}\ v_b(z_b) \tag{2.11b}$$

The solutions for the third region are obtained by substituting (2.11) into (2.1) and (2.2). Since the third region has the same properties as the first region, the parameters use the a subscript.

$$i_c = -\,j\ (\alpha/2)\ (\omega/\omega_{qa})\ (\omega_{qb}/\omega_{qa})\ (V_b/V_a)\ i_o \sin(\beta_{qa}z) \tag{2.12a}$$

$$v_c = (\alpha/2)\ (\omega_{qb}/\omega_{qa})\ (V_b/V_a)^{\frac{1}{2}}\ v_{ob} \cos(\beta_{qa}z) \tag{2.12b}$$

The ratio of the maximum a-c velocity in the third region (v_{cm}) to the maximum a-c velocity in the first region (v_{am}) is

$$v_{cm}/v_{am} = (V_b/V_a)^{\frac{1}{2}} (R_b/R_a) (\omega_{pb}/\omega_{pa}) (v_{ob}/v_{oa}). \tag{2.13}$$

The d-c velocity is proportional to $(V_o)^{\frac{1}{2}}$, and the plasma frequency is inversely proportional to the square root of the d-c velocity. Thus (2.13) reduces to

$$v_{cm}/v_{am} = (R_b/R_a) (V_b/V_a)^{3/4}. \tag{2.14}$$

The ratio of the current maxima is identical to (2.14).

Examination of (2.14) indicates that the best amplification is obtained if the values of the potential and plasma reduction factor in the second drift-tube region are increased. The value of R_b can be increased by increasing the drift-tube radius, as shown in Fig. 2.1. If the size of the drift tube is not increased, the value of R_b is less than R_a because the normalized beam radius $(\beta_{eb}b)$ decreases as the drift-tube potential is increased. The variations in the envelopes of the current and velocity modulations are shown in Fig. 2.3, for a choice of drift tube and beam parameter values dealt with on a nonlinear basis in later chapters.

The nonlinear investigation includes only the first two regions. The value of maximum velocity in Region C, which occurs just after the second transition (z_b), is obtained by multiplying the value of the velocity just before the second transition by the ratio of the d-c velocities (v_{ob}/v_{oa}). This yields adequate information for demonstrating the velocity saturation effect. The modified Webster theory,

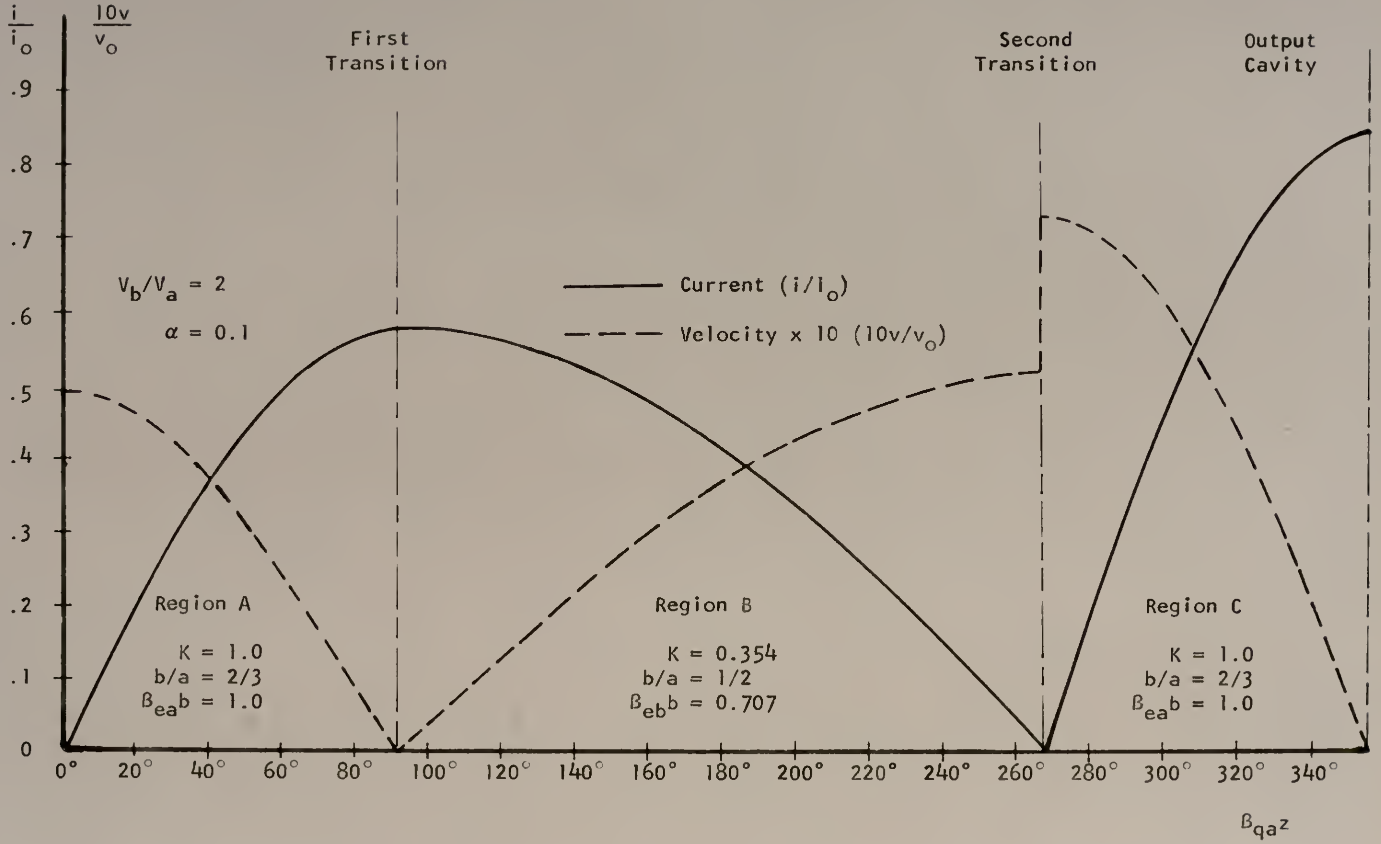

Fig. 2.3 - Space-charge-wave amplification with the first transition at a current maximum.

discussed in Chapter 1, can be utilized to predict the a-c current present in the output cavity located a quarter plasma wavelength beyond the second transition. The current prediction is obtained by replacing α in (1.3) by a new α', where α' is equal to $2v_{cm}/v_{oa}$, and substituting (1.3) into (1.1) in place of X_o. In addition β_p is replaced by $R_1\beta_p$ to account for the effect of the fringe field.

An expression similar to (2.14) results if the first transition is made at one-half of a plasma wavelength ($\beta_{qa} z_a = 180°$). The entrance conditions for the second drift region are

$$i_i(z_a) = 0 \tag{2.15a}$$

$$v_i(z_a) = (\alpha/2)\ (V_a/V_b)^{\frac{1}{2}}\ v_{oa}. \tag{2.15b}$$

The new solutions for the second drift space are found by applying (2.15) to (2.1) and (2.2).

$$i_b = -\ j\ (\alpha/2)\ (\omega/\omega_{qb})\ (V_a/V_b)\ i_o\ \sin(\beta_{qb} z) \tag{2.16a}$$

$$v_b = (\alpha/2)\ (V_a/V_b)^{\frac{1}{2}}\ v_{oa}\ \cos(\beta_{qb} z) \tag{2.16b}$$

The second drift tube must be one-fourth of a reduced plasma wavelength long in order to allow the second transition to occur at a current maximum. The entrance conditions for the third region are

$$i_i(z_b) = (\alpha/2)\ (\omega/\omega_{qb})\ (V_a/V_b)\ i_o \tag{2.17a}$$

$$v_i(z_b) = 0. \tag{2.17b}$$

The solutions in the third region, assuming once again that this region possesses the same properties as the first region, are obtained by substituting (2.17) into (2.1) and (2.2).

$$i_c = (\alpha/2)\ (\omega/\omega_{qb})\ (V_a/V_b)\ i_o \cos(\beta_{qa} z) \qquad (2.18a)$$

$$v_c = -\ j\ (\alpha/2)\ (R_a/R_b)\ (V_a/V_b)^{3/4}\ v_{oa} \sin(\beta_{qa} z) \qquad (2.18b)$$

The variations in the envelopes of the current and velocity modulations, with the first transition occurring at the point of maximum velocity variation, are shown in Fig. 2.4. The ratio of the maximum current or velocity in the third region to the corresponding maximum value in the first region is

$$i_{cm}/i_{am} = v_{cm}/v_{am} = (R_a/R_b)\ (V_a/V_b)^{3/4}. \qquad (2.19)$$

It is apparent from examining (2.19) that in order to obtain maximum amplification it is necessary to decrease the drift-tube potential and radius in the second region. This is just the opposite approach from that of the first analysis; however, comparison of (2.14) and (2.19) indicates that the degree of amplification is the same. The only difference comes in the length of the drift-tube sections. With the first transition occurring at a current maximum, all drift tubes are one-fourth of a reduced plasma wavelength long; whereas, in the second approach, the first and third sections must be one-half of a plasma wavelength long in order to obtain the desired current amplification.

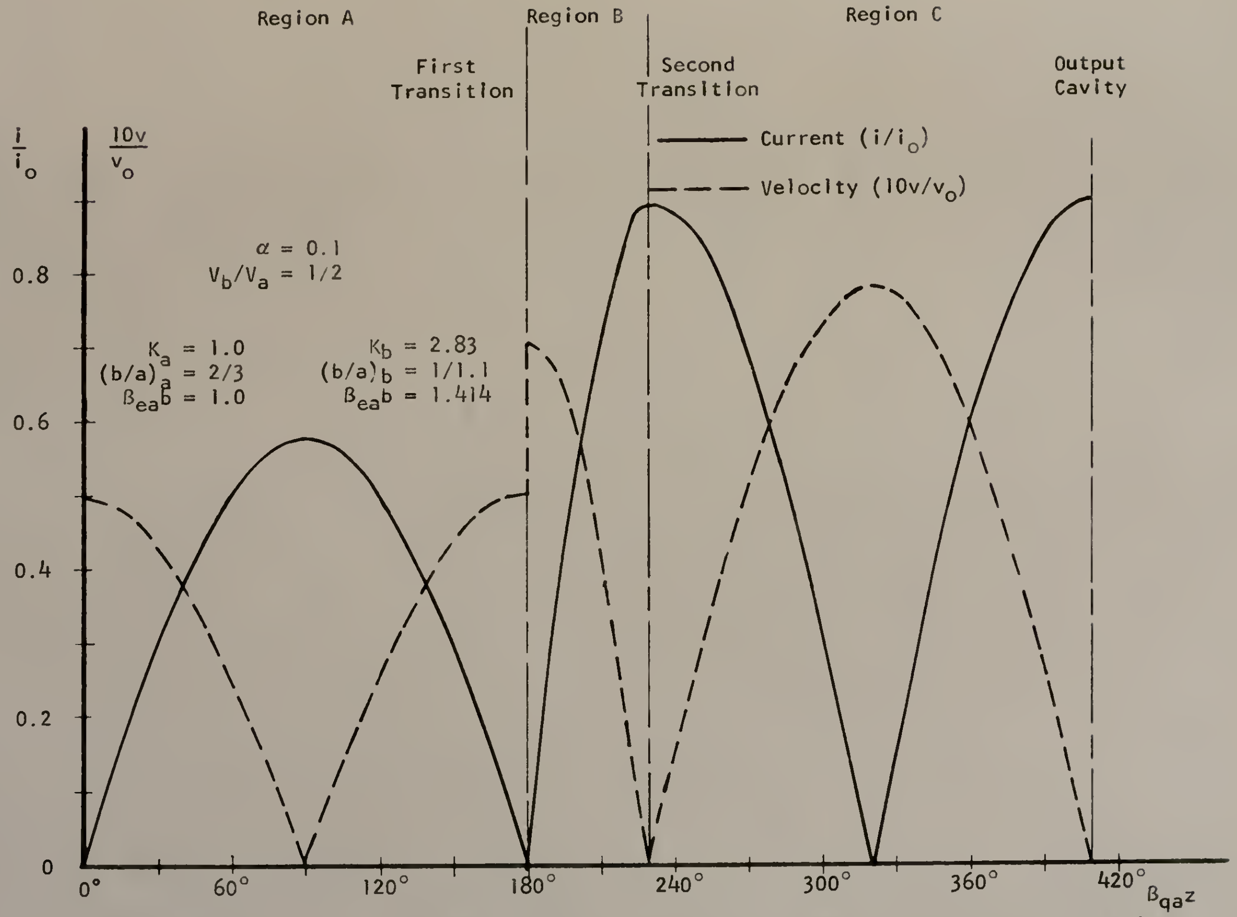

Fig. 2.4 - Space-charge-wave amplification with the first transition at a velocity maximum.

Conclusions Based on Small-Signal Theory

The small-signal theory predicts that the amplification is independent of the degree of voltage modulation, i.e., it is independent of α. The experimental fact that amplifiers actually reach saturation quite quickly as α increases cannot be ascertained from this small-signal theory. This theory also predicts that the best amplification is obtained if the voltage is decreased at a velocity maximum, and increased at a velocity minimum. Because the small-signal solution for a-c velocity has a minimum value of zero, no reduction in the a-c velocity occurs if the beam voltage is increased at the point of zero a-c velocity. If the transition is located at some other point, then the amplitude of the a-c velocity is reduced. These simple results are contrasted in Chapter 6 with the results obtained by a nonlinear theory. Among other things, it is shown that the best amplification is not obtained by placing the d-c velocity transitions at positions corresponding to multiples of a quarter plasma wavelength, and that saturation effects quickly come into play as the signal amplitude is increased.

CHAPTER 3

DERIVATION OF SPACE-CHARGE-WAVE EQUATIONS USING THE METHOD OF SUCCESSIVE APPROXIMATIONS

Synopsis

Following the approach used by Paschke, the electron beam is considered as a plasma, where the effect of the individual electron is ignored. The nonlinear partial differential equation which describes the polarization of an electron is derived by examining the current flow in an infinitesimal beam element. Linear equations are obtained by the method of successive approximations.

Assumptions

In order to simplify the analysis the following assumptions are made:

1. The electron velocity is small compared with the velocity of light.
2. The r-f electric field component in the axial direction is approximately constant over the beam cross section.
3. The effects of temperature, particle collisions, and potential depression caused by space charge are ignored.
4. Ion mass is assumed to be infinite, hence the ions are not

affected by r-f fields.

5. The d-c charge density of the ions ($|\rho_o|$) cancels the d-c charge density of the electrons (ρ_o).
6. The velocity, in keeping with the polarization coordinate system, is a single-valued function of space, i.e., electron overtaking does not occur.
7. The effect of the transverse electric field associated with the plasma surrounded by a conducting cylinder is accounted for by using the appropriate plasma reduction factor.
8. All variables are assumed to be functions only of the independent variables time (t) and axial position (z).
9. An infinite magnetic field confines the motion of the electron beam to the axial direction.

Derivation of the Space-Charge-Wave Equations

Several relations between position, current, velocity, and charge density are needed in order to derive the nonlinear space-charge-wave equations which describe the electron plasma. The charge density is given by

$$\rho_t = \rho_o + \rho(z,t). \tag{3.1}$$

The convection-current density is related to the charge density and velocity by

$$i_t = i_o + i = (\rho_o + \rho)(v_o + v), \tag{3.2}$$

where

$$i_o = \rho_o v_o. \tag{3.3}$$

The a-c current density and charge density are related by the principle of continuity of current,

$$- \partial i/\partial z = \partial\rho/\partial t. \tag{3.4}$$

Applying Newton's notation to partial differential equations gives

$$\partial f/\partial z \equiv f', \tag{3.5a}$$

and

$$\partial f/\partial t \equiv \dot{f}, \tag{3.5b}$$

where f is any function of axial position (z) and time (t). Thus applying (3.5) to (3.4) gives

$$- i' = \dot{\rho}. \tag{3.4}$$

The velocity at any point in the plasma is a function of the effect of the space-charge forces at that point. Using Newton's law of motion this relationship is given by

$$\dot{v} + (v_o + v)\, v' = - \eta E. \tag{3.6}$$

There is an associated electric field transverse to the z-axis whenever an electron beam of finite size is in the vicinity of a metallic drift tube. This transverse electric field, which is time varying, indicates the presence of a displacement current (M) per unit length of beam. This coupling current enters into the continuity equation for the total current flowing through an infinitesimal length of beam as shown in Fig. 3.1.

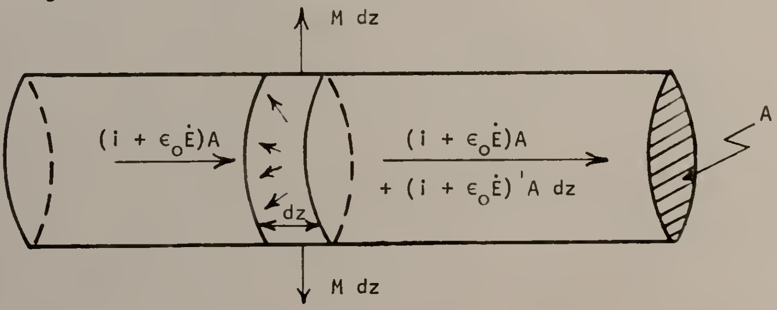
M dz
$(i + \epsilon_o\dot{E})A$
dz
$(i + \epsilon_o\dot{E})A$
$+ (i + \epsilon_o\dot{E})'A\,dz$
A
M dz

Fig. 3.1 - Current flow in an infinitesimal beam element.

Summation of the currents shown in Fig. 3.1 gives

$$i' + \epsilon_o(\dot{E})' + M/A = 0. \tag{3.7}$$

At this point a new variable (z_p) is introduced. This variable represents the polarization, or displacement, of an electron from its position in the unmodulated beam. This choice of variable is in keeping with the polarization system of coordinates established by Bobroff [29]. The polarization is related to the electric field due to space-charge by the relation

$$-\rho_o z_p = \epsilon_o E + f, \tag{3.8}$$

where *f* is the coupling flux which represents the presence of the transverse electric field. The coupling flux is related to the coupling current (M) by the relation

$$(\dot{f})' = M/A. \tag{3.9}$$

Substitution of (3.8) and (3.9) into (3.7) gives

$$i' = \rho_o(\dot{z}_p)'. \tag{3.10}$$

Integration of (3.10) with respect to z yields

$$i = \rho_o \dot{z}_p. \tag{3.11}$$

Comparison of (3.10) and (3.4) in terms of i' gives

$$\dot{\rho} = -\rho_o(\dot{z}_p)'. \tag{3.12}$$

Integration of (3.12) with respect to time yields

$$\rho = -\rho_o z_p'. \tag{3.13}$$

The velocity is obtained by substituting relations for i and ρ into (3.2).

$$v = \frac{v_o z_p' + \dot{z}_p}{1 - z_p'} \tag{3.14}$$

An equation for velocity is obtained by solving (3.8) for E and substituting the result into (3.6).

$$\dot{v} + (v_o + v)\, v' = \eta(\rho_o z_p + f)/\epsilon_o \tag{3.15}$$

Substituting (3.14) into (3.15) results in an equation involving only the polarization (z_p) of the electron. The final form is a nonlinear, second-order partial differential equation of fourth-degree.

$$\begin{aligned} & z_p'' + 2(\dot{z}_p)'/v_o + \ddot{z}_p/v_o^2 - \eta(\rho_o z_p + f)/\epsilon_o v_o^2 \\ & + 2[\, \dot{z}_p(\dot{z}_p)' - z_p'\ddot{z}_p - (\dot{z}_p)' z_p' \dot{z}_p \,]/v_o^2 \\ & +[\ddot{z}_p(z_p')^2 + z_p''\, (\dot{z}_p)^2]/v_o^2 + 2[z_p''\dot{z}_p - (\dot{z}_p)'\, z_p']/v_o \\ & + \eta(\rho_o z_p + f)\, [3z_p' - 3(z_p')^2 + (z_p')^3\,]/\epsilon_o v_o^2 = 0 \end{aligned} \tag{3.16}$$

The velocity is related to the polarization (z_p) through (3.14), and the current density is related to the polarization through (3.11).

Method of Successive Approximations

The solution to (3.16) is obtained by the technique known as the method of successive approximations. In this approach it is assumed that the polarization may be expressed as

$$z_p = \sum_{n=1}^{3} z_n, \tag{3.17}$$

where it is assumed that z_n is proportional to α^n. Three equations are formulated by substituting (3.17) into (3.16) and separating terms by powers of α. The variables $\underline{i}$, $\underline{v}$, and $\underline{f}$ are also related to α by series similar to (3.17).

Substitution of (3.17) into (3.16) leads to a first-order equation of the form

$$(z_1)'' + 2(\dot{z}_1)'/v_o + \ddot{z}_1/v_o^2 - (\eta/\epsilon_o)(\rho_o z_1 + f_1)/v_o^2 = 0. \quad (3.18)$$

Equation (3.18) has a solution (z_1) which is directly proportional to α. This solution should be identical to the Hahn-Ramo small-signal solution, which is also a linear function of α. The Hahn-Ramo solution is obtained from (3.18) provided,

$$\rho_o z_1 + f_1 \equiv R_1^2 \rho_o z_1. \quad (3.19a)$$

This is another way of saying that the small-signal plasma reduction factors may be utilized to account for the effect of the fringe field. Following the technique used to obtain (3.19a), Paschke has approximated the second-order and third-order fringe effects by the relations

$$\rho_o z_2 + f_2 = \langle R_{0,2}^2 \rangle \rho_o z_2 \quad (3.19b)$$

$$\rho_o z_3 + f_3 = \langle R_{1,3}^2 \rangle \rho_o z_3. \quad (3.19c)$$

The notation $\langle R_{0,2} \rangle$ follows the example of Engler, and indicates that

R_2, the value of reduction factor associated with $2\beta_e b$, is utilized when seeking the second harmonic portion of the second-order solution, whereas $R_0 = 0$ is used with the d-c portion of the second-order solution. The third-order solution has a component of fundamental frequency and a third harmonic portion. Hence, R_1 is used with the fundamental frequency portion, and R_3 with the third harmonic. The value of R_3 is determined by examining the reduction factor curve of fixed b/a at the point $3\beta_e b$. Olving [22] has shown that the application of plasma reduction factors is valid for thin beams ($\beta_e b < 1$).

Substituting (3.19a) into (3.18) gives

$$z_1'' + 2\,(\dot{z}_1)'/v_o + \ddot{z}_1/v_o^2 + (R_1\beta_p)^2\, z_1 = 0, \tag{3.20}$$

where the plasma wave-number (β_p) is defined as

$$\beta_p = \omega_p/v_o = \sqrt{\eta|\rho o|/e_o}/v_o. \tag{3.21}$$

Three linear partial differential equations are obtained from (3.16) by substituting (3.17) and (3.19) into (3.16) and separating according to powers of α.

$$z_1'' + 2(\dot{z}_1)'/v_o + \ddot{z}_1/v_o^2 + (\beta_p R_1)^2\, z_1 = 0 \tag{3.22a}$$

$$z_2'' + 2(\dot{z}_2)'/v_o + \ddot{z}_2/v_o^2 + \beta_p^2 < R_{0,2}^2 > z_2 = 3(R_1\beta_p)^2\, z_1 z_1'$$

$$- 2\,[\dot{z}_1\,(\dot{z}_1)' - \ddot{z}_1 z_1']/v_o^2 - 2\,[z_1''\,\dot{z}_1 - (\dot{z}_1)'\,z_1']/v_o \tag{3.22b}$$

$$z_3'' + 2(\dot{z}_3)'/v_o + \ddot{z}_3/v_o^2 + \beta_p^2 < R_{1,3}^2 > z_3 =$$

$$2\,[\, z_1'\ddot{z}_2 + z_2'\ddot{z}_1 - \dot{z}_1(\dot{z}_2)' - \dot{z}_2(\dot{z}_1)']/v_o^2$$

$$+ [\, 2(\dot{z}_1)'\, z_1'\dot{z}_1 - \ddot{z}_1(z_1')^2 - z_1''(\dot{z}_1)^2]/v_o^2$$

$$+ 2\,[(\dot{z}_1)'\, z_2' + (\dot{z}_2)'\, z_1' - z_1''\,\dot{z}_2 - z_2''\,\dot{z}_1]/v_o$$

$$+ \beta_p^2\,[3z_1' < R_{0,2}^2 > z_2 - 3 < R_{1,3}^2 > z_1(z_1')^2 + 3z_2' < R_{1,3}^2 > z_1] \tag{3.22c}$$

The velocity may also be expressed as a series solution

$$v = \sum_{n=1}^{3} v_n, \tag{3.23}$$

where v_n is proportional to α^n.

Expanding the denominator of (3.14) into a power series yields

$$v = (v_o\, z_p' + \dot{z}_p)\ [1 + z_p' + (z_p')^2 + (z_p')^3 + \dots\ ]. \tag{3.24}$$

Equations for the first-, second-, and third-order velocity terms are obtained by substituting (3.17) into (3.24) and comparing coefficients of powers of α.

$$v_1 = v_o\, z_1' + \dot{z}_1 \tag{3.25a}$$

$$v_2 = v_1\, z_1' + \dot{z}_2 + v_o\, z_2' \tag{3.25b}$$

$$v_3 = v_o\, z_3' + \dot{z}_3 + v_1\, z_2' + v_2\, z_1' \tag{3.25c}$$

The solution for the electron polarization (z_p) is obtained by first solving the linear, homogeneous, partial differential equation (3.22a) for the first-order solution (z_1). This solution is substituted into the right hand side of (3.22b) in order to evaluate the forcing function. The second-order polarization (z_2) is obtained by solving the linear, nonhomogenous equation (3.22b). The third-order polarization is obtained by solving (3.22c), after first substituting the solutions for z_1 and z_2 into the right hand side of (3.22c) to evaluate the forcing function. For this investigation a third-order approximation is considered to be sufficient to determine the saturation effect. Consequently, the electron polarization (z_p) is approximated by the sum of z_1, z_2, and z_3.

CHAPTER 4

GENERAL SOLUTIONS FOR THE SPACE-CHARGE-WAVE EQUATIONS

Synopsis

In this chapter the general solutions for the first-, second-, and third-order components of the polarization, current, and velocity are derived. Unlike the analyses of Paschke and Engler, boundary conditions are not substituted upon completion of each order of the solution. Consequently, the general solutions are considerably more complex than the solutions obtained in their reports. Both Engler and Paschke restricted their analysis to the investigation of a single drift region, corresponding to Region A of this report. Since the primary investigation in this report is the effect of drift-tube potential and reduction factor changes on the amplification process, at least two unique drift regions are needed. The additional labor required to obtain a general solution is necessary since the particular solution in Region B is obtained by comparison of the general solution obtained in this chapter with the particular solution for Region A obtained in the next chapter.

First-Order Solutions

Since the small-signal solution to the space-charge-wave equation has a time dependence given by $e^{j(\omega t - \beta_e z)}$, a solution of the form

$$z_1 = F_1(z)\cos(\omega t - \beta_e z) + G_1(z)\sin(\omega t - \beta_e z) \tag{4.1}$$

is chosen. Equations for the functions $F_1(z)$ and $G_1(z)$ are obtained by substituting (4.1) into (3.22a).

$$\begin{aligned}&[F_1''(z) + (R_1\beta_p)^2 F_1(z)]\cos(\omega t - \beta_e z)\\&+ [G_1''(z) + (R_1\beta_p)^2 G_1(z)]\sin(\omega t - \beta_e z) = 0\end{aligned} \tag{4.2}$$

Since (4.2) must hold for all values of time,

$$F_1''(z) + (R_1\beta_p)^2 F_1(z) = 0 \tag{4.3a}$$

$$G_1''(z) + (R_1\beta_p)^2 G_1(z) = 0. \tag{4.3b}$$

The product $R_1\beta_p$ is called the reduced plasma wave number and is defined by the symbol (β_{q1}). The solutions to (4.3) are

$$F_1(z) = A\cos(\beta_{q1}z) + B\sin(\beta_{q1}z) \tag{4.4a}$$

$$G_1(z) = C\cos(\beta_{q1}z) + D\sin(\beta_{q1}z). \tag{4.4b}$$

The general solution for the first-order polarization (z_1) is obtained by substituting (4.4) into (4.1). The polarization is normalized by multiplying (4.1) by β_{q1a}. The normalized first-order polarization is given by

$$\bar{z}_1 = \beta_{q1a}\, z_1 = [\bar{A}\cos(\beta_{q1}z) + \bar{B}\sin(\beta_{q1}z)]\cos(\omega t - \beta_e z)$$
$$+ [\bar{C}\cos(\beta_{q1}z) + \bar{D}\sin(\beta_{q1}z)]\sin(\omega t - \beta_e z), \qquad (4.5)$$

where the bar ($^-$) indicates that the parameter has been multiplied by β_{q1a}. The subscript a of β_{q1a} indicates that this is the value of β_{q1} in Region A. The absence of a second subscript for the other terms in (4.5) simply indicates that the terms are applicable for either region. The particular solutions for Region A or Region B have double-subscripted terms.

The first-order current (i_1) is found by substituting (4.5) into (3.11).

$$i_1/i_o = BE\,[\bar{C}\cos(\beta_{q1}z) + \bar{D}\sin(\beta_{q1}z)]\cos(\omega t - \beta_e z)$$
$$- BE\,[\bar{A}\cos(\beta_{q1}z) + \bar{B}\sin(\beta_{q1}z)]\sin(\omega t - \beta_e z), \qquad (4.6)$$

where

$$BE = \beta_e/\beta_{q1a}.$$

The first-order velocity is found by substituting (4.5) into (3.25a).

$$v_1/v_o = BQ1\,[\bar{B}\cos(\beta_{q1}z) - \bar{A}\sin(\beta_{q1}z)]\cos(\omega t - \beta_e z)$$
$$+ BQ1\,[\bar{D}\cos(\beta_{q1}z) - \bar{C}\sin(\beta_{q1}z)]\sin(\omega t - \beta_e z), \qquad (4.7)$$

where

$$BQ1 = \beta_{q1}/\beta_{q1a}.$$

Second-Order Solutions

The substitution of (4.5) into (3.22b) determines the forcing function for the second-order polarization equation.

$$z_2'' + 2\,(\dot{z}_2)'/v_o + \ddot{z}_2/v_o^2 + \beta_p^2 < R_{0,2}^2 > z_2 = ff_2, \qquad (4.8)$$

where

$$\begin{aligned} ff_2 = {} & K_1 \cos(2\beta_{q1}z) + K_2 \sin(2\beta_{q1}z) \\ & + [K_3 + K_4 \cos(2\beta_{q1}z) + K_5 \sin(2\beta_{q1}z)] \cos 2(\omega t - \beta_e z) \\ & + [K_6 + K_7 \cos(2\beta_{q1}z) + K_8 \sin(2\beta_{q1}z)] \sin 2(\omega t - \beta_e z). \end{aligned} \qquad (4.9)$$

The constants K_1 through K_8 are defined in Appendix B. The general solution for z_2 is of the form

$$z_2 = F_0(z) + F_2(z) \cos 2(\omega t - \beta_e z) + G_2(z) \sin 2(\omega t - \beta_e z). \qquad (4.10)$$

The reduction factor R_0 is associated with the d-c portion of (4.8), and R_2 with the second harmonic portion. Three equations are obtained by substituting (4.10) into (4.8) and comparing coefficients of the same function of time.

$$F_0''(z) + (R_0\beta_p)^2\, F_0(z) = K_1 \cos(2\beta_{q1}z) + K_2 \sin(2\beta_{q1}z) \qquad (4.11a)$$

$$F_2''(z) + (R_2\beta_p)^2\, F_2(z) = K_3 + K_4 \cos(2\beta_{q1}z) + K_5 \sin(2\beta_{q1}z) \qquad (4.11b)$$

$$G_2''(z) + (R_2\beta_p)^2\ G_2(z) = K_6 + K_7 \cos(2\beta_{q1} z) + K_8 \sin(2\beta_{q1} z) \quad (4.11c)$$

Since $R_0 = 0$, the solution to (4.11a) is found by integrating twice with respect to z.

$$F_0(z) = -\ [K_1 \cos(2\beta_{q1} z) + K_2 \sin(2\beta_{q1} z)]/(2\beta_{q1})^2 + E\ z + H, \quad (4.12)$$

where E and H are constants of integration. The complementary function for (4.11b) is

$$F_2(z)_c = I \sin(\beta_{q2} z) + J \cos(\beta_{q2} z), \quad (4.13)$$

where

$$\beta_{q2} = R_2\beta_p. \quad (4.14)$$

The form of the particular integral is determined by the forcing function portion of (4.11b).

$$F_2(z)_p = C_1 + C_2 \cos(2\beta_{q1} z) + C_3 \sin(2\beta_{q1} z) \quad (4.15)$$

The arbitrary constants C_1, C_2, and C_3 are evaluated by substituting (4.15) into (4.11b) and comparing coefficients.

$$F_2(z)_p = [K_3 + g\ \{K_4 \cos(2\beta_{q1} z) + K_5 \sin(2\beta_{q1} z)\}]/(\beta_{q2})^2, \quad (4.16)$$

where

$$g = (1 - 4\ s^2)^{-1},$$

and $$s = \beta_{q1}/\beta_{q2}.$$

The general solution to (4.11b) is the sum of (4.13) and (4.16). Comparison of (4.11b) and (4.11c) indicates that the form of the solution to (4.11c) is identical to (4.16) provided K_3 is replaced by K_6, etc. The complementary function involves two new constants of integration called L and M. The general solution for z_2 is the sum of the general solutions for $F_0(z)$, $F_2(z)$, and $G_2(z)$. As in the case of the first-order solutions, the second-order solutions are normalized.

$$\begin{aligned}\bar{z}_2 = {} & E\,\bar{z} + \bar{H} - \beta_{q1a}\,[K_1 \cos(2\beta_{q1}z) + K_2 \sin(2\beta_{q1}z)]/(2\beta_{q1})^2 \\ & + [\bar{I}\sin(\beta_{q2}z) + \bar{J}\cos(\beta_{q2}z) + \beta_{q1a}\,\{K_3 + g\,K_4\cos(2\beta_{q1}z) \\ & + g\,K_5\sin(2\beta_{q1}z)\}/(\beta_{q2})^2]\cos 2(\omega t - \beta_e z) + [\bar{L}\sin(\beta_{q2}z) \\ & + \bar{M}\cos(\beta_{q2}z) + \beta_{q1a}\,\{K_6 + g\,K_7\cos(2\beta_{q1}z) + g\,K_8\sin(2\beta_{q1}z)\} \\ & /(\beta_{q2})^2]\sin 2(\omega t - \beta_e z) \qquad (4.17)\end{aligned}$$

The second-order current is found by applying (4.17) to (3.11).

$$\begin{aligned} i_2/I_o = {} & 2\,BE\,[\bar{M}\cos(\beta_{q2}z) + \bar{L}\sin(\beta_{q2}z) + \beta_{q1a}\,\{K_6 + g\,K_7 \\ & \cdot\cos(2\beta_{q1}z) + g\,K_8\sin(2\beta_{q1}z)\}/(\beta_{q2})^2]\cos 2(\omega t - \beta_e z) \\ & - 2\,BE\,[\bar{J}\cos(\beta_{q2}z) + \bar{I}\sin(\beta_{q2}z) + \beta_{q1a}\,\{K_3 + g\,K_4 \\ & \cdot\cos(2\beta_{q1}z) + g\,K_5\sin(2\beta_{q1}z)\}/(\beta_{q2})^2]\sin 2(\omega t - \beta_e z) \qquad (4.18)\end{aligned}$$

The second-order velocity is found by substituting (4.5), (4.7), and (4.17) into (3.25b).

$$
\begin{aligned}
v_2/v_o = {} & E + BE\ BQ1\ P_{10}/2 + (BQ1)^2\ P_2/4 - [K_2/(6\beta_{q1})] \cos(2\beta_{q1}z) \\
& + [K_1/(6\beta_{q1})] \sin(2\beta_{q1}z) + [BQ2\ \bar{I} \cos(\beta_{q2}z) - BQ2\ \bar{J} \\
& \cdot \sin(\beta_{q2}z) - K_6/\beta_e + (1 + 2s^2)\ g\ \{K_5 \cos(2\beta_{q1}z) - K_4 \\
& \cdot \sin(2\beta_{q1}z)\}/(3\beta_{q1})] \cos 2(\omega t - \beta_e z) + [BQ2\ \bar{L} \cos(\beta_{q2}z) \\
& - BQ2\ \bar{M} \sin(\beta_{q2}z) + K_3/\beta_e + (1 + 2s^2)\ g\ \{K_8 \cos(2\beta_{q1}z) \\
& - K_7 \sin(2\beta_{q1}z)\}/(3\beta_{q1})] \sin 2(\omega t - \beta_e z) \qquad (4.19)
\end{aligned}
$$

Third-Order Solutions

The forcing function for the third-order polarization equation is evaluated by substituting solutions for z_1 and z_2 into (3.22c).

$$
\begin{aligned}
& z_3'' + 2(\dot{z}_3)'/v_o + \ddot{z}_3/v_o^2 + < R_{1,3}^2 > \beta_p^2\ z_3 = [K_9 \cos(\beta_{q1}z) \\
& + K_{10} \cos(b_1\beta_{q2}z) + K_{11} \cos(b_2\beta_{q2}z) + K_{12} \cos(3\beta_{q1}z) + K_{13} \sin(\beta_{q1}z) \\
& + K_{14} \sin(b_1\beta_{q2}z) + K_{15} \sin(b_2\beta_{q2}z) + K_{16} \sin(3\beta_{q1}z)] \cos(\omega t - \beta_e z) \\
& + [K_{17} \cos(\beta_{q1}z) + K_{18} \cos(b_1\beta_{q2}z) + K_{19} \cos(b_2\beta_{q2}z) + K_{20} \\
& \cdot \cos(3\beta_{q1}z) + K_{21} \sin(\beta_{q1}z) + K_{22} \sin(b_1\beta_{q2}z) + K_{23} \sin(b_2\beta_{q2}z)
\end{aligned}
$$

$$+ K_{24} \sin(3\beta_{q1} z)] \sin(\omega t - \beta_e z) \qquad (4.20)$$

Only that portion of the forcing function which is of fundamental frequency has been retained. The other portion, which is a third harmonic function of time, and hence is associated with the generation of a third harmonic component of polarization, is omitted. The reason for this omission is simply that the problem is concerned with the fundamental frequency, and harmonic components are carried only when they are required to evaluate solutions which involve fundamental frequency components. The notation $< R_{1,3}^2 >$ is replaced by R_1^2 because of the omission of the third harmonic component.

The form of the general solution for the third-order polarization is

$$z_3 = F_3(z) \cos(\omega t - \beta_e z) + G_3(z) \sin(\omega t - \beta_e z). \qquad (4.21)$$

The equations needed to determine $F_3(z)$ and $G_3(z)$ are obtained by substituting (4.21) into (4.20) and comparing coefficients of the same function of time.

$$F_3''(z) + (R_1\beta_p)^2 F_3(z) = A_1 \qquad (4.22a)$$

$$G_3''(z) + (R_1\beta_p)^2 G_3(z) = B_1, \qquad (4.22b)$$

where A_1 represents the coefficient of $\cos(\omega t - \beta_e z)$ and B_1 of $\sin(\omega t - \beta_e z)$ as given in (4.20). The solutions of the complementary functions of (4.22) are

$$F_3(z)_c = P\cos(\beta_{q1}z) + Q\sin(\beta_{q1}z) \tag{4.23a}$$

$$G_3(z)_c = R\cos(\beta_{q1}z) + S\sin(\beta_{q1}z). \tag{4.23b}$$

The solutions for the particular integrals are determined by the forcing function in (4.20). Since $\cos(\beta_{q1}z)$ is part of both the forcing function and the complementary function, the general form of the particular integral must be modified to include the term $c_1\, z\cos(\beta_{q1}z)$. A similar substitution is made for the $\sin(\beta_{q1}z)$ term. The various coefficients are evaluated by substituting the general form into (4.20) and comparing with the forcing function. The general solutions for $F_3(z)$ and $G_3(z)$ are

$$\begin{aligned} F_3(z) = {} & [P - K_{13}z/(2\beta_{q1})]\cos(\beta_{q1}z) + [Q + K_9 z/(2\beta_{q1})]\sin(\beta_{q1}z) \\ & + [K_{10}\cos(b_1\beta_{q2}z) + K_{14}\sin(b_1\beta_{q2}z)]/(b_3\beta_{q2}^2) \\ & - [K_{11}\cos(b_2\beta_{q2}z) + K_{15}\sin(b_2\beta_{q2}z)]/(b_4\beta_{q2}^2) \\ & - [K_{12}\cos(3\beta_{q1}z) + K_{16}\sin(3\beta_{q1}z)]/(8\beta_{q1}^2) \end{aligned} \tag{4.24}$$

$$\begin{aligned} G_3(z) = {} & [R - K_{21}z/(2\beta_{q1})]\cos(\beta_{q1}z) + [S + K_{17}z/(2\beta_{q1})]\sin(\beta_{q1}z) \\ & + [K_{18}\cos(b_1\beta_{q2}z) + K_{22}\sin(b_1\beta_{q2}z)]/(b_3\beta_{q2}^2) \\ & - [K_{19}\cos(b_2\beta_{q2}z) + K_{23}\sin(b_2\beta_{q2}z)]/(b_4\beta_{q2}^2) \\ & - [K_{20}\cos(3\beta_{q1}z) + K_{24}\sin(3\beta_{q1}z)]/(8\beta_{q1}^2). \end{aligned} \tag{4.25}$$

The general solution for the normalized third-order polarization is

$$\bar{z}_3 = \bar{F}_3(z) \cos(\omega t - \beta_e z) + \bar{G}_3(z) \sin(\omega t - \beta_e z), \qquad (4.26)$$

where the bar ($\bar{\ }$) indicates that the term is multiplied by β_{q1a}.

The third-order current is obtained by substituting (4.26) into (3.11).

$$i_3/i_o = BE\, \bar{G}_3(z) \cos(\omega t - \beta_e z) - BE\, \bar{F}_3(z) \sin(\omega t - \beta_e z) \qquad (4.27)$$

The third-order velocity is determined by substituting z_1, z_2, z_3, v_1, and v_2 into (3.25c).

$$v_3/v_o = [\bar{F}_3{}'(z) + F_a(z) + F_c(z)] \cos(\omega t - \beta_e z)$$

$$+ [\bar{G}_3{}'(z) + F_b(z) + F_d(z)] \sin(\omega t - \beta_e z), \qquad (4.28)$$

where $\bar{F}_3{}'(z)$ and $\bar{G}_3{}'(z)$ are the derivatives with respect to $\underline{z}$ of $\bar{F}_3(z)$ and $\bar{G}_3(z)$ respectively, and the functions $F_a(z)$, $F_b(z)$, $F_c(z)$, and $F_d(z)$ are defined in Appendix B.

In this chapter the general solutions to the space-charge-wave equations are determined. Boundary conditions are applied in the next chapter at the input gap to determine the particular solutions in Region A. In the following chapter, boundary conditions are applied at the point where the drift tube properties change to determine the particular solutions in Region B. The solutions and variables which apply in one particular region will be denoted by a second subscript. Thus the first-order polarization in Region A will be denoted as z_{1a}, while in Region B, the solution is denoted as z_{1b}.

CHAPTER 5

PARTICULAR SOLUTIONS FOR REGION OF FIRST DRIFT TUBE

Synopsis

In this chapter particular solutions are obtained from the general solutions of Chapter 4 by applying boundary conditions at the input cavity located at $\bar{z} = 0$. The solutions for this initial drift-tube region, known as Region A, are utilized as entrance conditions for obtaining solutions for Region B. The information obtained from the solutions in Region A pertains to a basic two-cavity klystron amplifier, driven at low signal levels, with the nonlinear beam effects taken into account. The phenomena investigated include current saturation, shift in the locations of velocity and current maxima and minima as signal voltage increases, phase shift, and second harmonic current generation. All constants identified with Region A will bear an a subscript. Numerical data used to plot the various curves presented in this chapter were obtained by use of a Fortran compiler applied to the IBM 709 computer.

Boundary Conditions

A signal voltage (V_s) is applied to a pair of closely-spaced grids located at $\bar{z} = 0$. The signal voltage is given by

$$V_s(t) = V_m \sin(\omega t), \tag{5.1}$$

where ω is the angular frequency at which the voltage varies. A previously unmodulated beam of electrons passes through the pair of grids. The effect of this a-c voltage on the electron beam is the establishment of velocity modulation. The extent of the effect is determined by applying the principles of continuity of current and conservation of energy. The usual klystron assumptions [30] discussed in the following sections are applied at the input gap.

Continuity of current

The principle of continuity of current is used to determine the initial current at $\bar{z} = 0$. Since the beam is unmodulated before entering the gridded gap, the current modulation upon exit is assumed to be negligible. Hence,

$$\bar{i}_1(0) = \bar{i}_2(0) = \bar{i}_3(0) = 0. \tag{5.2}$$

This conclusion is based on the assumption that the two grids are so closely spaced that there is no time for electron bunching to occur, i.e., the transit time is zero. Using the assumption of closely-spaced grids, it may be assumed that the beam coupling coefficient (μ) is unity. For gaps with finite grid spacing the coefficient is always less than one. Since it is assumed that the transit time is zero, it follows that the initial polarization (z_p), or displacement from the undisturbed position, is also zero. This condition is used to complete the second-order polarization solution.

Conservation of energy

The velocity of the electron beam upon exit from the input cavity is obtained by applying the principle of conservation of energy at $\bar{z} = 0$, along with the assumption that $\mu = 1$.

$$(m/2)\ (v_a^2 - v_{oa}^2) = -e\ V_m \sin(\omega t) \tag{5.3}$$

Transposing,

$$v_a^2 = v_{oa}^2 + 2\ \eta\ V_m\ \sin(\omega t). \tag{5.4}$$

Since

$$v_{oa}^2 = 2\ \eta\ V_a, \tag{5.5}$$

where V_a is the potential of the drift tube in Region A, (5.4) may be written as

$$v_a^2 = 2\ \eta\ [V_a + V_m\ \sin(\omega t)]. \tag{5.6}$$

The velocity in Region A is obtained by factoring V_a, taking the square root, and replacing $\sqrt{2\ \eta\ V_a}$ by v_{oa}.

$$v_a = v_{oa}\sqrt{1 + (V_m/V_a)\ \sin(\omega t)} \tag{5.7}$$

The ratio V_m/V_a is by definition the voltage modulation index (α).

$$\alpha \equiv V_m/V_a. \tag{5.8}$$

Application of the binomial expansion to (5.7) yields

$$v_a = v_{oa}\,[1 + (\alpha/2)\,\sin(\omega t) - (\alpha/2)^2\,\sin^2(\omega t)/2 + (\alpha/2)^3 \cdot \sin^3(\omega t)/2 + \ldots\,]. \tag{5.9}$$

Completing the square and cube in (5.9) gives

$$v_a = v_{oa}\,[1 + (\alpha/2)\,\sin(\omega t) - (\alpha/4)^2\,\{1 - \cos(2\omega t)\} + (\alpha/4)^3\,\{3\,\sin(\omega t) - \sin(3\omega t)\} + \ldots\,]. \tag{5.10}$$

By applying Paschke's method of successive approximations the beam velocity may be written as

$$v_a = v_{oa} + v_{1a} + v_{2a} + v_{3a}, \tag{5.11}$$

where v_{na} is proportional to α^n. The various velocity terms may be evaluated at $\bar{z} = 0$ by comparing (5.10) and (5.11) by powers of α.

$$\bar{v}_{1a}(0) = (\alpha/2)\,\sin(\omega t) \tag{5.12a}$$

$$\bar{v}_{2a}(0) = -\,(\alpha/4)^2\,[1 - \cos(2\omega t)] \tag{5.12b}$$

$$\bar{v}_{3a}(0) = (\alpha/4)^3\,[3\,\sin(\omega t) - \sin(3\omega t)], \tag{5.12c}$$

where

$$\bar{v}_{na}(0) \equiv v_{na}(0)/v_{oa}. \qquad n = 1,2,3 \tag{5.12d}$$

First-Order Solutions

Two of the first-order constants of integration are evaluated by applying (5.2) to (4.6).

$$\bar{i}_1(0) = x_a\ [\bar{C}_a \cos(\omega t) - \bar{A}_a \sin(\omega t)] = 0, \qquad (5.13)$$

where

$$x_a = \beta_{ea}/\beta_{q1a}. \qquad (5.14)$$

Since (5.13) must hold for all values of time,

$$\bar{A}_a = \bar{C}_a = 0. \qquad (5.15)$$

The other two constants are determined by applying (5.12a) and (5.15) to (4.7).

$$\bar{v}_{1a}(0) = \bar{B}_a \cos(\omega t) + \bar{D}_a \sin(\omega t) = (\alpha/2) \sin(\omega t) \qquad (5.16)$$

Hence,

$$\bar{B}_a = 0 \qquad (5.17a)$$

$$\bar{D}_a = \alpha/2. \qquad (5.17b)$$

The first-order variations are obtained by substituting (5.15) and (5.17) into (4.6) and (4.7).

$$\bar{i}_{1a} = x_a\ (\alpha/2) \sin(\bar{z}) \cos(\omega t - x_a\bar{z}) \qquad (5.18a)$$

$$\bar{v}_{1a} = (\alpha/2)\cos(\bar{z})\sin(\omega t - x_a\bar{z}), \tag{5.18b}$$

where

$$\bar{z} = \beta_{q1a}z. \tag{5.19}$$

These solutions are identical with the small-signal solutions obtained by Hahn [1] and Ramo [2].

Second-Order Solutions

Before obtaining the second-order solutions, it is necessary to evaluate $\bar{K}_1$ through $\bar{K}_8$ as given in Appendix B. The values in Region A are obtained by substituting (5.15) and (5.17) into the general expressions.

$$\bar{K}_{1a} = \bar{K}_{3a} = \bar{K}_{4a} = \bar{K}_{8a} = 0 \tag{5.20a}$$

$$\bar{K}_{2a} = 3(\alpha/4)^2 \tag{5.20b}$$

$$\bar{K}_{5a} = -3(\alpha/4)^2 \tag{5.20c}$$

$$\bar{K}_{6a} = x_a(\alpha/4)^2 \tag{5.20d}$$

$$\bar{K}_{7a} = 3x_a(\alpha/4)^2 \tag{5.20e}$$

Two of the second-order constants of integration are obtained by substituting (5.2) and (5.20) into (4.18).

$$\begin{aligned} \bar{I}_{2a}(0) = 2\, x_a\, [\bar{M}_a + s_a t_a\, (\alpha/4)^2\, (1 + 3\, g_a)] \cos(2\omega t) \\ - 2\, x_a \bar{J}_a \sin(2\omega t) = 0. \end{aligned} \qquad (5.21)$$

Hence,

$$\bar{J}_a = 0 \qquad (5.22a)$$

$$\bar{M}_a = -\, s_a t_a g_a\, (1 - s_a^{\,2})\, (\alpha/2)^2. \qquad (5.22b)$$

The remaining second-order constants are determined by substituting (5.12b) and (5.20) into (4.19) and comparing functions of time.

$$\begin{aligned} \bar{v}_{2a}(0) = E_a + (\alpha/4)^2 - (1/2)\, (\alpha/4)^2 + (\bar{L}_a/s_a) \sin(2\omega t) \\ + [\bar{I}_a/s_a - (\alpha/4)^2 - (1 + 2\, s_a^{\,2})\, g_a\, (\alpha/4)^2] \\ \cdot \cos(2\omega t) = -\, (\alpha/4)^2\, [1 - \cos(2\omega t)]. \end{aligned} \qquad (5.23)$$

Hence,

$$E_a = -(3/8)\, (\alpha/2)^2 \qquad (5.24a)$$

$$\bar{I}_a = 3\, (\alpha/4)^2\, s_a g_a\, (1 - 2\, s_a^{\,2}) \qquad (5.24b)$$

$$\bar{L}_a = 0. \qquad (5.24c)$$

In the discussion of boundary conditions, it was mentioned that the initial polarization (z_p) is zero provided the grids are closely spaced. The remaining constant (H_a) is determined by applying this boundary condition, (5.20), (5.22), and (5.24) to (4.17).

$$\bar{H}_a = 0 \qquad (5.24d)$$

The second-order current is found by substituting (5.22) and (5.24) into (4.18).

$$\begin{aligned} \bar{i}_{2a} = {} & (1/2)\ (\alpha/2)^2\ t_a^{\,2}[1 + 3\ g_a \cos(2\bar{z}) - 4\ g_a\ (1 - s_a^{\,2}) \\ & \cdot \cos(\bar{z}/s_a)] \cos 2(\omega t - x_a\bar{z}) + (3/2)\ (\alpha/2)^2 \\ & \cdot t_a g_a\ [s_a \sin(2\bar{z}) - (1 - 2\ s_a^{\,2}) \sin(\bar{z}/s_a)] \\ & \cdot \sin 2(\omega t - x_a\bar{z}) \end{aligned} \qquad (5.25)$$

The second-order velocity is found by substituting (5.22) and (5.24) into (4.19).

$$\begin{aligned} \bar{v}_{2a} = {} & - (\alpha/4)^2\ [\cos^2 (z) + \{1 - 3\ g_a\ (1 - 2\ s_a^{\,2}) \cos(\bar{z}/s_a) \\ & + g_a\ (1 + 2\ s_a^{\,2}) \cos(2\bar{z})\} \cos 2(\omega t - x_a\bar{z}) + x_a g_a \\ & \cdot \{(1 + 2\ s_a^{\,2}) \sin(2\bar{z}) - 4\ s_a(1 - s_a^{\,2}) \sin(\bar{z}/s_a)\} \\ & \cdot \sin 2(\omega t - x_a\bar{z})] \end{aligned} \qquad (5.26)$$

Third-Order Solutions

In order to evaluate the third-order solutions, the parameters $\bar{K}_9$ through $\bar{K}_{24}$, as defined in Appendix B, must be evaluated for Region A. Equations (5.15), (5.17), (5.20), (5.22), and (5.24) are used to evaluate these parameters.

$$\bar{K}_{9a} = (9/4)\ (\alpha/2)^3\ t_a s_a g_a \tag{5.27a}$$

$$\bar{K}_{10a} = (3/4)\ (\alpha/2)^3\ x_a g_a\ [2\ s_a\ (b_{2a} - s_a{}^2) - (\ 6\ s_a + 1)/(4\ s_a)] \tag{5.27b}$$

$$\bar{K}_{11a} = -\ (3/4)\ (\alpha/2)^3\ x_a g_a\ [2\ s_a\ (b_{1a} - s_a{}^2) + (6\ s_a - 1)/(4\ s_a)] \tag{5.27c}$$

$$\bar{K}_{12a} = (15/4)\ (\alpha/2)^3\ s_a t_a g_a \tag{5.27d}$$

$$\bar{K}_{13a} = \bar{K}_{14a} = \bar{K}_{15a} = \bar{K}_{16a} = 0 \tag{5.27e}$$

$$\bar{K}_{17a} = \bar{K}_{18a} = \bar{K}_{19a} = \bar{K}_{20a} = 0 \tag{5.27f}$$

$$\bar{K}_{21a} = (\alpha/4)^3\ g_a\ [54\ s_a{}^2 + 2\ x_a{}^2 + 14\ t_a{}^2 - 16\ s_a{}^2\ t_a{}^2 - 9]/2 \tag{5.27g}$$

$$\bar{K}_{22a} = -\ 2\ (\alpha/4)^3\ b_{1a}\ (g_a/s_a)\ [9\ (1 - 2\ s_a{}^2)/4 + x_a t_a b_{2a}\ (b_{4a} - 2s_a{}^2)] \tag{5.27h}$$

$$\bar{K}_{23a} = -\ 2\ (\alpha/4)^3\ b_{2a}\ (g_a/s_a)\ [9\ (1 - 2\ s_a{}^2)/4 + x_a t_a b_{1a} (b_{3a} + 2\ s_a{}^2)] \tag{5.27i}$$

$$\bar{K}_{24a} = (\alpha/4)^3\ g_a\ [90\ s_a{}^2 - 9 + 14\ t_a{}^2 - 2\ x_a{}^2]/2 \tag{5.27j}$$

Two of the third-order constants of integration are evaluated by applying (5.2) to (4.27).

$$\bar{i}_3(0) = x_a\ \bar{G}_3(0)\ \cos(\omega t) - x_a\ \bar{F}_3(0)\ \sin(\omega t) = 0 \tag{5.28}$$

Since this condition must hold for any value of time,

$$\bar{G}_3(0) = 0 \tag{5.29a}$$

$$\bar{F}_3(0) = 0. \tag{5.29b}$$

Applying (5.29) to (4.24) and (4.25) gives

$$\bar{P}_a + \bar{K}_{10}\, s_a{}^2/b_{3a} - \bar{K}_{11}\, s_a{}^2/b_{4a} - \bar{K}_{12}/8 = 0 \tag{5.30a}$$

$$\bar{R}_a + \bar{K}_{18}\, s_a{}^2/b_{3a} - \bar{K}_{19}\, s_a{}^2/b_{4a} - \bar{K}_{20}/8 = 0. \tag{5.30b}$$

The third-order constants $\bar{P}_a$ and $\bar{R}_a$ are found by transposing (5.30) and applying (5.27f).

$$\bar{P}_a = \bar{K}_{12}/8 + s_a{}^2\, [\bar{K}_{11}/b_{4a} - \bar{K}_{10}/b_{3a}] \tag{5.31}$$

$$\bar{R}_a = 0 \tag{5.32}$$

The remaining third-order constants are determined by applying (5.12c) to (4.28).

$$\begin{aligned}\bar{v}_{3a}(0) &= [\bar{F}_{3a}{}'(0) + F_{aa}(0) + F_{ca}(0)]\cos(\omega t)\\ &\quad + [\bar{G}_{3a}{}'(0) + F_{ba}(0) + F_{da}(0)]\sin(\omega t)\\ &= 3\,(\alpha/4)^3 \sin(\omega t),\end{aligned} \tag{5.33}$$

where $\bar{F}_3{}'(0)$ implies differentiation of $\bar{F}_3(z)$ with respect to z and evaluation at z = 0. Applying (5.27) to the derivatives of (4.24) and (4.25) gives

$$\bar{F}_{3a}'(0) = \bar{Q}_a \tag{5.34a}$$

$$\bar{G}_{3a}'(0) = \bar{S}_a + (s_a b_{1a}/b_{3a})\,\bar{K}_{22a} - \bar{K}_{21a}/2 - (s_a b_{2a}/b_{4a})\bar{K}_{23a}$$
$$- (3/8)\,\bar{K}_{24a}. \tag{5.34b}$$

The values of $F_a(z)$ through $F_d(z)$ for Region A, and evaluated at $z = 0$, are

$$F_{aa}(0) = 0 \tag{5.35a}$$

$$F_{ba}(0) = -\,9\,(\alpha/4)^3 \tag{5.35b}$$

$$F_{ca}(0) = 0 \tag{5.35c}$$

$$F_{da}(0) = -\,3\,(\alpha/4)^3. \tag{5.35d}$$

Substituting (5.34) and (5.35) into (5.33) gives

$$\bar{Q}_a \cos(\omega t) + [\bar{S}_a - \bar{K}_{21a}/2 + (s_a b_{1a}/b_{3a})\,\bar{K}_{22a} - (s_a b_{2a}/b_{4a})$$
$$\cdot\bar{K}_{23a} - (3/8)\,\bar{K}_{24a} - 12\,(\alpha/4)^3]\sin(\omega t) = 3\,(\alpha/4)^3 \sin(\omega t). \tag{5.36}$$

The third-order constants are evaluated by comparing functions of time.

$$\bar{Q}_a = 0 \tag{5.37}$$

$$\bar{S}_a = \bar{K}_{21a}/2 - (s_a b_{1a}/b_{3a})\,\bar{K}_{22a} + (3/8)\,\bar{K}_{24a} + (s_a b_{2a}/b_{4a})\,\bar{K}_{23a}$$
$$+ 15\,(\alpha/4)^3 \tag{5.38}$$

Since the third-order constants have been established, the third-order solutions for the current and velocity can be evaluated.

$$\begin{aligned}\bar{i}_{3a} = x_a\alpha^3 \, &[A_6 \sin(\bar{z}) + A_7 \sin(b_{1a}\bar{z}/s_a) + A_8 \sin(b_{2a}\bar{z}/s_a) \\ &+ A_9 \sin(3\bar{z}) + A_{10}\, \bar{z} \cos(\bar{z})] \cos(\omega t - x_a\bar{z}) - x_a\alpha^3 \\ &\cdot [A_1 \cos(\bar{z}) + A_2 \cos(b_{1a}\bar{z}/s_a) + A_3 \cos(b_{2a}\bar{z}/s_a) + A_4 \\ &\cdot \cos(3\bar{z}) + A_5\, z \sin(\bar{z})] \sin(\omega t - x_a\bar{z}) \qquad (5.39)\end{aligned}$$

$$\begin{aligned}\bar{v}_{3a} = \alpha^3 \, &[A_{11}\, \bar{z} \cos(\bar{z}) + A_{12} \sin(\bar{z}) + A_{13} \sin(b_{1a}\bar{z}/s_a) \\ &+ A_{14} \sin(b_{2a}\bar{z}/s_a) + A_{15} \sin(3\bar{z})] \cos(\omega t - x_a\bar{z}) + \alpha^3 \\ &\cdot [A_{16}\, \bar{z} \sin(\bar{z}) + A_{17} \cos(\bar{z}) + A_{18} \cos(b_{1a}\bar{z}/s_a) + A_{19} \\ &\cdot \cos(b_{2a}\bar{z}/s_a) + A_{20} \cos(3\bar{z})] \sin(\omega t - x_a\bar{z}) \qquad (5.40)\end{aligned}$$

The constants A_1 through A_{20} are evaluated in Appendix B.

Results

The fundamental component of current is found by adding (5.18) and (5.39).

$$\bar{i}_{fa} = \bar{i}_{1a} + \bar{i}_{3a} \qquad (5.41)$$

In Fig. 5.1 the amplitude of the fundamental frequency current is plotted against distance along the beam axis ($\tilde{z}$) for three values of α. The small-signal solution (i_{1a}) is also shown for the purpose of demonstrating saturation effects. Several interesting points are noted from examination of this figure. These are separately discussed below. The amplitude of the fundamental frequency velocity, along with the corresponding small-signal solution, is shown in Fig. 5.2.

Saturation of fundamental current

Small-signal theory predicts an increase in the amplitude of the fundamental current, which is linearly proportional to α; however, it is apparent from Fig. 5.1 that the amount of increase becomes proportionally smaller as α increases. This saturation effect is a well-known experimental fact. There is some reason to doubt that the apparent growth in current with distance for $\alpha = 0.3$, as ascertained from this theory, is physically real, inasmuch as this data comes from a region where overtaking has occurred.[2] Fig. 5.3 shows the effect of saturation as maximum current is plotted against α. It should be noted that the apparent increase in the slope past $\alpha = 0.3$ is well outside the range where this third-order approximation is valid.

Locations of velocity and current maxima and minima

It is also apparent from Fig. 5.1 and Fig. 5.2 that the locations of the maximum and minimum current and velocity shift as α is increased. The locations of the maximum and minimum values of current and velocity

---

[2] The concept of overtaking is discussed in Appendix C.

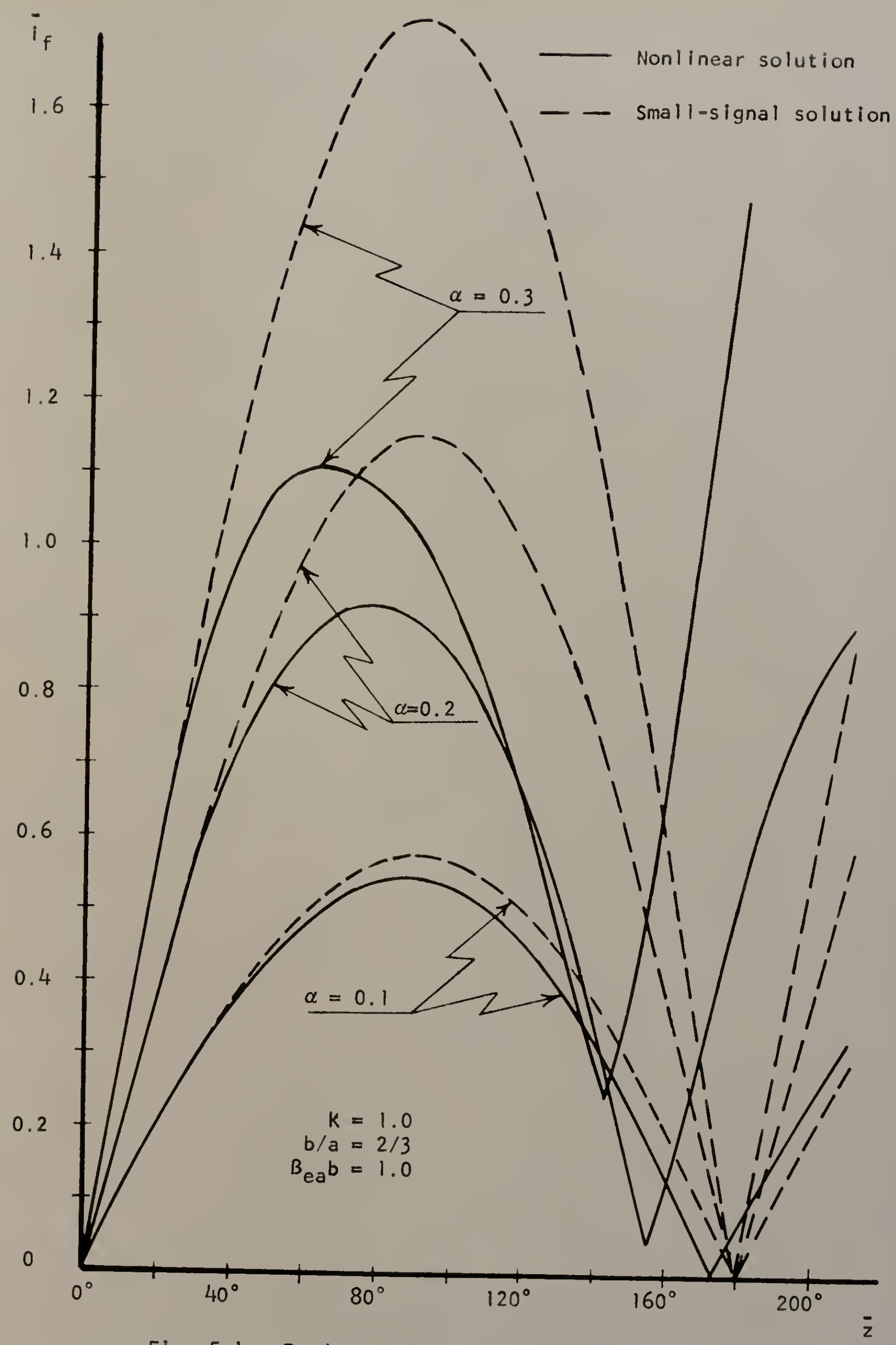

Fig. 5.1 - Fundamental frequency current vs. position.

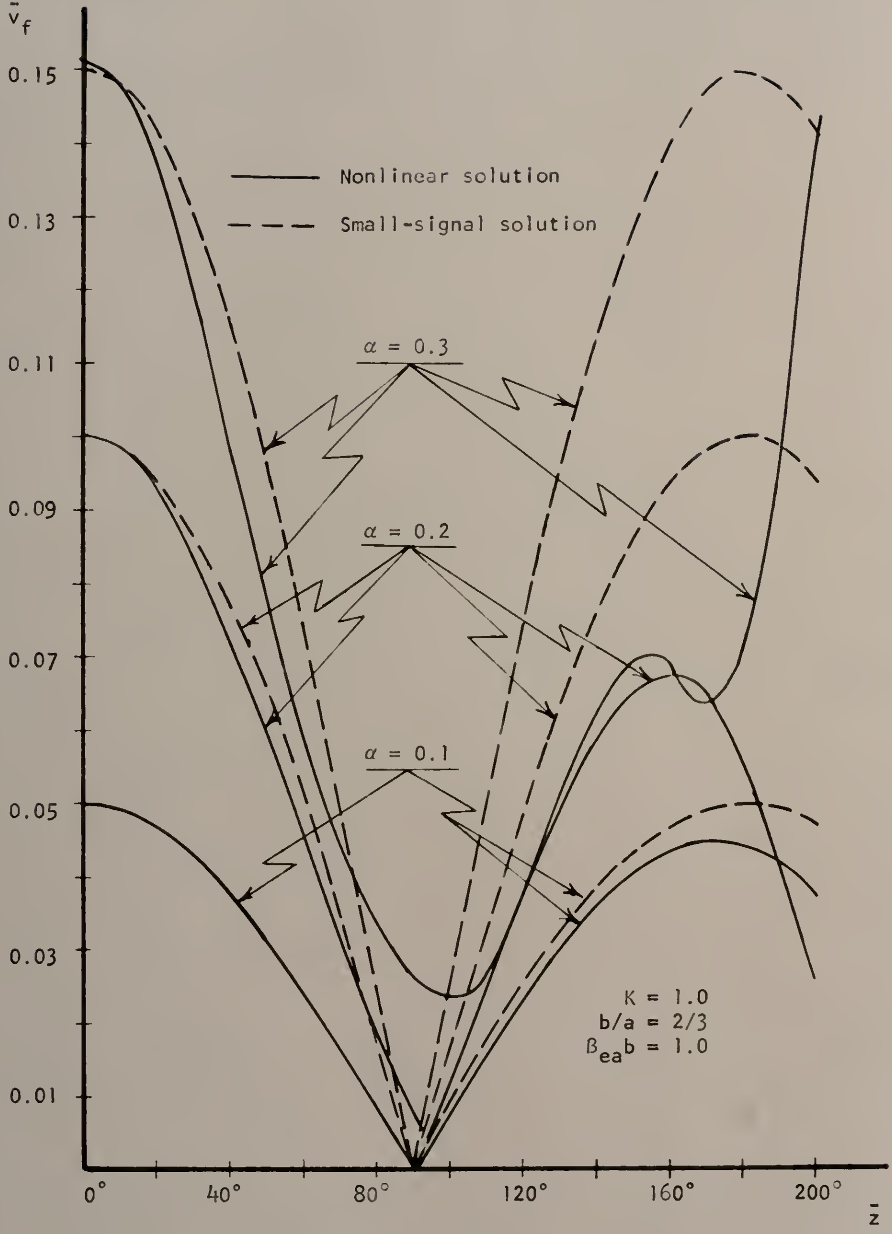

Fig. 5.2 - Fundamental frequency velocity vs. position.

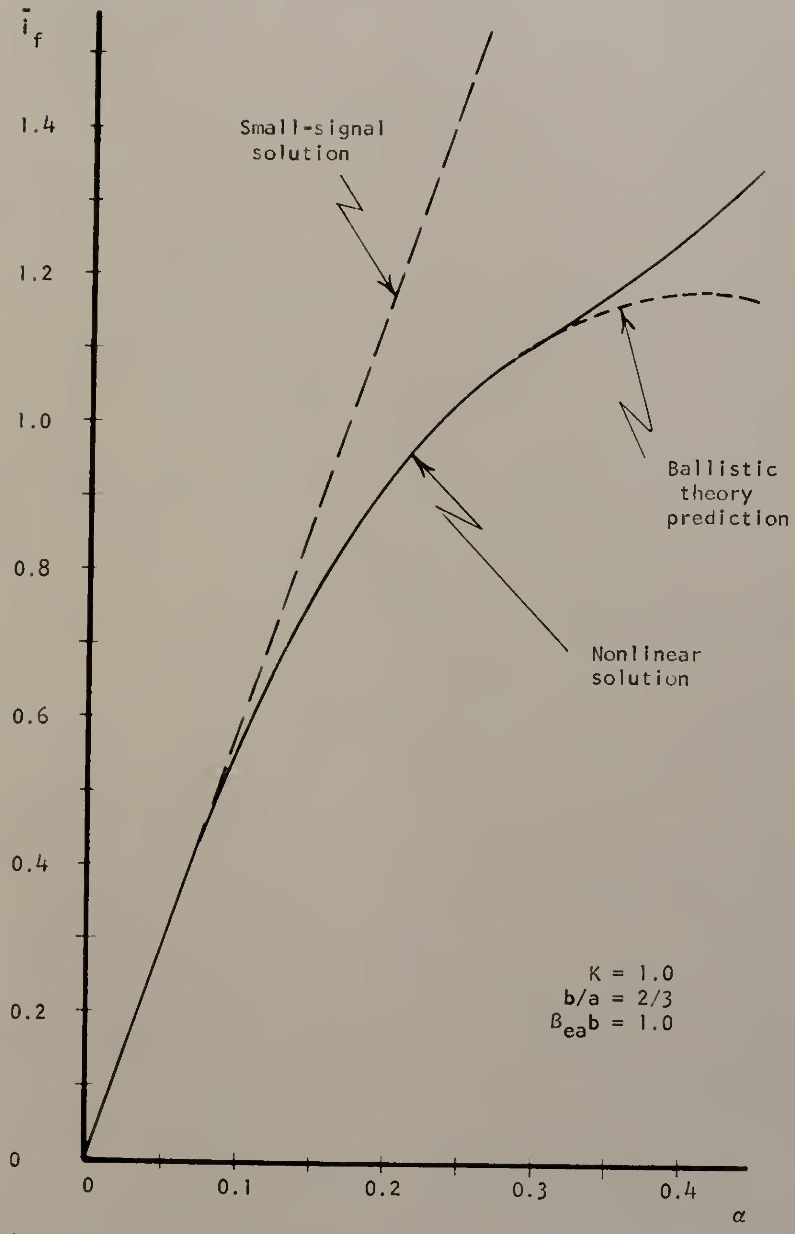

Fig. 5.3 - Maximum fundamental frequency current as a function of α.

as a function of α are shown in Fig. 5.4. These shifts from the locations predicted by small-signal theory are appreciable even for a moderate value of α such as 0.2. This shift in position has been experimentally observed by Mihran [13].

Phase shift

Since this analysis is a nonlinear approach, phase shift should be expected. The fundamental current is given by the sum of (5.18) and (5.39), and may be expressed in the form

$$\bar{i}_{fa} = \bar{I}_{fa} \cos(\omega t - x_a \bar{z} - \theta_f). \tag{5.42}$$

Examination of (5.39) shows the presence of both a cos(ωt) and a sin(ωt) component. The first-order term, as given by (5.18), has only a cos(ωt) component. Hence, the magnitude of the fundamental current is given by

$$\bar{I}_{fa} = \sqrt{(\bar{i}_{1a} + \bar{i}_{3ac})^2 + (\bar{i}_{3as})^2} \ , \tag{5.43}$$

where the subscripts c and s indicate cos(ωt) and sin(ωt) coefficients, respectively. The phase shift is given by

$$\theta_{fa} = \tan^{-1}\left[\frac{\bar{i}_{3as}}{\bar{i}_{1a} + \bar{i}_{3ac}}\right] . \tag{5.44}$$

The phase shift increases markedly with increasing α, as indicated in Fig. 5.5. This phase shift is evaluated at the point of maximum current

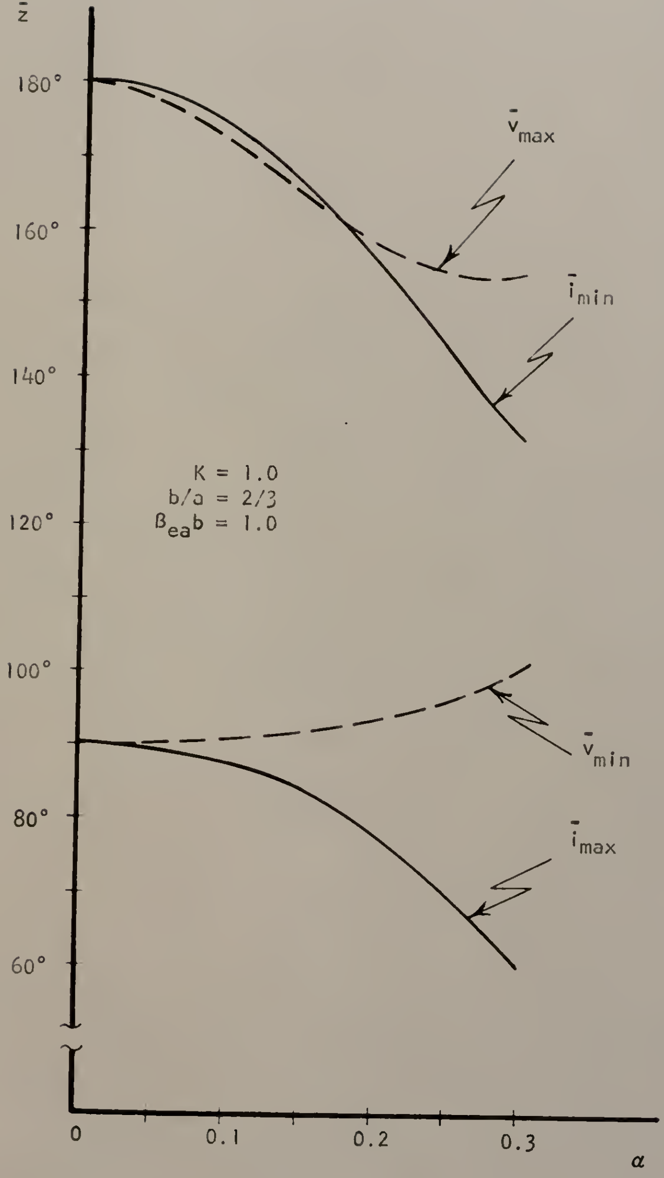

Fig. 5.4 - Location of current and velocity maxima and minima as a function of α.

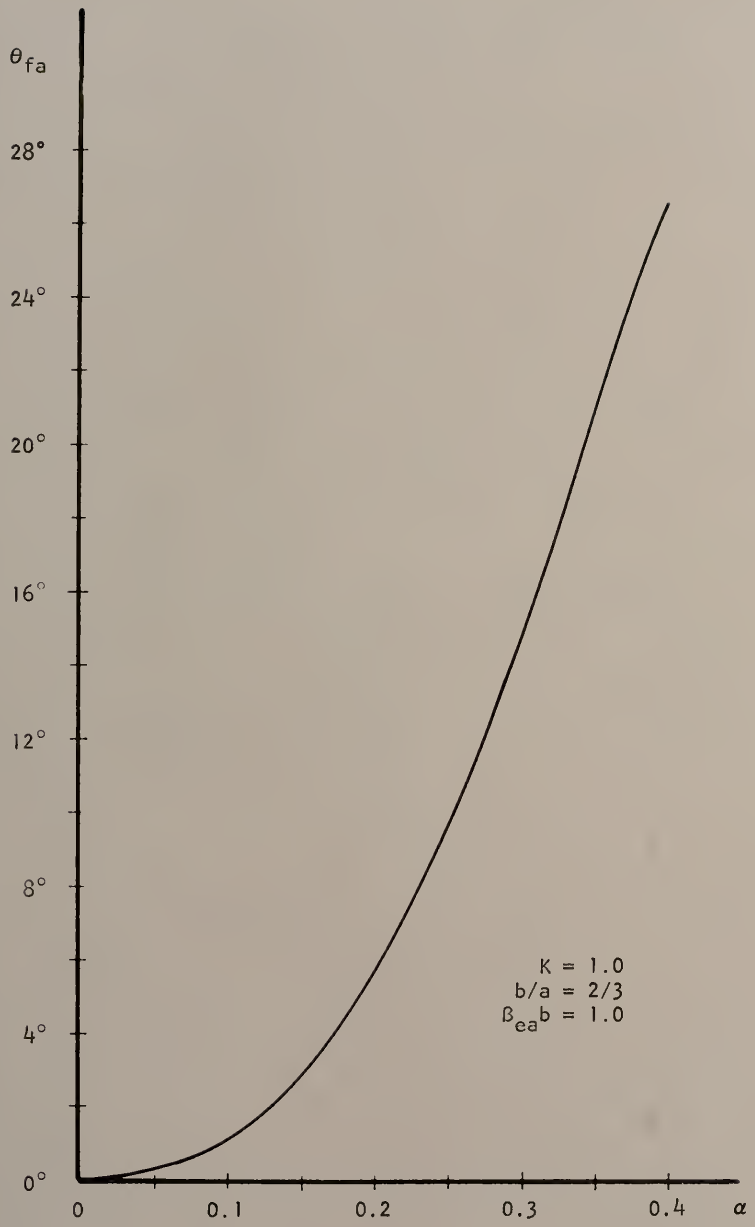

Fig. 5.5 - Phase shift at the point of maximum current as a function of α.

for each value of α. These results indicate that the technique of ignoring the out-of-phase component, as employed by Paschke [23, 24], leads to considerable error, particularly for larger values of α.

Second harmonic generation

The magnitude of second harmonic current is shown in Fig. 5.6. Examination of (5.25) indicates that the magnitude of second harmonic current increases as the square of the value of α. Comparison of Fig. 5.1 and Fig. 5.6 would tend to indicate that better performance could be obtained by tuning the klystron output cavity to the second harmonic rather than the fundamental. This conclusion is unwarranted, however, since the fundamental current solution is based on terms from the first-order and third-order solutions, with the third-order term contributing to saturation. On the other hand, the second harmonic solution shown neglects an additional second harmonic term which would be contributed by a fourth-order solution, and therefore fails to show saturation effects. The second harmonic solution obtained by this third-order approximation is analogous to the fundamental frequency solution obtained by small-signal analysis.

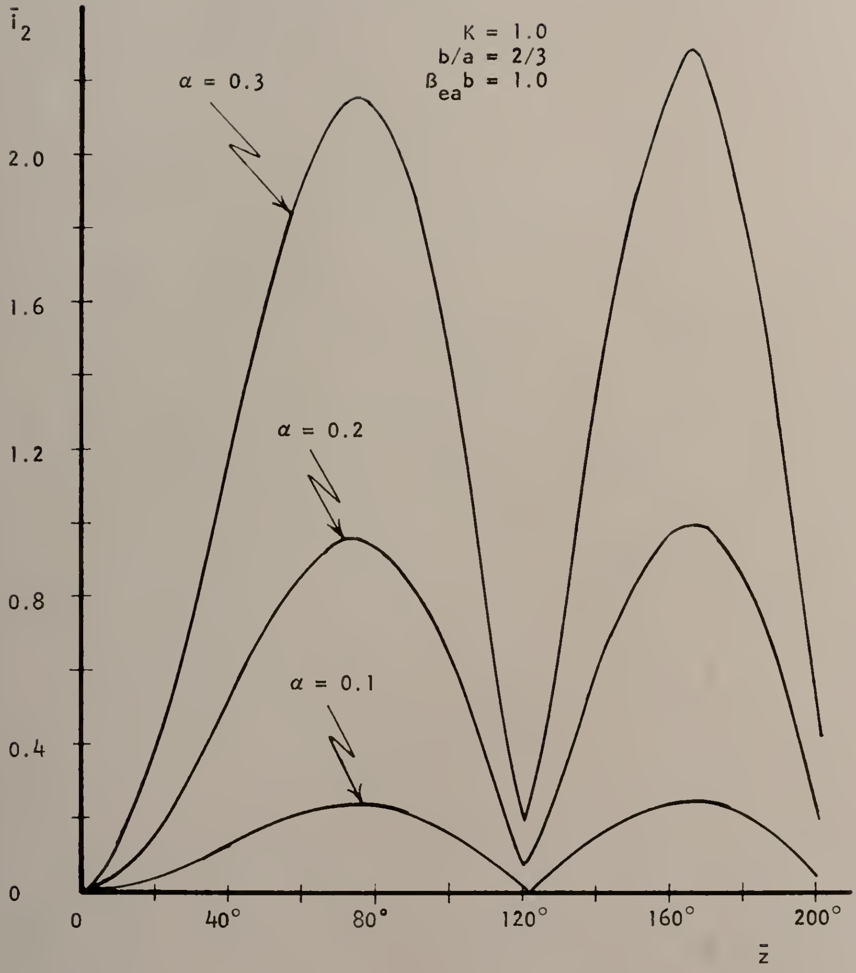

Fig. 5.6 - Second harmonic current vs. position.

CHAPTER 6

PARTICULAR SOLUTIONS FOR REGION OF SECOND DRIFT TUBE

Synopsis

In this chapter methods are investigated for amplifying the current beyond that obtained in the simple two-cavity klystron discussed in the previous chapter. The model for the space-charge-wave amplifier is identical to a two-cavity klystron, except the drift tube is divided into sections, each of which may have a different potential and a different diameter. The additional amplification results from changes in the drift tube potential and radius. Both of these changes effect the value of the plasma reduction factor (R_1). This amplifier represents a combination of the velocity-jump amplifier proposed by Tien and Field [3], and the rippled-wall amplifier investigated by Birdsall and Whinnery [4]. A third method for obtaining amplification is to vary the beam diameter; however, this technique is not considered because of the additional complexity introduced both in the theoretical analysis and in construction of a working unit. The analysis includes the effect of placing the transition in either the vicinity of maximum velocity modulation, or in the vicinity of minimum velocity modulation. The investigation also includes a search for the optimum location of the transition, in so far as concerns the achievement of maximum current modulation at some point further down the beam. The solutions for current and velocity are obtained from the general solutions in Chapter 4, by applying boundary conditions at the transition. All data for the figures in this chapter are obtained from computations performed by the IBM 709 computer. The data for the input to the transition are obtained from the solutions for Region A, using the beam parameters specified in Chapter 5.[3]

Boundary Conditions

The modulated electron beam drifts under the influence of space-charge forces until it reaches the position $\bar{z} = Z_a$, at which point the second drift tube is positioned. The drift-tube potential changes from V_a to V_b at the junction of the two tubes. From the conservation of energy,

$$(m/2)\ (v_b^2 - v_a^2) = |e|\ (V_b - V_a),$$

or

$$v_b^2 = 2\ \eta\ (V_b - V_a) + v_a^2. \qquad (6.1)$$

Using the relation

$$v_o^2 = 2\ \eta\ V, \qquad (6.2)$$

---

[3] To help insure that the computer program for Region B was correct, computations were performed without making any change in either drift-tube potential or plasma reduction factor. The results of these computations were compared with the solutions for Region A extended through the distance covered by Region B. The results were identical to three significant figures. The solutions obtained for Region A were compared with the solutions obtained by Engler [26].

(6.1) may be expressed as

$$v_b = \sqrt{v_{ob}^2 - v_{oa}^2 + v_a^2}\ , \qquad (6.3)$$

or

$$v_b = v_{ob}\sqrt{1 + (v_a^2 - v_{oa}^2)/v_{ob}^2}\ . \qquad (6.4)$$

Expanding (6.4) in a binomial series gives

$$v_b \cong v_{ob}\ [1 + y/2 - y^2/8 + y^3/16], \qquad (6.5a)$$

where

$$y = (v_a^2 - v_{oa}^2)/v_{ob}^2. \qquad (6.5b)$$

The velocity (v_a) may be written as a power series in α according to the method of successive approximations.

$$v_a = v_{oa} + v_{1a} + v_{2a} + v_{3a}, \qquad (6.6)$$

where the various order terms (v_n) are proportional to α^n. Substitution of (6.6) into (6.5b) yields

$$y = [2\ v_{oa}\ (v_{1a} + v_{2a} + v_{3a}) + v_{1a}^2 + v_{2a}^2 + v_{3a}^2$$
$$+ 2\ (v_{1a}\ v_{2a} + v_{1a}\ v_{3a} + v_{2a}\ v_{3a})]/v_{ob}^2. \qquad (6.7)$$

It is assumed that the a-c terms are all considerably smaller than the d-c terms.[4] Consequently, (6.7) may be approximated by

$$y \cong 2\, v_{oa}\, (v_{1a} + v_{2a} + v_{3a})/v_{ob}^{2}. \qquad (6.8)$$

Equation (6.8) is substituted into (6.5a), and the approximation that $v_{na}/v_{oa} << 1$ is applied. The resulting velocity in Region B is

$$v_b = v_{ob}\, [1 + v_{oa}\, (v_{1a} + v_{2a} + v_{3a})/(v_{ob})^{2}]. \qquad (6.9)$$

The method of successive approximations is applied to v_b. Comparison of terms in (6.9) yields

$$v_{nb}(Z_a) = \sqrt{V_a/V_b}\; v_{na}(Z_a). \quad n = 1, 2, 3 \qquad (6.10)$$

Essentially this is the small-signal assumption used in the analysis of the velocity-jump amplifier by Tien and Field; however, the solution in Region B contains second-order and third-order terms in addition to the small-signal solution.

The second boundary condition is the continuity of current. Hutter [11] shows that the current is continuous across a velocity jump by using kinematic considerations, and alternately as a limiting case of the Llewellyn-Peterson equations.

---

[4] For $\alpha = 0.2$ the largest a-c velocity term is approximately 10 per cent of the d-c velocity.

Consequently,

$$i_{nb}\,(Z_a) = i_{na}\,(Z_a). \qquad n = 1,\ 2,\ 3 \tag{6.11}$$

First-Order Solutions

The first-order current in Region B is found from (4.6).

$$\begin{aligned}\bar{i}_{1b} = {} & BE_b\,[\bar{C}_b \cos(BQ1_b\,\bar{z}) + \bar{D}_b \sin(BQ1_b\,\bar{z})] \cos(\omega t - BE_b\,\bar{z}) \\ & - BE_b\,[\bar{A}_b \cos(BQ1_b\,\bar{z}) + \bar{B}_b \sin(BQ1_b\,\bar{z})] \sin(\omega t - BE_b\,\bar{z})\end{aligned} \tag{6.12}$$

The first-order current in Region A is obtained from (5.18a), and is evaluated at the boundary $\bar{z} = Z_a$.

$$\bar{i}_{1a}(Z_a) = (\alpha/2)\; x_a \sin(Z_a) \cos(\omega t - x_a\, Z_a) \tag{6.13}$$

Two equations for the first-order constants are determined by applying the continuity of current condition to (6.12) and (6.13). The two equations are obtained by comparing coefficients of cos(ωt) and sin(ωt).

$$\begin{aligned}(\alpha/2)\; x_a \sin(Z_a) \cos(x_a\, Z_a) = {} & \\ & BE_b\,[\bar{C}_b \cos(BQ1_b\, Z_a) + \bar{D}_b \sin(BQ1_b\, Z_a)] \cos(BE_b\, Z_a) \\ & + BE_b\,[\bar{A}_b \cos(BQ1_b\, Z_a) + \bar{B}_b \sin(BQ1_b\, Z_a)] \sin(BE_b\, Z_a)\end{aligned} \tag{6.14a}$$

$$
\begin{aligned}
(\alpha/2)\, x_a \sin(Z_a) \sin(x_a Z_a) = {} & \\
& BE_b\, [\bar{C}_b \cos(BQl_b\, Z_a) + \bar{D}_b \sin(BQl_b\, Z_a)] \sin(BE_b\, Z_a) \\
& - BE_b\, [\bar{A}_b \cos(BQl_b\, Z_a) + \bar{B}_b \sin(BQl_b\, Z_a)] \cos(BE_b\, Z_a)
\end{aligned}
\tag{6.14b}
$$

The other two equations needed to evaluate the four constants are derived from the velocity boundary condition. The first-order velocity in Region A is obtained from (5.18b).

$$
\bar{v}_{1a}(Z_a) = (\alpha/2) \cos(Z_a) \sin(\omega t - x_a Z_a) \tag{6.15}
$$

The first-order velocity in Region B is found from (4.7).

$$
\begin{aligned}
\bar{v}_{1b}(\bar{z}) = {} & \sqrt{V_b/V_a}\, BQl_b\, [\bar{B}_b \cos(BQl_b\, \bar{z}) - \bar{A}_b \sin(BQl_b\, \bar{z})] \\
& \cdot \cos(\omega t - BE_b\, \bar{z}) + \sqrt{V_b/V_a}\, BQl_b\, [\bar{D}_b \cos(BQl_b\, \bar{z}) \\
& - \bar{C}_b \sin(BQl_b\, \bar{z})] \sin(\omega t - BE_b\, \bar{z})
\end{aligned}
\tag{6.16}
$$

The first-order velocity (v_{1b}) is normalized with respect to the d-c velocity (v_{oa}) in Region A, rather than with respect to the d-c velocity (v_{ob}) in Region B. This is done in order that the two normalized first-order velocity terms, $\bar{v}_{oa}$ and $\bar{v}_{ob}$, may be compared directly. The boundary condition (6.10) is applied to (6.15) and (6.16). The remaining two equations needed to evaluate the first-order constants are obtained by comparing coefficients of $\cos(\omega t)$ and $\sin(\omega t)$.

$$- (\alpha/2)\ (V_a/V_b)\ \cos(Z_a)\ \sin(x_a\ Z_a) =$$

$$BQ1_b\ [\bar{B}_b \cos(BQ1_b\ Z_a) - \bar{A}_b \sin(BQ1_b\ Z_a)]\ \cos(BE_b\ Z_a)$$

$$- BQ1_b\ [\bar{D}_b \cos(BQ1_b\ Z_a) - \bar{C}_b \sin(BQ1_b\ Z_a)]\ \sin(BE_b\ Z_a) \qquad (6.17a)$$

$$(\alpha/2)\ (V_a/V_b)\ \cos(Z_a)\ \cos(x_a\ Z_a) =$$

$$BQ1_b\ [\bar{B}_b \cos(BQ1_b\ Z_a) - \bar{A}_b \sin(BQ1_b\ Z_a)]\ \sin(BE_b\ Z_a)$$

$$+ BQ1_b\ [\bar{D}_b \cos(BQ1_b\ Z_a) - \bar{C}_b \sin(BQ1_b\ Z_a)]\ \cos(BE_b\ Z_a) \qquad (6.17b)$$

The first-order solutions are established once the constants $\bar{A}_b$, $\bar{B}_b$, $\bar{C}_b$, and $\bar{D}_b$ are evaluated and substituted into (6.10) and (6.16). Cramer's Rule[5] is used to evaluate the constants.

Second-Order Solutions

The second-order current in Region B is obtained from (4.18).

$$\bar{i}_{2b}(\bar{z}) = 2\ BE_b\ [Y_{1b}(\bar{z}) + \bar{M}_b \cos(BQ2_b\ \bar{z}) + \bar{L}_b \sin(BQ2_b\ \bar{z})]$$

$$\cdot \cos 2(\omega t - BE_b\ \bar{z}) - 2\ BE_b [Y_{2b}(\bar{z}) + \bar{J}_b \cos(BQ2_b\ \bar{z})$$

---

[5] See Appendix D for a discussion of the solutions for these constants.

$$+ \bar{i}_b \sin(BQ2_b\, \bar{z})] \sin 2(\omega t - BE_b\, \bar{z}), \tag{6.18}$$

where

$$Y_{1b}(\bar{z}) = s_b\, [\bar{K}_{6b} + g_b\, \bar{K}_{7b} \cos(2\ BQ1_b\, \bar{z}) + g_b\, \bar{K}_{8b} \sin(2BQ1_b\, \bar{z})]/BQ2_b \tag{6.19}$$

$$Y_{2b}(\bar{z}) = s_b\, [\bar{K}_{3b} + g_b\, \bar{K}_{4b} \cos(2\ BQ1_b\, \bar{z}) + g_b\, \bar{K}_{5b} \sin(2\ BQ1_b\, \bar{z})]/BQ2_b. \tag{6.20}$$

The second-order current in Region A is obtained from (5.25), and evaluated at the transition (Z_a).

$$i_{2a}(Z_a) = Y_{1a}(Z_a) \cos 2(\omega t - x_a\, Z_a) + Y_{2a}(Z_a)$$

$$\cdot \sin 2(\omega t - x_a\, Z_a), \tag{6.21}$$

where

$$Y_{1a}(Z_a) = (1/2)\ (\alpha/2)^2\ t_a^{\ 2}\ [1 + 3\ g_a \cos(2\ Z_a)$$

$$- 4\ g_a\ (1 - s_a^{\ 2}) \cos(Z_a/s_a)] \tag{6.22}$$

$$Y_{2a}(Z_a) = (3/2)\ (\alpha/2)^2\ t_a\ g_a\ [s_a \sin(2\ Z_a)$$

$$- (1 - 2\ s_a^{\ 2}) \sin(Z_a/s_a)]. \tag{6.23}$$

Equation (6.18) is equated to (6.21), using the boundary condition for continuity of current given by (6.11), and coefficients of cos(ωt) and sin(ωt) are compared.

$$\begin{aligned} &Y_{1a}(Z_a) \cos(2\ x_a\ Z_a) - Y_{2a}(Z_a) \sin(2\ x_a\ Z_a) = \\ &\quad 2BE_b\ [Y_{1b}(Z_a) + \bar{M}_b \cos(BQ2_b\ Z_a) + \bar{L}_b \sin(BQ2_b\ Z_a)] \\ &\quad \cdot \cos(2\ BE_b\ Z_a) + 2\ BE_b\ [Y_{2b}(Z_a) + \bar{J}_b \cos(BQ2_b\ Z_a) \\ &\quad + \bar{I}_b \sin(BQ2_b\ Z_a)] \sin(2BE_b\ Z_a) \end{aligned} \tag{6.24a}$$

$$\begin{aligned} &Y_{1a}(Z_a) \sin(2\ x_a\ Z_a) + Y_{2a}(Z_a) \cos(2\ x_a\ Z_a) = \\ &\quad 2\ BE_b\ [Y_{1b}(Z_a) + \bar{M}_b \cos(BQ2_b\ Z_a) + \bar{L}_b \sin(BQ2_b\ Z_a)] \\ &\quad \cdot \sin(2\ BE_b\ Z_a) - 2\ BE_b\ [Y_{2b}(Z_a) + \bar{J}_b \cos(BQ2_b\ Z_a) \\ &\quad + \bar{I}_b \sin(BQ2_b\ Z_a)] \cos(2\ BE_b\ Z_a) \end{aligned} \tag{6.24b}$$

The second-order velocity in Region B is obtained from (4.19), and normalized with respect to v_{oa}.

$$\begin{aligned} \bar{v}_{2b}(\bar{z}) = &\sqrt{V_b/V_a}\ [E_b + BE_b\ BQ1_b\ P_{10b}/2 + (BQ1_b)^2\ P_{2b}/4 \\ &- (\bar{K}_{2b}/6) \cos(2\ BQ1_b\ \bar{z}) + (\bar{K}_{1b}/6) \sin(2\ BQ1_b\ \bar{z})] \\ &+ \sqrt{V_b/V_a}\ [BQ2_b\ \{\bar{I}_b \cos(BQ2_b\ \bar{z}) - \bar{J}_b \sin(BQ2_b\ \bar{z})\} \\ &+ Y_{3b}(\bar{z})] \cos 2(\omega t - BE_b\ \bar{z}) + \sqrt{V_b/V_a}\ [BQ2_b\ \{\bar{L}_b \\ &\cdot \cos\ (BQ2_b\ \bar{z}) - \bar{M}_b \sin(BQ2_b\ \bar{z})\} + Y_{4b}(\bar{z})] \\ &\cdot \sin 2(\omega t - BE_b\ \bar{z}), \end{aligned} \tag{6.25}$$

where

$$Y_{3b}(\bar{z}) = -\bar{K}_{6b}/x_b + (g_b/3)\,(1 + 2\,s_b^{2})\,[\bar{K}_{5b}\cos(2\,\mathrm{BQ1}_b\,\bar{z})$$

$$-\bar{K}_{4b}\sin(2\,\mathrm{BQ1}_b\,\bar{z})] \tag{6.26}$$

$$Y_{4b}(\bar{z}) = \bar{K}_{3b}/x_b + (g_b/3)\,(1 + 2\,s_b^{2})\,[\bar{K}_{8b}\cos(2\,\mathrm{BQ1}_b\,\bar{z})$$

$$-\bar{K}_{7b}\sin(2\,\mathrm{BQ1}_b\,\bar{z})]\,. \tag{6.27}$$

The second-order velocity in Region A is found from (5.26), and evaluated at the point of discontinuity (Z_a).

$$\bar{v}_{2a}(Z_a) = -(\alpha/4)^2\,[\cos^2(Z_a) + Y_{3a}(Z_a)\cos 2(\omega t - x_a\,Z_a)$$

$$+\,Y_{4a}(Z_a)\sin 2(\omega t - x_a\,Z_a)], \tag{6.28}$$

where

$$Y_{3a}(Z_a) = 1 + g_a\,(1 + 2\,s_a^{2})\cos(2\,Z_a) - 3\,g_a\,(1 - 2\,s_a^{2})\cos(Z_a/s_a) \tag{6.29a}$$

$$Y_{4a}(Z_a) = x_a\,g_a\,(1 + 2\,s_a^{2})\sin(2\,Z_a) - 4\,g_a\,t_a\,(1 - s_a^{2})\sin(Z_a/s_a). \tag{6.29b}$$

Equations (6.25) and (6.28) are compared at $\bar{z} = Z_a$ by using the boundary condition of (6.10). Three equations for the second order constants are obtained by comparing the coefficients of $\cos(\omega t)$, and $\sin(\omega t)$, and the time independent terms.

$$-(\alpha/4)^2\,(V_a/V_b)\cos^2(Z_a) = E_b + (1/2)\,\mathrm{BE}_b\,\mathrm{BQ1}_b\,P_{10b} + (1/4)$$

$$\cdot (BQ1_b)^2 \; P_{2b} - (1/6) \; \bar{K}_{2b} \cos(2 \; BQ1_b \; Z_a) + (1/6) \; \bar{K}_{1b}$$

$$\cdot \sin(2 \; BQ1_b \; Z_a) \qquad (6.30)$$

$$-(\alpha/4)^2 \; (V_a/V_b) \; [Y_{3a}(Z_a) \cos(2 \; x_a \; Z_a) - Y_{4a}(Z_a) \sin(2 \; x_a \; Z_a)]$$

$$= [BQ2_b \; \{\bar{I}_b \cos(BQ2_b \; Z_a) - \bar{J}_b \sin(BQ2_b \; Z_a)\} + Y_{3b}(Z_a)]$$

$$\cdot \cos(2 \; BE_b \; Z_a) - [BQ2_b \; \{ \bar{L}_b \cos(BQ2_b \; Z_a) - \bar{M}_b \sin(BQ2_b \; Z_a)\}$$

$$+ Y_{4b}(Z_a)] \sin(2 \; BE_b \; Z_a) \qquad (6.31a)$$

$$-(\alpha/4)^2 \; (V_a/V_b) \; [Y_{3a}(Z_a) \sin(2 \; x_a \; Z_a) + Y_{4a}(Z_a) \cos(2 \; x_a \; Z_a)]$$

$$= [BQ2_b \; \{\bar{I}_b \cos(BQ2_b \; Z_a) - \bar{J}_b \sin(BQ2_b \; Z_a)\} + Y_{3b}(Z_a)]$$

$$\cdot \sin(2 \; BE_b \; Z_a) + [BQ2_b \; \{\bar{L}_b \cos(BQ2_b \; Z_a) - \bar{M}_b \sin(BQ2_b \; Z_a)\}$$

$$+ Y_{4b}(Z_a)] \cos(2 \; BE_b \; Z_a) \qquad (6.31b)$$

The second-order constant E_b may be obtained from (6.30).

$$E_b = - (\alpha/4)^2 \; (V_a/V_b) \cos^2 (Z_a) - (1/2) \; BE_b \; BQ1_b \; P_{10b} - (1/4)$$

$$\cdot \; (BQ1_b)^2 \; P_{2b} + (1/6) \; \bar{K}_{2b} \cos(2 \; BQ1_b \; Z_a) - (1/6) \; \bar{K}_{1b}$$

$$\cdot \; \sin(2 \; BQ1_b \; Z_a) \qquad (6.32)$$

Equations (6.24) and (6.31) represent a set of four equations in the four second-order constants. The solutions to this set of equations are also discussed in Appendix D.

Third-Order Solutions

The third-order current in Region B is obtained from (4.27).

$$\begin{aligned}\bar{i}_{3b}(\bar{z}) = {} & BE_b\,[\bar{R}_b \cos(BQ1_b\,\bar{z}) + \bar{S}_b \sin(BQ1_b\,\bar{z}) + Y_{5b}(\bar{z})] \\ & \cdot \cos(\omega t - BE_b\,\bar{z}) - BE_b\,[\bar{P}_b \cos(BQ1_b\,\bar{z}) + \bar{Q}_b \\ & \cdot \sin(BQ1_b\,\bar{z}) + Y_{6b}(\bar{z})]\,\sin(\omega t - BE_b\,\bar{z}),\end{aligned} \tag{6.33}$$

where

$$\begin{aligned}Y_{5b}(\bar{z}) = {} & (\bar{z}/2)\,[\bar{K}_{17b} \sin(BQ1_b\,\bar{z}) - \bar{K}_{21b} \cos(BQ1_b\,\bar{z})] + (s_b/b_{3b}) \\ & \cdot [\bar{K}_{18b} \cos(BQ2_b\,b_{1b}\,\bar{z}) + \bar{K}_{22b} \sin(BQ2_b\,b_{1b}\,\bar{z})]/BQ2_b \\ & - (s_b/b_{4b})\,[\bar{K}_{19b} \cos(BQ2_b\,b_{2b}\,\bar{z}) + \bar{K}_{23b} \sin(BQ2_b\,b_{2b}\,\bar{z})] \\ & /BQ2_b - [\bar{K}_{20b} \cos(3\,BQ1_b\,\bar{z}) + \bar{K}_{24b} \sin(3\,BQ1_b\,\bar{z})]/(8\,BQ1_b)\end{aligned} \tag{6.34}$$

$$\begin{aligned}Y_{6b}(\bar{z}) = {} & (\bar{z}/2)\,[\bar{K}_{9b} \sin(BQ1_b\,\bar{z}) - \bar{K}_{13b} \cos(BQ1_b\,\bar{z})] + (s_b/b_{3b}) \\ & \cdot [\bar{K}_{10b} \cos(BQ2_b\,b_{1b}\,\bar{z}) + \bar{K}_{14b} \sin(BQ2_b\,b_{1b}\,\bar{z})]/BQ2_b \\ & - (s_b/b_{4b})\,[\bar{K}_{11b} \cos(BQ2_b\,b_{2b}\,\bar{z}) + \bar{K}_{15b} \sin(BQ2_b\,b_{2b}\,\bar{z})]/BQ2\end{aligned}$$

$$- [\bar{K}_{12b} \cos(3\ BQ1_b\ \bar{z}) + \bar{K}_{16b} \sin(3\ BQ1_b\ \bar{z})]/(8\ BQ1_b). \tag{6.35}$$

The third-order current in Region A is obtained from (5.39) and evaluated at the transition (Z_a).

$$\bar{I}_{3a}(Z_a) = Y_{5a}(Z_a) \cos(\omega t - x_a\ Z_a) - Y_{6a}(Z_a) \sin(\omega t - x_a\ Z_a), \tag{6.36}$$

where

$$Y_{5a}(Z_a) = x_a\ \alpha^3\ [A_6 \sin(Z_a) + A_7 \sin(b_{1a}\ Z_a/s_a) + A_8 \sin(b_{2a}\ Z_a/s_a)$$
$$+ A_9 \sin(3\ Z_a) + A_{10}\ Z_a \cos(Z_a)] \tag{6.37}$$

$$Y_{6a}(Z_a) = x_a\ \alpha^3\ [A_1 \cos(Z_a) + A_2 \cos(b_{1a}\ Z_a/s_a) + A_3 \cos(b_{2a}\ Z_a/s_a)$$
$$+ A_4 \cos(3\ Z_a) + A_5\ Z_a \sin(Z_a)]. \tag{6.38}$$

Equations (6.33) and (6.36) are compared at $\bar{z} = Z_a$ by using the continuity of current boundary condition. Equating coefficients of $\cos(\omega t)$ and $\sin(\omega t)$ yields two of the equations needed to evaluate the third-order constants.

$$Y_{5a}(Z_a) \cos(x_a\ Z_a) + Y_{6a}(Z_a) \sin(x_a\ Z_a) =$$
$$BE_b\ [\bar{R}_b \cos(BQ1_b\ Z_a) + \bar{S}_b \sin(BQ1_b\ Z_a) + Y_{5b}(Z_a)]$$
$$\cdot \cos(BE_b\ Z_a) + BE_b\ [\bar{P}_b \cos(BQ1_b\ Z_a) + \bar{Q}_b$$
$$\cdot \sin(BQ1_b\ Z_a) + Y_{6b}(Z_a)] \sin(BE_b\ Z_a) \tag{6.39a}$$

$$Y_{5a}(Z_a)\ \sin(x_a\ Z_a) - Y_{6a}(Z_a)\ \cos(x_a\ Z_a) =$$

$$BE_b\ [\bar{R}_b\ \cos(BQ1_b\ Z_a) + \bar{S}_b\ \sin(BQ1_b\ Z_a) + Y_{5b}(Z_a)]$$

$$\cdot\ \sin(BE_b\ Z_a) - BE_b\ [\bar{P}_b\ \cos(BQ1_b\ Z_a) + \bar{Q}_b\ \sin(BQ1_b\ Z_a)$$

$$+ Y_{6b}(Z_a)]\ \cos(BE_b\ Z_a) \tag{6.39b}$$

The third-order velocity in Region A is obtained from (5.40) and evaluated at $\bar{z} = Z_a$.

$$\bar{v}_{3a}(Z_a) = Y_{7a}(Z_a)\ \cos(\omega t - x_a\ Z_a) + Y_{8a}(Z_a)\ \sin(\omega t - x_a\ Z_a), \tag{6.40}$$

where

$$Y_{7a}(Z_a) = \alpha^3\ [A_{11}\ Z_a\ \cos(Z_a) + A_{12}\ \sin(Z_a) + A_{13}\ \sin(b_{1a}\ Z_a/s_a)$$

$$+ A_{14}\ \sin(b_{2a}\ Z_a/s_a) + A_{15}\ \sin(3\ Z_a)] \tag{6.41a}$$

$$Y_{8a}(Z_a) = \alpha^3\ [A_{16}\ Z_a\ \sin(Z_a) + A_{17}\ \cos(Z_a) + A_{18}\ \cos(b_{1a}\ Z_a/s_a)$$

$$+ A_{19}\ \cos(b_{2a}\ Z_a/s_a) + A_{20}\ \cos(3\ Z_a)]. \tag{6.41b}$$

The third-order velocity in Region B is obtained from (4.28). The third-order velocity is normalized with respect to v_{oa} rather than v_{ob}. This is accomplished by multiplying (4.28) by $\sqrt{V_b/V_a}$.

$$\bar{v}_{3b}(\bar{z}) = \sqrt{V_b/V_a}\ [BQ1_b\ \bar{Q}_b\ \cos(BQ1_b\ \bar{z}) - BQ1_b\ \bar{P}_b\ \sin(BQ1_b\ \bar{z})$$

$$+ Y_{7b}(\bar{z}) \,]\, \cos(\omega t - BE_b\, \bar{z}) + \sqrt{V_b/V_a}\, [BQ1_b\, \bar{S}_b \cos(BQ1_b\, \bar{z})$$

$$- BQ1_b\, \bar{R}_b \sin(BQ1_b\, \bar{z}) + Y_{8b}(\bar{z})] \sin(\omega t - BE_b\, \bar{z}), \tag{6.42}$$

where

$$\begin{aligned} Y_{7b}(\bar{z}) = {} & BQ1_b\, (\bar{z}/2)\, [\bar{K}_{9b} \cos(BQ1_b\, \bar{z}) + \bar{K}_{13b} \sin(BQ1_b\, \bar{z})] \\ & + (b_{2b}\, s_b/b_{4b})\, [\bar{K}_{11b} \sin(BQ2_b\, b_{2b}\, \bar{z}) - \bar{K}_{15b} \cos(BQ2_b\, b_{2b}\, \bar{z})] \\ & + (b_{1b}\, s_b/b_{3b})\, [\bar{K}_{14b} \cos(BQ2_b\, b_{1b}\, \bar{z}) - \bar{K}_{10b} \sin(BQ2_b\, b_{1b}\, \bar{z})] \\ & + (3/8)\, [\bar{K}_{12b} \sin(3\, BQ1_b\, \bar{z}) - \bar{K}_{16b} \cos(3\, BQ1_b\, \bar{z})] + F_{ab}(\bar{z}) \\ & + F_{cb}(\bar{z}) + (\bar{K}_{9b}/2) \sin(BQ1_b\, \bar{z}) - (\bar{K}_{13b}/2) \cos(BQ1_b\, \bar{z}) \end{aligned} \tag{6.43a}$$

$$\begin{aligned} Y_{8b}(\bar{z}) = {} & BQ1_b\, (\bar{z}/2)\, [\bar{K}_{21b} \sin(BQ1_b\, \bar{z}) + \bar{K}_{17b} \cos(BQ1_b\, \bar{z})] \\ & + (b_{1b}\, s_b/b_{3b})\, [\bar{K}_{22b} \cos(BQ2_b\, b_{1b}\, \bar{z}) - \bar{K}_{18b} \sin(BQ2_b\, b_{1b}\, \bar{z})] \\ & + (b_{2b}\, s_b/b_{4b})\, [\bar{K}_{19b} \sin(BQ2_b\, b_{2b}\, \bar{z}) - \bar{K}_{23b} \cos(BQ2_b\, b_{2b}\, \bar{z})] \\ & + (3/8)\, [\bar{K}_{20b} \sin(3\, BQ1_b\, \bar{z}) - \bar{K}_{24b} \cos(3\, BQ1_b\, \bar{z})] + F_{bb}(\bar{z}) \\ & + F_{db}(\bar{z}) + (\bar{K}_{17b}/2) \sin(BQ1_b\, \bar{z}) - (\bar{K}_{21b}/2) \cos(BQ1_b\, \bar{z}). \end{aligned} \tag{6.43b}$$

The remaining pair of equations required to evaluate the third-order constants are obtained by comparing (6.40) and (6.42) at $\bar{z} = Z_a$, using the boundary condition given by (6.10).

$$
\begin{aligned}
&(V_a/V_b)\ [Y_{7a}\ (Z_a)\cos(x_a\ Z_a) - Y_{8a}\ (Z_a)\sin(x_a\ Z_a)] = \\
&\quad BQ1_b\ [\bar{Q}_b \cos(BQ1_b\ Z_a) - \bar{P}_b \sin(BQ1_b\ Z_a)] \cos(BE_b\ Z_a) \\
&\quad - BQ1_b\ [\bar{S}_b \cos(BQ1_b\ Z_a) - \bar{R}_b \sin(BQ1_b\ Z_a)] \sin(BE_b\ Z_a) \\
&\quad + Y_{7b}\ (Z_a)\cos(BE_b\ Z_a) - Y_{8b}\ (Z_a)\sin(BE_b\ Z_a) \qquad (6.44a)
\end{aligned}
$$

$$
\begin{aligned}
&(V_a/V_b)\ [Y_{7a}\ (Z_a)\sin(x_a\ Z_a) + Y_{8a}\ (Z_a)\cos(x_a\ Z_a)] = \\
&\quad BQ1_b\ [\bar{Q}_b \cos(BQ1_b\ Z_a) - \bar{P}_b \sin(BQ1_b\ Z_a)] \sin(BE_b\ Z_a) \\
&\quad + BQ1_b\ [\bar{S}_b \cos(BQ1_b\ Z_a) - \bar{R}_b \sin(BQ1_b\ Z_a)] \cos(BE_b\ Z_a) \\
&\quad + Y_{7b}\ (Z_a)\sin(BE_b\ Z_a) + Y_{8b}\ (Z_a)\cos(BE_b\ Z_a) \qquad (6.44b)
\end{aligned}
$$

Equations (6.39) and (6.44) comprise a set of four equations in the four third-order constants. The solutions for this set of equations are discussed in Appendix D. The third-order solutions, given by (6.33) and (6.42), are complete once these four constants have been evaluated.

Transition Near a Velocity Maximum

According to the small-signal results of (2.16), the best amplification for a transition near a velocity maximum is achieved if the drift-tube voltage (V_b) is reduced, and the plasma reduction factor (R_{1b}) is also reduced by decreasing the drift-tube radius (a) in Region B. These parameters are changed in relation to the values they possessed in Region A. The conclusions drawn from the small-signal analysis are that best amplification is obtained if the voltage and radius are changed at the exact location of maximum velocity variation, and that the amplification obtained is independent of α, i.e., the amplifier does not saturate.

The effect of varying the drift-tube radius is demonstrated in Fig. 6.1 for a fixed voltage transition, $V_b = V_a/2$. It is seen from Fig. 6.1, that a 10 per cent increase in amplification is achieved if the b/a ratio is changed from 0.667 to 0.91 in Region B; whereas, the gain drops about 5 per cent if the ratio is changed to 0.5 in Region B. Comparison with the solution for Region A, which corresponds to the conventional two-cavity klystron, shows that a 25 per cent increase in amplification is achieved by changing the b/a value to 0.91 and reducing the potential by a factor of two in Region B. The major contribution to the increased amplification, however, comes from the change in drift-tube voltage, rather than the change in drift-tube radius.

The effect of varying the drift-tube voltage is demonstrated in Fig. 6.2 for a b/a transition from 0.667 to 0.91. The amplification increases as the drift-tube potential in Region B decreases. The curve for $V_b = V_a/10$ also demonstrates another important consideration, namely the location of the output cavity. If the position of the second cavity is shifted by five degrees in relation to its optimum value, the amplification is reduced to such an extent that a much smaller voltage transition would yield better amplification. The actual shape of the curve for a ten to one change in potential is somewhat in doubt, as overtaking occurs over

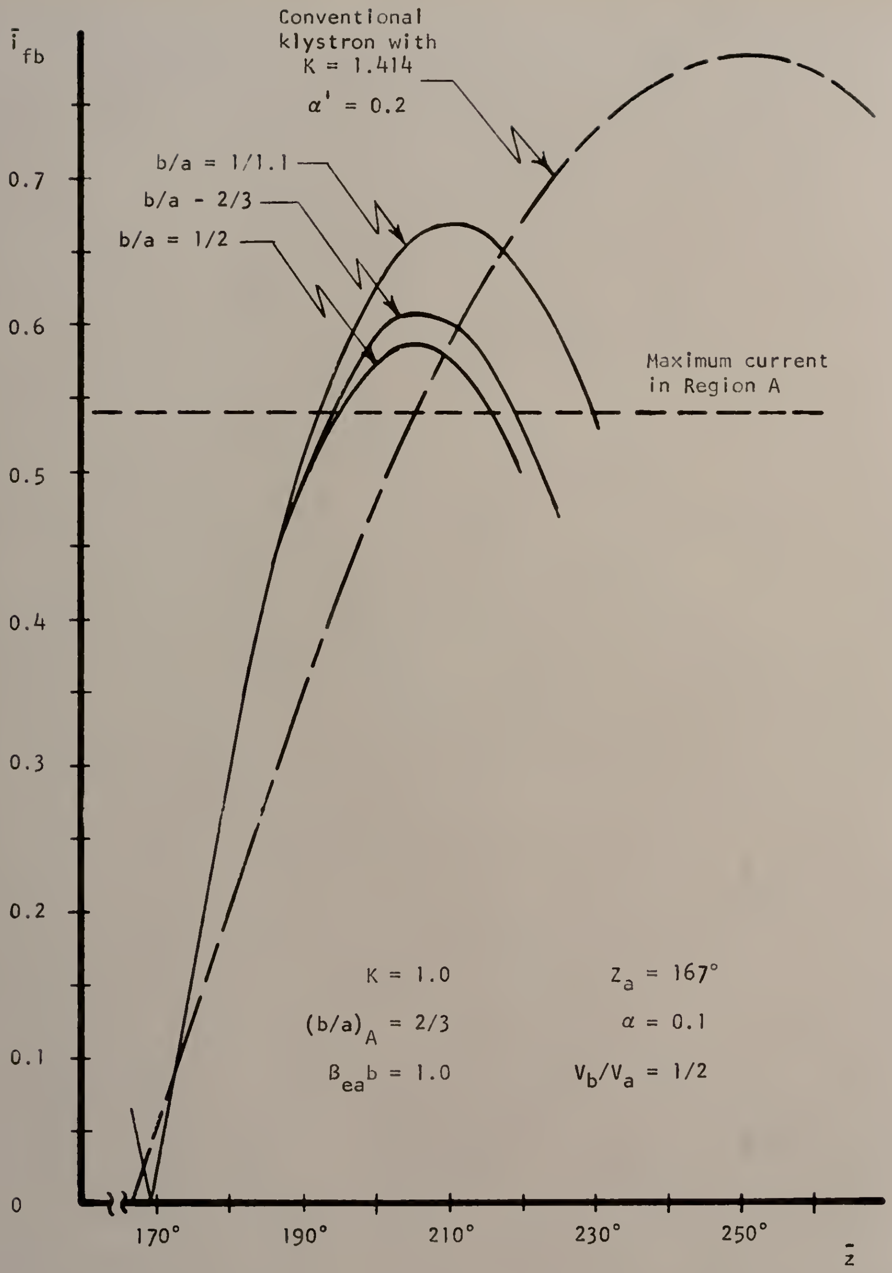

Fig. 6.1 - Current in Region B as a function of the drift-tube radius.

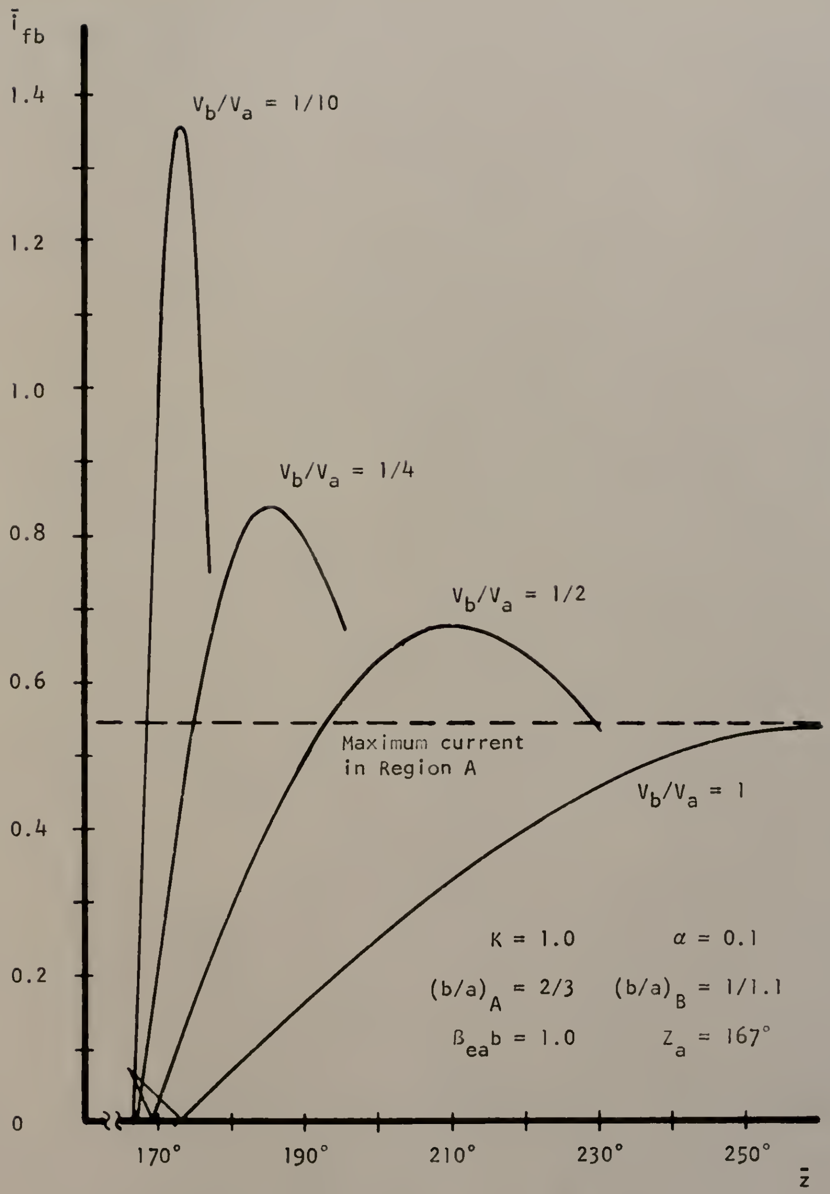

Fig. 6.2 - Current in Region B as a function of the drift-tube voltage.

a considerable portion of the cycle. It is also evident from examination of Fig. 6.2 that the optimum length of the second drift tube is a definite function of the voltage ratio; whereas, the curves in Fig. 6.1 show that the change in optimum length with plasma reduction factor is negligible,

Small-signal theory predicts that the location of the velocity-jump must be at the point of maximum velocity variation. In order to investigate how the predicted amplification is affected by the nonlinear theory, the location of the transition is varied. The maximum current obtained at some point in Region B for a particular transition location is plotted in Fig. 6.3 against the location of the transition. The optimum location for $\alpha = 0.1$ is actually about twenty-two degrees closer to the input cavity than the point where maximum velocity variation occurs. The optimum amplification is about 5 per cent above that obtained by locating the transition at the point of maximum velocity variation. It should be noted that the position of the cavity is not too critical, in that a five degree shift in location from the optimum position results in less than a 1 per cent loss in amplification for this example. Thus the contributions to the over-all amplification due to changes in the drift-tube radius or location of the transition are negligible, at least for small values of α.

The reason for this increased current is the fact that while the velocity fluctuations are decreasing as the transition is moved toward the input, the current fluctuations are increasing. Since the current is continuous at the transition, the current excitation in Region B builds from the current amplitude at the transition. Thus a compromise

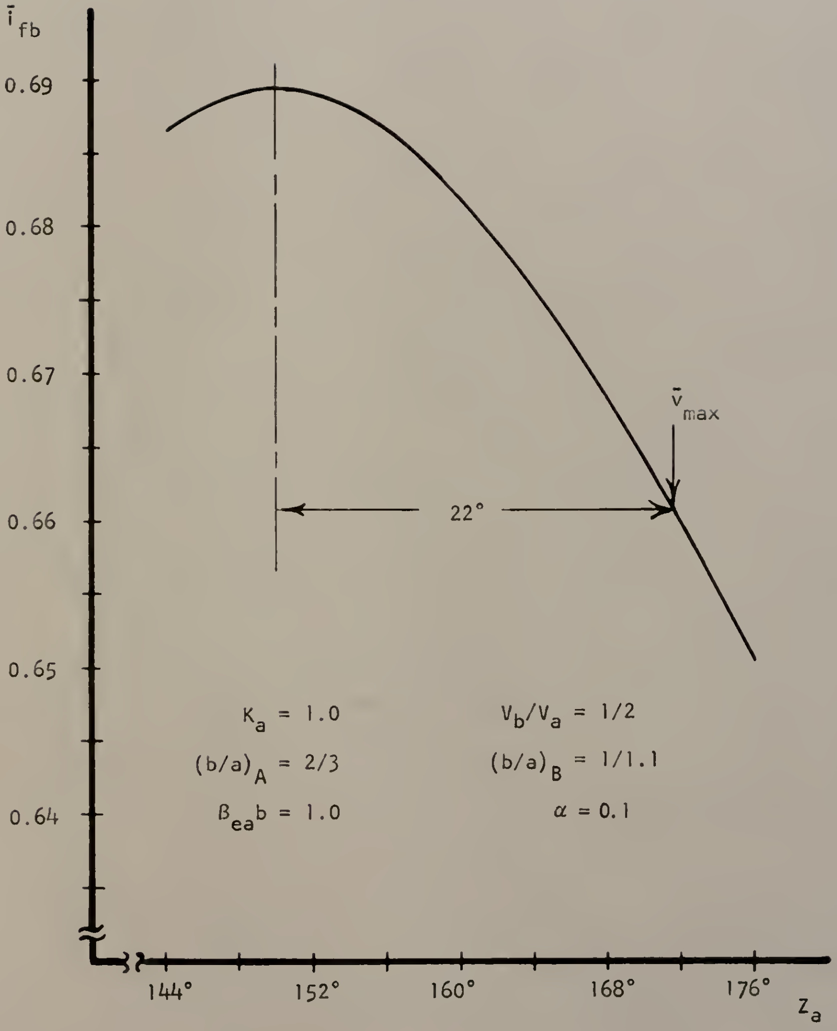

Fig. 6.3 - Maximum current in Region B as a function of the location of the first transition.

is made between maximum velocity excitation and virtually no initial current, and the case where little velocity excitation is achieved, but a large current is present at the transition. In the small-signal theory the location of maximum velocity and minimum current coincide, but this does not hold for the nonlinear analysis, as was previously shown in Fig. 5.4.

The fact that the velocity at the transition is less than the velocity at the entrance in Region A indicates that this amplifier design might not be correct. The curve labeled $\alpha' = 0.2$ in Fig. 6.1 supports this conclusion. This curve corresponds to the current obtainable from a conventional two-cavity klystron with the same signal voltage as the space-charge-wave amplifier, but employing the beam characteristics of Region B, namely the lower d-c potential which yields a beam of higher perveance. To exceed the current output of this klystron, it is necessary to use an amplifier which has the same initial beam characteristics, then employ an increase in drift-tube potential at the first transition, and finally return to the original potential at the second transition. The first transition is made near a velocity minimum, and the second near a velocity maximum. This type of velocity-jump amplifier was discussed on a linear basis in Chapter 2, and the small-signal results are shown in Fig. 2.3. In the next section this amplification process is investigated on a nonlinear basis, where it is shown that amplification is possible, at least for small values of α.

Transition Near a Velocity Minimum

The small-signal solutions for a transition at a velocity minimum are given in (2.9). It would appear that the variation in reduction factor is just as important a consideration as changing the potential because of the four to one ratio in the powers to which these parameters are varied. Since the current amplification is relatively insensitive to a voltage transition at a velocity minimum, a second transition is needed in the vicinity of a velocity maximum. As shown in the previous section, the best amplification is achieved at the velocity maximum if the drift-tube potential is reduced, and the reduction factor is decreased by reducing the drift-tube radius. Hence, the voltage and radius of the drift tube must be increased at the first transition, then returned to their original values at the second transition.

The effect of varying the drift-tube voltage is shown in Fig. 6.4. It is apparent that the velocity variations are relatively insensitive to the change in potential; however, the velocity definitely decreases as the drift-tube voltage in Region B increases. It is also apparent that the optimum location of the second transition is a definite function of the voltage ratio. The fact that the variations are relatively insensitive to changes in potential follows from (2.9b). The ratio of maximum velocity in Region B to maximum velocity in Region A is only proportional to the one-fourth power of the voltage ratio. However, it also appears at first glance that the velocity should increase with increasing values of V_b, rather than decrease. The explanation is found by examining

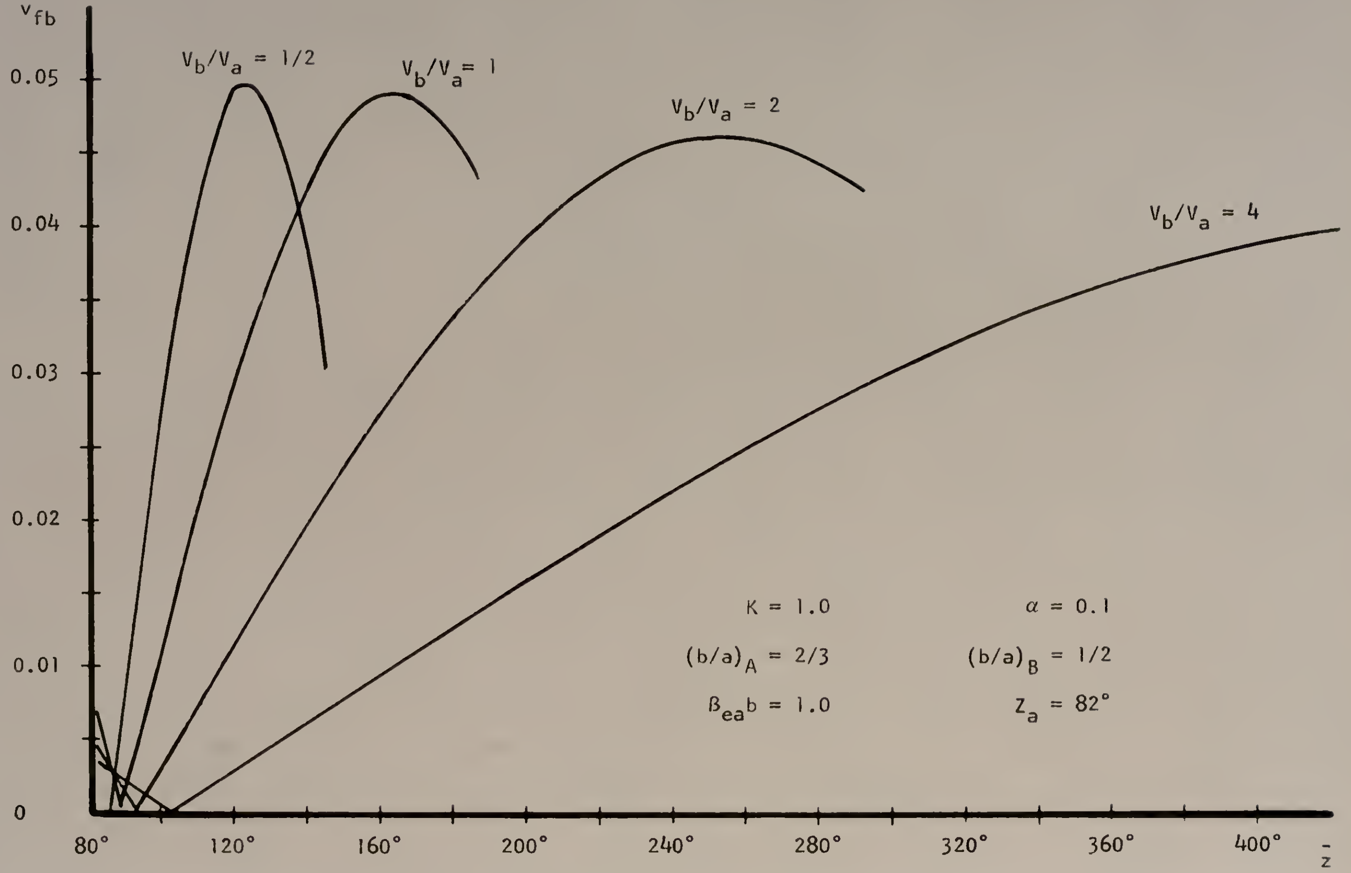

Fig. 6.4 - Velocity in Region B as a function of the drift-tube voltage.

the plasma reduction-factor curves shown in Fig. 2.1. As the voltage increases the normalized beam radius ($\beta_e b$) decreases, thus decreasing the value of the reduction factor. Since the ratio of reduction factors is raised to the first power, a small gain due to the increase in V_b is more than compensated by the decrease in R_{1b}.

The effect of varying the drift-tube radius in Region B is demonstrated in Fig. 6.5. The drift-tube radius in Region B should be increased because the best amplification is achieved for smaller values of b/a. It is apparent from Fig. 6.5 that the decrease in reduction factor resulting from the increase in drift-tube potential can be compensated at least partially by increasing the drift-tube radius. Amplification is achieved in the third section if the drift-tube potential is decreased at the second transition. The amplification can be further enhanced also by restoring the drift-tube radius to the value of Region A.

The principle purpose of the first transition is to change the drift-tube potential from a value V_a to a higher value V_b, without decreasing the velocity amplification, or perhaps to even increase it somewhat by increasing the drift-tube radius. The drift-tube potential is returned to the original value (V_a) at the second transition. The amplification resulting from the decrease in drift-tube potential was the subject of a preceding section.

The locations of the two transitions are quite important. Small-signal theory predicts that each drift tube should be a quarter plasma wavelength long. The velocity at the second transition is shown in

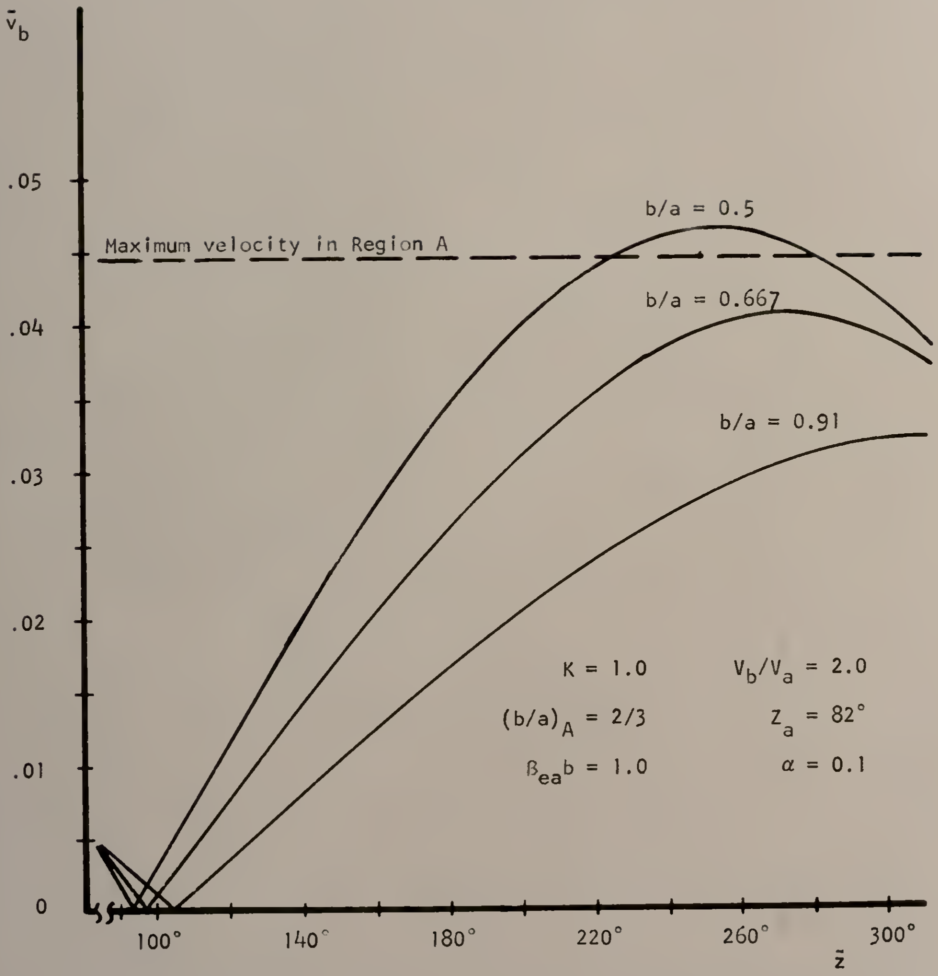

Fig. 6.5 - Velocity in Region B as a function of the drift-tube radius.

Fig. 6.6 for the case where the velocity is maximum, i.e., the transition locations are optimized, and for the case where each drift-tube section is a quarter plasma wavelength long. The maximum velocity obtained in Region A is also plotted for comparison. It is obvious that the velocity modulation can be improved by optimizing the transition locations. The optimum locations of the first and second transitions as a function of α are shown in Fig. 6.7 and 6.8 respectively.

If the second transition is located at the point of maximum a-c velocity in Region B, then the maximum velocity in the third region is obtained by multiplying the velocity at the transition by $\sqrt{V_b/V_a}$. The ratio of the maximum velocity in Region C to the maximum velocity in Region A is plotted in Fig 6.9 for the solutions predicted by the small-signal theory and by the nonlinear theory for the two aforementioned cases. The nonlinear theory definitely shows the effect of saturation. Although it is possible to improve the gain by optimizing the drift-tube lengths, it is apparent that for practical values of α the amplifier is useless. Perhaps for larger voltage jumps, the amplifier will not saturate at such a low value of α. Such a conclusion can only be verified by further computer work, and of course in the final analysis, by experimental investigation.

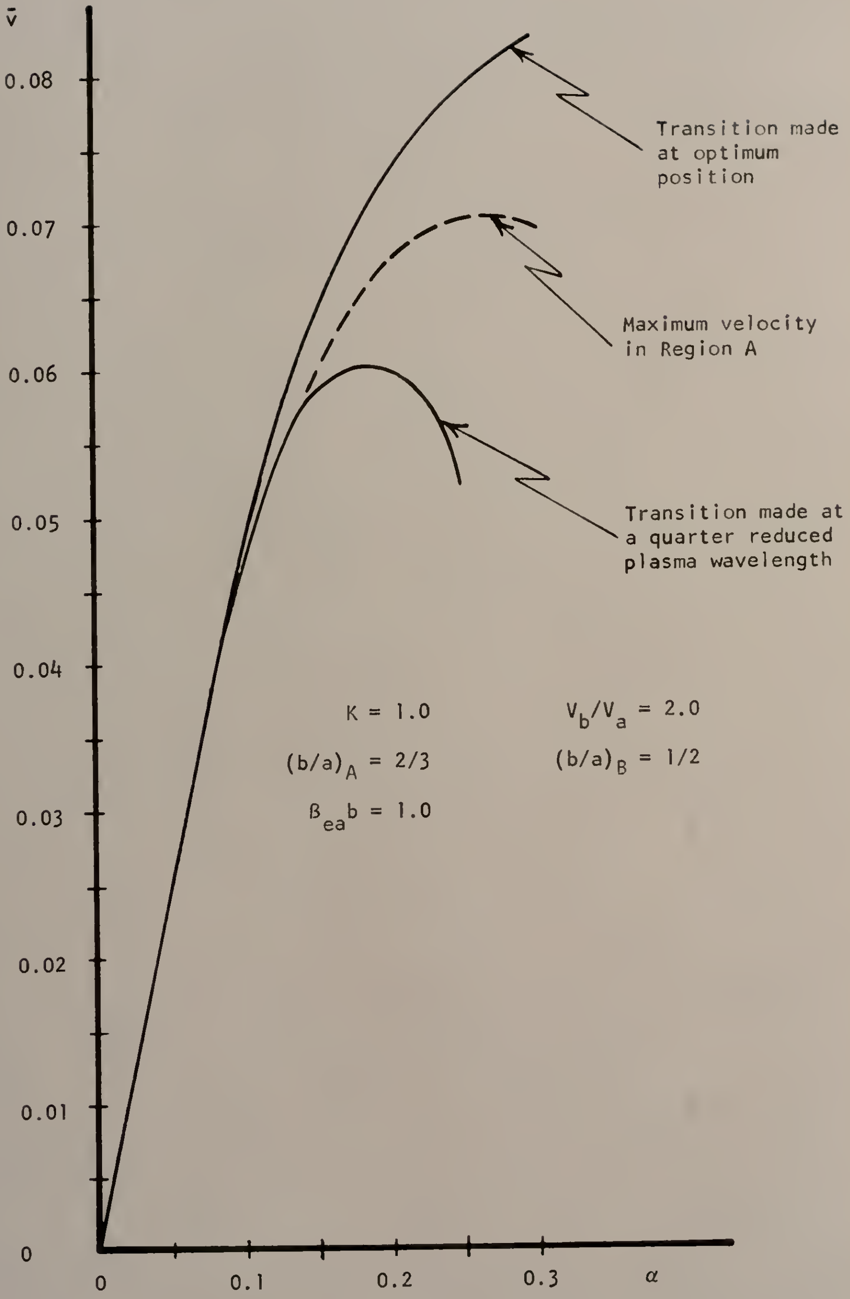

Fig. 6.6 - Maximum velocity in Region B as a function of α.

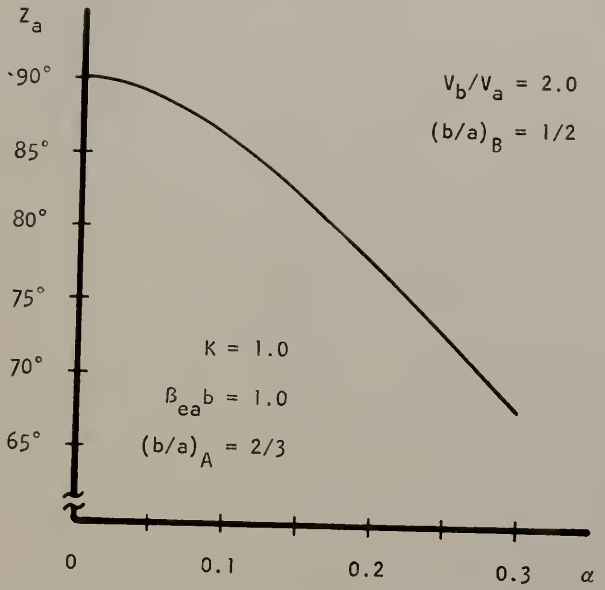

Fig. 6.7 - Location of the first transition for maximum velocity in Region B.

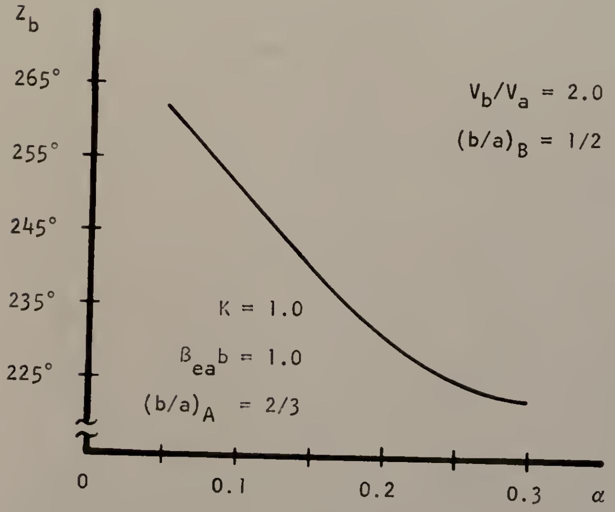

Fig. 6.8 - Location of the maximum velocity in Region B.

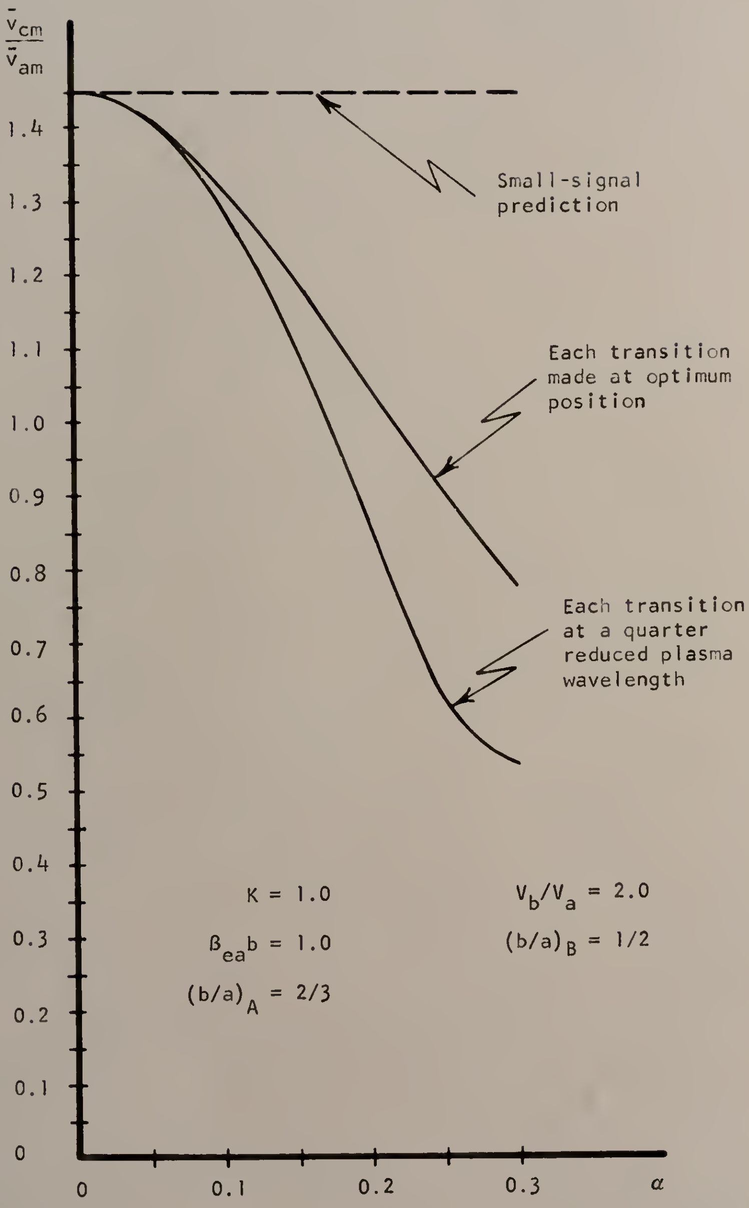

Fig. 6.9 - Effect of drift-tube lengths upon the velocity amplification.

CHAPTER 7

SUMMARY AND CONCLUSIONS

Tien and Field; Birdsall and Whinnery; Peter, Bloom and Ruetz; and others had utilized small-signal analyses to investigate the performance of a space-charge-wave amplifier which employed changes in the potential and radius of the drift tube at the point of minimum and maximum velocity variations to enhance the amplification. The amplifier was found to have excellent amplification properties which depended only upon the ratio of the potential change between sections, and to a lesser extent, upon the change in drift-tube radius. Experimental investigation, however, had shown that the amplifier definitely saturated at quite low signal levels, and therefore exhibited low efficiency.

The purpose of this dissertation was to study the saturation phenomena, and try to determine if the performance could be improved by adjusting the lengths of the drift-tube sections. A nonlinear theory proposed by Paschke for the study of the nonlinear effects in a basic two-cavity klystron was utilized. The nonlinear space-charge-wave equation was developed in Chapter 3, and the general solutions were obtained in Chapter 4 by employing the method of successive approximations as proposed by Paschke. In the following two chapters particular solutions for the first and second drift-tube sections were obtained by applying boundary conditions of conservation of energy and continuity of current to the transition locations.

The solutions for the first region applied to the conventional two-cavity klystron. Solutions for current and velocity were plotted in Fig. 5.1 and Fig. 5.2 for three values of the voltage modulation index (α). These solutions obtained from the nonlinear theory demonstrated the saturation phenomena, and also showed that the locations of minimum and maximum current and velocity deviated significantly from the multiples of quarter plasma wavelengths predicted by the small-signal theory. It was shown in Fig. 5.4 that the locations of the minimum and maximum current for $\alpha = 0.3$ are only approximately two-thirds of the distances predicted by small-signal theory. Consequently, if the first transition were placed a quarter plasma wavelength from the buncher it would not be at the position of minimum velocity, nor would a transition placed one-half of a plasma wavelength be at the point of maximum velocity variation.

The solutions for the second region gave information concerning the current and velocity after the space-charge-wave had undergone a velocity-jump. Several different combinations of voltage ratios, drift-tube radii, and transition locations were explored. These studies fell into two general catagories; a) transition near a velocity maximum, and b) transition near a velocity minimum.

For a transition near a velocity maximum it was determined that the best amplification was obtained if the voltage and radius of the second drift tube were decreased. The major effect was due to the voltage transition rather than the change in the drift-tube radius, as can be seen by comparison of Fig. 6.1 and Fig. 6.2. It was demonstrated in Fig. 6.3 that the best position for locating the transition was not at the point of maximum velocity variation, but some twenty-two degrees closer to the input. For larger values of α the shift would most likely be even greater since the beam acts in a more nonlinear fashion.

It was also demonstrated in Fig. 6.1 that if the amplifier utilized only two drift-tube sections, the current output was not as good as a conventional two-cavity klystron which had the same signal voltage applied to the input, but utilized the lower drift-tube voltage, and consequently the higher beam perveance, of the second section. Consequently, it was necessary to utilize an increase in potential at the first transition in order to insure that the same maximum beam perveance was available for the first section of both amplifiers. It was demonstrated in Fig. 6.4 and Fig. 6.5 that a single transition near a velocity minimum with an increase in potential did not produce a useful amplifier either. However, combining this transition with a second transition near a velocity maximum, where the drift-tube potential was decreased to the original value, produced an amplifier from which gain could be obtained.

A comparison was made in Fig. 6.6 of the velocity amplitude for a conventional klystron, and for the space-charge-wave amplifier first using quarter plasma wavelength sections, and then for the case where the drift-tube lengths had been optimized. It was evident that the amplifier had improved performance for larger input signals only if the drift-tube lengths were optimized. The required transition locations were shown in Fig. 6.7 for the first transition, and in Fig. 6.8 for the second transition. It was apparent that these locations were definite functions of α, and that the locations shifted toward the input as α increased. Comparison of Fig.

6.7 and Fig. 5.4 indicates that the first transition location definitely does not coincide with the point of minimum velocity variation as predicted by the small-signal theory, and in fact, closely follows the location of the maximum current.

The ratio of maximum velocity in the third region to the velocity initially introduced by the input signal was plotted in Fig. 6.9 for the small-signal theory and the nonlinear prediction for drift tubes with quarter plasma wavelength sections and optimized sections. It is apparent that the nonlinear theory indicates the saturation effect which was not predicted by small-signal theory, and that performance can be improved by optimizing the lengths of the drift tubes. However, it is also apparent that the improvement is not adequate, since the ratio still falls below unity for reasonably small input signals.

It should be pointed out again, however, that the theory utilized in this analysis is valid only to the point of electron crossover. For the parameters utilized in this investigation such crossover takes place for $\alpha = 0.15$, i.e., well below the point where saturation effects are a serious problem. Consequently, the saturation phenomena could not be completely analyzed by this theory. It is also possible that gain could have been achieved for larger values of α by utilizing a larger voltage jump. The two to one change in potential used for several of the curves is well below the changes utilized by Tien and Field in their original work. Only further computer investigations for various possible parameter combinations and detailed experimental work can yield a more complete picture of the saturation phenomena.

APPENDIX A

LIST OF PRINCIPLE SYMBOLS

a	Drift-tube radius, and subscript used to indicate a variable in Region A
b	Beam radius, and subscript used to indicate a variable in Region B
e	Electron charge ($- 1.6 \times 10^{-19}$coulomb)
f	Electric flux coupling beam and drift tube
i_f	Fundamental component of current density
i_o	Electron current density in unmodulated beam
i_t	Electron current density in modulated beam
i	A-c electron current density ($i_t - i_o$)
$\bar{i}$	Normalized electron current density (i/i_o)
j	$\sqrt{-1}$
m	Electron rest mass (9.1×10^{-31}kilogram)
n	Integer used to represent the harmonic number
s	$\beta_{q1}/\beta_{q2} = R_1/R_2$
t	Time
v_o	Electron velocity in unmodulated beam $\sqrt{2\eta V_o}$
v_t	Electron velocity in modulated beam
v	A-c component of electron velocity in modulated beam ($v_t - v_o$)
$\bar{v}$	Normalized component of a-c velocity (v/v_o)
z	Axial distance measured from input cavity
$\bar{z}$	Normalized axial distance ($\beta_{q1a}z$)

z_n	Component of electron polarization obtained from n^{th} order solution
z_p	Polarization, or displacement, of an electron from its position in the unmodulated beam
A	Beam cross sectional area
E	Electric field resulting from space charge
J_1	Bessel function of 1st order and 1st kind
K	Beam micro-perveance $(I_o\ 10^6/V_o^{3/2})$
M	Displacement current/unit length coupling drift tube and electron beam
R_n	Plasma reduction factor at frequency $n\omega$
V_m	Amplitude of a-c potential applied to input cavity
V_n	Drift-tube potential in Region N
X_o	Ballistic bunching parameter
X	Bunching parameter including space-charge effects
α	Voltage modulation index (V_m/V_{oa})
β_e	Electronic wave number (ω/v_o)
$\beta_e b$	Normalized beam radius
β_p	Plasma wave number (ω_p/v_o)
β_{qn}	Reduced plasma wave number $(R_n\beta_p)$
ϵ_o	Permittivity of free space $(8.854 \times 10^{-12}$ farads/meter)
ρ_o	Electron charge density in unmodulated beam
ρ_t	Electron charge density in modulated beam
ρ	A-c component of charge density in modulated beam
η	Ratio of $|e|/m$ $(1.76 \times 10^{11}$ coulomb/kilogram)
ω	Angular frequency of signal voltage to input cavity
ω_p	Angular frequency of plasma oscillation for a beam of infinite size $(\eta|\rho_o|/\epsilon_o)^{1/2}$

ω_q	Reduced plasma frequency of oscillation ($R_1 \omega_p$)
μ	Gap coupling coefficient
θ_f	Phase shift of fundamental component of current density

APPENDIX B

LIST OF PARAMETERS USED IN EQUATIONS

The following group of parameters is needed in order to express the parameters introduced in (4.11) in a compact fashion for computer analysis.

$x = \beta_e/\beta_{q1}$
$s = \beta_{q1}/\beta_{q2}$
$t = \beta_e/\beta_{q2}$
$g = (1 - 4s^2)^{-1}$
$b_1 = 1 - s$
$b_2 = 1 + s$
$b_3 = 2s - 1$
$b_4 = 2s + 1$
$BQ1 = \beta_{q1}/\beta_{q1a}$
$BQ2 = \beta_{q2}/\beta_{q1a}$
$BE = \beta_e/\beta_{q1a}$
$P_1 = \bar{A}\ \bar{B} + \bar{C}\ \bar{D}$
$P_2 = \bar{A}^2 + \bar{B}^2 + \bar{C}^2 + \bar{D}^2$
$P_3 = \bar{A}\ \bar{C} + \bar{B}\ \bar{D}$
$P_4 = \bar{A}^2 - \bar{B}^2 + \bar{C}^2 - \bar{D}^2$
$P_5 = \bar{A}\ \bar{D} + \bar{B}\ \bar{C}$
$P_6 = \bar{A}^2 + \bar{B}^2 - \bar{C}^2 - \bar{D}^2$

$P_7 = \bar{A}\,\bar{B} - \bar{C}\,\bar{D}$

$P_8 = \bar{A}^2 - \bar{B}^2 - \bar{C}^2 + \bar{D}^2$

$P_9 = \bar{A}\,\bar{C} - \bar{B}\,\bar{D}$

$P_{10} = \bar{A}\,\bar{D} - \bar{B}\,\bar{C}$

The following parameters are introduced in (4.11). The bar $(\bar{\ })$ indicates the parameter is normalized by dividing by β_{q1} .

$\bar{K}_1 = 1.5\ (BQ1)^2\ P_1$

$\bar{K}_2 = -\ 0.75\ (BQ1)^2\ P_4$

$\bar{K}_3 = x\ (BQ1)^2\ P_3/2$

$\bar{K}_4 = 1.5\ (BQ1)^2\ (P_7 - x\ P_9)$

$\bar{K}_5 = -\ 0.75\ (BQ1)^2\ (P_8 + 2\ x\ P_5)$

$\bar{K}_6 = -\ 0.25\ (BQ1)^2\ x\ P_6$

$\bar{K}_7 = 0.75\ (BQ1)^2\ (x\ P_8 + 2\ P_5)$

$\bar{K}_8 = 1.5\ (BQ1)^2\ (x\ P_7 - P_9)$

The following parameters are needed for describing the parameters introduced in (4.20).

$X_1 = 2x^2 + 3$

$X_2 = x^2 + 1$

$X_3 = 2x^2 - 1$

$X_4 = 2x^2 - 7$

$X_5 = x^2 - 1$

$X_6 = x^2 - 1.5$

$X_7 = x^2 - 3$

$T_1 = 4t^2 + 1$

$T_2 = 4t^2 - 1$

$H_a = BQ1\ (X_2\ \bar{A} + 2\ x\ \bar{D})$

$H_b = BQ1\ (X_2\ \bar{B} - 2\ x\ \bar{C})$

$H_c = BQ1\ (X_2\ \bar{C} - 2\ x\ \bar{B})$

$H_d = BQ1\ (X_2\ \bar{D} + 2\ x\ \bar{A})$

$H_e = 4t^2 + x^2 - 6s^2 - 3$

$H_f = 4t^2 + x^2/2 - 3$

$H_g = 6s^2 g\ X_1 + x^2\ X_2$

$H_h = s^2\ g\ X_1 + x^2/3$

$H_i = -\ s^2\ g\ X_4 + x^2/3$

$H_j = g\ (8t^2 - 3)/2 + 1/2 - x^2/6$

$K_a = BQ1\ (x\ \bar{A} + \bar{D})$

$K_b = BQ1\ (x\ \bar{B} - \bar{C})$

$K_c = BQ1\ (x\ \bar{C} - \bar{B})$

$K_d = BQ1\ (x\ \bar{D} + \bar{A})$

$K_e = BQ2\ (2\ t\ \bar{I} - \bar{M})$

$K_f = BQ2\ (2\ t\ \bar{M} - \bar{I})$

$K_g = BQ2\ (2\ t\ \bar{L} + \bar{J})$

$K_h = BQ2\ (2\ t\ \bar{J} + \bar{L})$

$K_i = BQ2\ (4\ x\ \bar{I} - T_1\ \bar{M}/s)$

$K_j = BQ2\ (4\ x\ \bar{J} + \bar{L}\ T_1/s)$

$K_k = BQ2\ (-4\ x\ \bar{M} + \bar{I}\ T_1/s)$

$K_m = BQ2\ (4\ x\ \bar{L} + \bar{J}\ T_1/s)$

$C_1 = BQ1\ (X_6\ \bar{K}_2 + H_g\ \bar{K}_5/6 + s\ t\ g\ X_4\ \bar{K}_7 + x\ (BE)^2\ X_5\ P_5/4)/2$

$C_2 = BQ1\ (X_6\ \bar{K}_1 + H_h\ \bar{K}_4 - s\ t\ g\ X_4\ \bar{K}_8 + (BE)^2\ X_5\ P_7/4)/2$

$$C_3 = BQ1\ (2\ x\ X_7\ \bar{K}_1/3 + x\ H_i\ \bar{K}_4 + s^2\ g\ X_1\ \bar{K}_8 + (BE)^2\ X_5\ P_9/4)/2$$

$$C_4 = -BQ1\ (2\ x\ X_7\ \bar{K}_2/3 + x\ H_i\ \bar{K}_5 - s^2\ g\ X_1\ \bar{K}_7 + (BE)^2\ X_5\ P_5/4)/2$$

$$C_5 = -\ (x\ \bar{K}_2 + 2\ s\ t\ g\ \bar{K}_5 + H_j\ \bar{K}_7)/2$$

$$C_6 = -\ (x\ \bar{K}_1 + 2\ s\ t\ g\ \bar{K}_4 - H_j\ \bar{K}_8)/2$$

$$C_7 = -\ (X_7\ \bar{K}_1/3 - H_j\ \bar{K}_4 + 2\ s\ t\ g\ \bar{K}_8)/2$$

$$C_8 = (X_7\ \bar{K}_2/3 - H_j\ \bar{K}_5 - 2\ s\ t\ g\ \bar{K}_7)/2$$

$$C_9 = g\ s\ t\ (\bar{K}_7\ H_a - \bar{K}_8\ H_b - \bar{K}_4\ H_c + \bar{K}_5\ H_d)$$

$$C_{10} = -\ s\ t\ g\ (\bar{K}_5\ H_a + \bar{K}_4\ H_b + \bar{K}_8\ H_c + \bar{K}_7\ H_d)$$

$$C_{11} = BQ1\ (x\ K_i + 1.5\ X_3\ K_f)/2$$

$$C_{12} = BQ1\ (-\ x\ K_j + 1.5\ X_3\ K_g)/2$$

$$C_{13} = BQ1\ (x\ K_m - 1.5\ X_3\ K_h)/2$$

$$C_{14} = BQ1\ (x\ K_k - 1.5\ X_3\ K_e)/2$$

$$C_{15} = (x\ K_f - 1.5\ BQ2\ T_2\ \bar{M}/s)/2$$

$$C_{16} = (x\ K_g - 1.5\ BQ2\ T_2\ \bar{L}/s)/2$$

$$C_{17} = (-\ x\ K_h + 1.5\ BQ2\ T_2\ \bar{J}/s)/2$$

$$C_{18} = (-\ x\ K_e + 1.5\ BQ2\ T_2\ \bar{I}/s)/2$$

$$C_{19} = s\ t\ g\ (\bar{K}_7\ H_a + \bar{K}_8\ H_b - \bar{K}_4\ H_c - \bar{K}_5\ H_d)$$

$$C_{20} = s\ t\ g\ (\bar{K}_8\ H_a - \bar{K}_7\ H_b - \bar{K}_5\ H_c + \bar{K}_4\ H_d)$$

$$C_{21} = s\ t\ g\ (\bar{K}_4\ H_a + \bar{K}_5\ H_b + \bar{K}_7\ H_c + \bar{K}_8\ H_d)$$

$$C_{22} = s\ t\ g\ (\bar{K}_5\ H_a - \bar{K}_4\ H_b + \bar{K}_8\ H_c - \bar{K}_7\ H_d)$$

$$C_{23} = s\ t\ g\ (\bar{K}_8\ H_a + \bar{K}_7\ H_b - \bar{K}_5\ H_c - \bar{K}_4\ H_d)$$

$$C_{24} = C_3 - 2\ BE\ X_7\ \bar{K}_1/3$$

$$C_{25} = C_4 + 2\ BE\ X_7\ \bar{K}_2/3$$

$$C_{26} = -\ C_1 + BQ1\ X_6\ \bar{K}_2$$

$$C_{27} = -\ C_2 + BQ1\ X_6\ \bar{K}_1$$

$$C_{28} = C_7 + X_7 \bar{K}_1/3$$

$$C_{29} = C_8 - X_7 \bar{K}_2/3$$

$$C_{30} = - C_5 - x \bar{K}_2$$

$$C_{31} = - C_6 - x \bar{K}_1$$

$$C_{32} = s\ t\ g\ (- \bar{K}_4 H_a + \bar{K}_5 H_b - \bar{K}_7 H_c + \bar{K}_8 H_d)$$

The following parameters are introduced in (4.20). The bar ($\bar{\ }$) indicates that the parameter is normalized by dividing by β_{q1} .

$$\begin{aligned}\bar{K}_9 &= BE(\bar{K}_6 \bar{A} - \bar{K}_3 \bar{C})H_e/2 + (K_c \bar{K}_3 - K_a \bar{K}_6) H_f - 2\ BQ1\ X_6 \bar{A}\ E + 2 \times K_a\ E \\ &\quad + \bar{A}\ C_1 - \bar{B}\ C_2 + \bar{C}\ C_3 - \bar{D}\ C_4 + K_a\ C_5 - K_b\ C_6 + K_c\ C_7 - K_d\ C_8 + C_{19} \\ &\quad + 2\ s\ t\ (\bar{K}_6 H_a - \bar{K}_3 H_c)\end{aligned}$$

$$\begin{aligned}\bar{K}_{10} &= \bar{A}\ C_{11} + \bar{B}\ C_{12} + \bar{C}\ C_{13} + \bar{D}\ C_{14} + K_a\ C_{15} + K_b\ C_{16} + K_c\ C_{17} + K_d\ C_{18} \\ &\quad + BE\ (H_a \bar{M} + H_b \bar{L} - H_c \bar{J} - H_d \bar{I})\end{aligned}$$

$$\begin{aligned}\bar{K}_{11} &= \bar{A}\ C_{11} - \bar{B}\ C_{12} + \bar{C}\ C_{13} - \bar{D}\ C_{14} + K_a\ C_{15} - K_b\ C_{16} + K_c\ C_{17} - K_d\ C_{18} \\ &\quad + BE\ (H_a \bar{M} - H_b \bar{L} - H_c \bar{J} + H_d \bar{I})\end{aligned}$$

$$\bar{K}_{12} = \bar{A}\ C_1 + \bar{B}\ C_2 + \bar{C}\ C_3 + \bar{D}\ C_4 + K_a\ C_5 + K_b\ C_6 + K_c\ C_7 + K_d\ C_8 + C_9$$

$$\begin{aligned}\bar{K}_{13} &= BQ1\ (x\ H_e \bar{K}_6/2 - 2\ X_6\ E)\ \bar{B} + \bar{K}_3\ (K_d H_f - BQ1 \times H_e \bar{D}/2) \\ &\quad + K_b\ (2 \times E - H_f \bar{K}_6) + C_{20} + 2\ s\ t\ (\bar{K}_6 H_b - \bar{K}_3 H_d) \\ &\quad - (\bar{A}\ C_2 + \bar{B}\ C_1 + \bar{C}\ C_4 + \bar{D}\ C_3 + K_a\ C_6 + K_b\ C_5 + K_c\ C_8 + K_d\ C_7)\end{aligned}$$

$$\begin{aligned}\bar{K}_{14} &= \bar{A}\ C_{12} - \bar{B}\ C_{11} + \bar{C}\ C_{14} - \bar{D}\ C_{13} + K_a\ C_{16} - K_b\ C_{15} + K_c\ C_{18} - K_d\ C_{17} \\ &\quad + BE\ (H_a \bar{L} - H_b \bar{M} - H_c \bar{I} + H_d \bar{J})\end{aligned}$$

$$\begin{aligned}\bar{K}_{15} &= \bar{A}\ C_{12} + \bar{B}\ C_{11} + \bar{C}\ C_{14} + \bar{D}\ C_{13} + K_a\ C_{16} + K_b\ C_{15} + K_c\ C_{18} + K_d\ C_{17} \\ &\quad + BE\ (H_a \bar{L} + H_b \bar{M} - H_c \bar{I} - H_d \bar{J})\end{aligned}$$

$$\bar{K}_{16} = -\bar{A}\ C_2 + \bar{B}\ C_1 - \bar{C}\ C_4 + \bar{D}\ C_3 - K_a\ C_6 + K_b\ C_5 - K_c\ C_8 + K_d\ C_7 + C_{23}$$

$$\begin{aligned}\bar{K}_{17} &= \bar{A}\ C_{24} - \bar{B}\ C_{25} + \bar{C}\ C_{26} - \bar{D}\ C_{27} + K_a\ C_{28} - K_b\ C_{29} + K_c\ C_{30} \\ &\quad - K_d\ C_{31} - 2\ BQ1\ X_6 \bar{C}\ E - (1/2)BE\ (\bar{A} \bar{K}_3 + \bar{C} \bar{K}_6)\ H_e + (K_a \bar{K}_3\end{aligned}$$

$$+ K_c \bar{K}_6) H_f + 2 x K_c E - 2 s t (\bar{K}_3 H_a + \bar{K}_6 H_c) - C_{21}$$

$$\bar{K}_{18} = \bar{A} C_{13} + \bar{B} C_{14} - \bar{C} C_{11} - \bar{D} C_{12} + K_a C_{17} + K_b C_{18} - K_c C_{15} - K_d C_{16}$$

$$- BE (H_a \bar{J} + H_b \bar{I} + H_c \bar{M} + H_d \bar{L})$$

$$\bar{K}_{19} = \bar{K}_{18} + 2 (- \bar{B} C_{14} + \bar{D} C_{12} - K_b C_{18} + K_d C_{16}) + 2 (H_b \bar{I} + H_d \bar{L}) BE$$

$$\bar{K}_{20} = \bar{A} C_{24} + \bar{B} C_{25} + \bar{C} C_{26} + \bar{D} C_{27} + K_a C_{28} + K_b C_{29} + K_c C_{30} + K_d C_{31}$$

$$+ C_{32}$$

$$\bar{K}_{21} = - (\bar{A} C_{25} + \bar{B} C_{24} + \bar{C} C_{27} + \bar{D} C_{26} + K_a C_{29} + K_b C_{28} + K_c C_{31}$$

$$+ K_d C_{30}) - BQ1\ 2\ X_6 \bar{D} E -(1/2) BE(\bar{K}_3 \bar{B} + \bar{D} \bar{K}_6) H_e + (\bar{K}_3 K_b$$

$$+ \bar{K}_6 K_d) H_f + 2 x K_d E - 2 s t (\bar{K}_3 H_b + \bar{K}_6 H_d) - C_{22}$$

$$\bar{K}_{22} = \bar{A} C_{14} - \bar{B} C_{13} - \bar{C} C_{12} + \bar{D} C_{11} + K_a C_{18} - K_b C_{17} - K_c C_{16} + K_d C_{15}$$

$$- BE (H_a \bar{I} - H_b \bar{J} + H_c \bar{L} - H_d \bar{M})$$

$$\bar{K}_{23} = \bar{K}_{22} + 2 (\bar{B} C_{13} - \bar{D} C_{11} + K_b C_{17} - K_d C_{15}) - 2 BE (H_b \bar{J} + H_d \bar{M})$$

$$\bar{K}_{24} = - \bar{A} C_{25} + \bar{B} C_{24} - \bar{C} C_{27} + \bar{D} C_{26} - K_a C_{29} + K_b C_{28} - K_c C_{31}$$

$$+ K_d C_{30} + C_{10}$$

The following functions of _z_ are needed in (4.28).

$$F_a(z) = f_1(z) [\bar{B} \cos (\beta_{q1} z) - \bar{A} \sin (\beta_{q1} z)] + f_2(z) [\bar{D} \cos (\beta_{q1} z)$$

$$- \bar{C} \sin (\beta_{q1} z)]$$

$$F_b(z) = f_2(z) [\bar{B} \cos (\beta_{q1} z) - \bar{A} \sin (\beta_{q1} z)] + f_3(z) [\bar{D} \cos (\beta_{q1} z)$$

$$- \bar{C} \sin (\beta_{a1} z)]$$

$$F_c(z) = - f_4(z) [K_c \cos (\beta_{q1} z) + K_d \sin (\beta_{q1} z)]/2 + f_5(z) [K_a \cos(\beta_{q1} z)$$

$$+ K_b \sin (\beta_{q1} z)]/2$$

$$F_d(z) = - f_5(z) [K_c \cos (\beta_{q1} z) + K_d \sin (\beta_{q1} z)]/2 - f_6(z) [K_a \cos (\beta_{q1} z)$$

$$+ K_b \sin (\beta_{q1} z)]/2$$

where

$$f_1(z) = BQ1\ [2E - 2\ s\ t\ \bar{K}_6 + \{2\ s^2\ g\ (\bar{K}_5 - x\ \bar{K}_7) - \bar{K}_2\}\cos\ (2\beta_{q1}z)$$
$$+ \{\bar{K}_1 - 2\ s^2\ g\ (\bar{K}_4 + x\ \bar{K}_8)\}\sin\ (2\beta_{q1}z) - K_f\cos\ (\beta_{q2}z)$$
$$- K_g\sin\ (\beta_{q2}z)]/2$$

$$f_2(z) = BQ1\ [2\ s\ t\ \bar{K}_3 + 2\ s^2\ g\ \{(x\ \bar{K}_4 + \bar{K}_8)\cos\ (2\beta_{q1}z) + (x\ \bar{K}_5 - \bar{K}_7)$$
$$\cdot\sin\ (2\beta_{q1}z)\} + K_h\cos\ (\beta_{q2}z) + K_e\sin\ (\beta_{q2}z)]/2$$

$$f_3(z) = BQ1\ [2\ E - \bar{K}_2\cos\ (2\beta_{q1}z) + \bar{K}_1\sin\ (2\beta_{q1}z)] - f_1(z)$$

$$f_4(z) = 2\ E + BE\ BQ1\ P_{10} + (1/2)(BQ1)^2\ P_2 - \bar{K}_6/x$$
$$+ (1/3)\ [g\ (1 + 2\ s^2)\ \bar{K}_5 - \bar{K}_2]\cos\ (2\beta_{q1}z)$$
$$- (1/3)\ [g\ (1 + 2\ s^2)\ \bar{K}_4 - \bar{K}_1]\sin\ (2\beta_{q1}z)$$
$$+ BQ2\ [\bar{I}\cos\ (\beta_{q2}z) - \bar{J}\sin\ (\beta_{q2}z)]$$

$$f_5(z) = \bar{K}_3/x + (1/3)\ g\ (1 + 2\ s^2)\ [\bar{K}_8\cos\ (2\beta_{q1}z) - \bar{K}_7\sin\ (2\beta_{q1}z)]$$
$$+ BQ2\ [\bar{L}\cos\ (\beta_{q2}z) - \bar{M}\sin\ (\beta_{q2}z)]$$

$$f_6(z) = f_4(z) - 4\ E - 2\ BE\ BQ1\ P_{10} - (BQ1)^2\ P_2$$
$$+ 2\ [\bar{K}_2\cos\ (2\beta_{q1}z) - \bar{K}_1\sin\ (2\beta_{q1}z)]/3$$

The following constants are associated with the third-order solutions in Region A.

$$A_1 = - A_2 - A_3 - A_4$$

$$A_2 = (3/128)\ g_a\ t_a [8\ s_a^2\ (b_{2a} - s_a^2) - (6\ s_a + 1)]/b_{3a}$$

$$A_3 = (3/128)\ g_a\ t_a\ [8\ s_a^2\ (b_{1a} - s_a^2) + (6\ s_a - 1)]\ /b_{4a}$$

$$A_4 = - (15/256)\ s_a\ t_a\ g_a$$

$$A_5 = - (12/5)\ A_4$$

$$A_6 = 15/64 - A_7\ b_{1a}/s_a - A_8\ b_{2a}/s_a - 3\ A_9 - A_{10}$$

$$A_7 = - s_a\ b_{1a}\ g_a\ [9\ (1 - 2\ s_a^2) + 4\ x_a\ t_a\ b_{2a}\ (b_{4a} - 2\ s_a^2)]/(128\ b_{3a})$$

$$A_8 = s_a\ b_{2a}\ g_a\ [9\ (1 - 2\ s_a^2) + 4\ x_a\ t_a\ b_{1a}\ (b_{3a} + 2\ s_a^2)]/(128\ b_{4a})$$

$$A_9 = - g_a [9 (10 s_a^2 - 1) + 2 x_a^2 (7 s_a^2 - 1)]/1024$$

$$A_{10} = - g_a [t_a^2 (7 - 8 s_a^2) + 27 s_a^2 + x_a^2 - 9/2]/128$$

$$A_{11} = A_5$$

$$A_{12} = A_5 - A_1 + x_a g_a (1 - 28 s_a^2)/128$$

$$A_{13} = x_a g_a [2 s_a (7 - 10 s_a^2) + 3 (1 - 2 s_a^2)]/128 - A_2 b_{1a}/s_a$$

$$A_{14} = x_a g_a [2s_a (7 - 10 s_a^2) - 3 (1 - 2 s_a^2)]/128 - A_3 b_{2a}/s_a$$

$$A_{15} = x_a g_a (1 - 16 s_a^2)/128 - 3 A_4$$

$$A_{16} = - A_{10}$$

$$A_{17} = A_6 + A_{10} + g_a (1 + 8 s_a^2) X_2/128 - (5 - 2 t_a^2)/64$$

$$A_{18} = A_7 b_{1a}/s_a - g_a [2 x_a t_a (1 - s_a^2) b_{4a} + 3 (1 - 2 s_a^2)]/64$$

$$A_{19} = A_8 b_{2a}/s_a - g_a [2 x_a t_a (1 - s_a^2) b_{3a} + 3 (1 - 2 s_a^2)]/64$$

$$A_{20} = 3 A_9 - (3 + x_a^2 - 12 g_a s_a^2)/128$$

APPENDIX C

DISCUSSION OF ELECTRON OVERTAKING

The space-charge-wave equations derived from the plasma model are valid only so long as the electron velocity is a single-valued function of position, consistent with the polarization system of coordinates. The problem remains to identify just when this limitation is violated. Physically, the location at which overtaking occurs is the point where the change in polarization ($\bar{z}_p$) exceeds the change in position along the beam axis ($\bar{z}$). Hence, overtaking occurs when the slope of $\bar{z}_p$ verses $\bar{z}$ is greater than one.

Engler [26] has investigated the problem on the assumption that the polarization can be represented by the first-order solution ($\bar{z}_1$) alone. This solution is obtained by substituting (5.15) and (5.17) into (4.5).

$$\bar{z}_1 = (\alpha/2)\ \sin(\bar{z})\ \sin(\omega t - x_a\ \bar{z}) \tag{C.1}$$

Taking the partial derivative of (C.1) with respect to $\bar{z}$ gives

$$\begin{aligned} \bar{z}_1{}' = (\alpha/2)\ [\ - x_a\ \sin(\bar{z})\ \cos(\omega t - x_a\ \bar{z}) \\ + \cos(\bar{z})\ \sin(\omega t - x_a\ \bar{z})\ ]. \end{aligned} \tag{C.2}$$

Equation (C.2) may be written as a single function of time in the form

$$\bar{z}_1{}' = (\alpha/2)\sqrt{x_a^2 \sin^2(\bar{z}) + \cos^2(\bar{z})} \quad \cos(\omega t - x_a \bar{z} - \Phi). \qquad (C.3)$$

Overtaking first occurs when $\bar{z}_1{}' = 1$. Since $x_a > 1$, the coefficient of $\cos(\omega t)$ can be maximized for a given value of α if $\bar{z} = 90^\circ$. Thus the maximum value of α is

$$\alpha_{max} = 2/x_a. \qquad (C.4)$$

Engler mentions that if higher-degree terms for the polarization are retained, the value of α_{max} may be raised.

To confirm this conclusion all three orders of terms in the polarization expression are retained. The total polarization is the sum of (4.5), (4.17), and (4.21), where the results of Chapter 5 are utilized to evaluate the coefficients. Since the actual polarization can be found only for explicit values of time, the polarization is computed for $\omega t = 0^\circ$ and $\omega t = 90^\circ$.

Fig. C.1 shows how the polarization varies as a function of α. The saturation effect, which is present for the current envelope, is also demonstrated here. The important point to note is the fact that the magnitude of the polarization and the portion of the cycle for which overtaking occurs both rise with increasing values of α. Fig. C.1 indicates that overtaking is present over most of the cycle for $\alpha = 0.3$.

Fig. C.2 shows the change in polarization with time. Although the polarization at any point on the beam definitely changes with time, the overall pattern seems to be nearly the same regardless of the value of time chosen. The patterns are not identical, however, as the second-

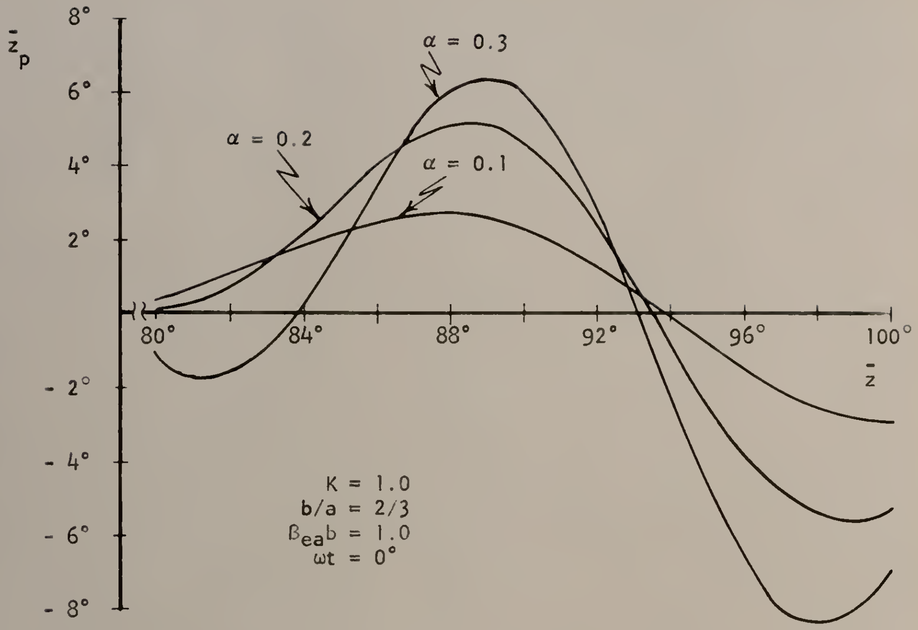

Fig. C.1 - Polarization as a function of α.

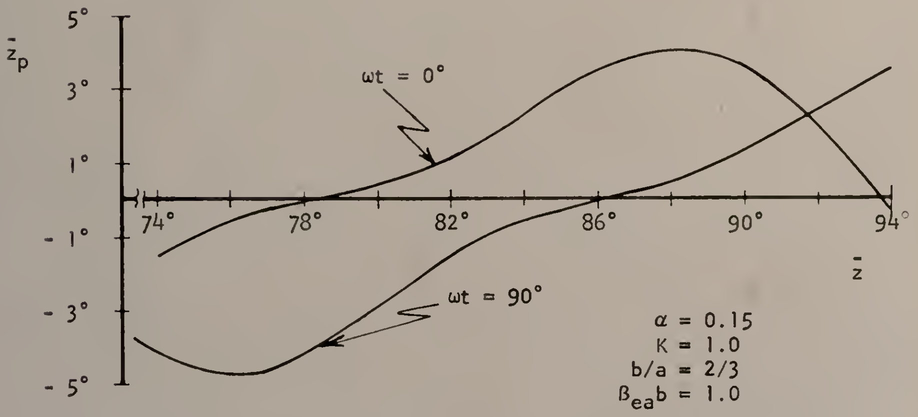

Fig. C.2 - Polarization as a function of ωt.

order term ($\bar{z}_2$) contains a time-independent function of position. Thus it may be concluded that overtaking will be spotted for a given value of α regardless of the time value used; however, the location along the beam at which overtaking occurs is a function of the time.

Careful examination of Fig. C.2 shows that overtaking occurs in the vicinity of 92^o for $\omega t = 0$. With the set of parameters used in Region A, (C.4) predicts that $\alpha_{max} = 0.175$. Hence, by including higher-order terms, overtaking is shown to occur for a smaller value of α_{max} rather than a larger value as predicted by Engler. It is also apparent that the degree of overtaking is slight, and the value of α_{max} predicted by (C.4) is an acceptable guide to follow.

APPENDIX D

METHOD FOR OBTAINING SOLUTIONS FOR THE CONSTANTS OF INTEGRATION IN REGION B

In this appendix the procedure for solving four simultaneous equations using Cramer's rule is discussed. In Chapter 6 solutions for the first-, second-, and third-order constants of integration, which are required to obtain particular solutions in Region B, are each left in the form of four simultaneous equations. The first-order constants are found in (6.14) and (6.17), the second-order in (6.24) and (6.31), and the third-order in (6.39) and (6.44).

Consider the following system of equations:

$$F_1 = C_1 S_1 + C_2 S_2 + C_3 S_3 + C_4 S_4 \qquad \text{(D.1a)}$$

$$F_2 = C_5 S_1 + C_6 S_2 + C_7 S_3 + C_8 S_4 \qquad \text{(D.1b)}$$

$$F_3 = C_9 S_1 + C_{10} S_2 + C_{11} S_3 + C_{12} S_4 \qquad \text{(D.1c)}$$

$$F_4 = C_{13} S_1 + C_{14} S_2 + C_{15} S_3 + C_{16} S_4. \qquad \text{(D.1d)}$$

The solutions to this set of equations are

$$S_1 = [F_1 M_{11} - F_2 M_{21} + F_3 M_{31} - F_4 M_{41}]/D \qquad \text{(D.2a)}$$

$$S_2 = [- F_1 M_{12} + F_2 M_{22} - F_3 M_{32} + F_4 M_{42}]/D \qquad (D.2b)$$

$$S_3 = [F_1 M_{13} - F_2 M_{23} + F_3 M_{33} - F_4 M_{43}]/D \qquad (D.2c)$$

$$S_4 = [- F_1 M_{14} + F_2 M_{24} - F_3 M_{34} + F_4 M_{44}]/D. \qquad (D.2d)$$

The symbol D represents the fourth-order determinant formed by the coefficients C_1 through C_{16}. The symbol M_{mn} represents the minor formed when the mth row and nth column are deleted from D. In general these solutions would appear to be quite complicated, since there are sixteen unique minors which must be evaluated. In addition there are three sets of such equations which must be evaluated, one for each order solution in Region B.

The work is considerably simplified, however, when the equations which (D.1) represent are examined. The first important point is the fact that for a particular order solution there are only four unique constants. These constants are the products of sine and cosine terms. For the first-order solution they are

$$C_1 = \cos(BQ1_b\ Z_a)\ \sin(BE_b\ Z_a) \qquad (D.3a)$$

$$C_2 = \sin(BQ1_b\ Z_a)\ \sin(BE_b\ Z_a) \qquad (D.3b)$$

$$C_3 = \cos(BQ1_b\ Z_a)\ \cos(BE_b\ Z_a) \qquad (D.3c)$$

$$C_4 = \sin(BQ1_b\ Z_a)\ \cos(BE_b\ Z_a). \qquad (D.3d)$$

The four first-order equations may be put in the form

$$F_1 = \quad C_1\ S_1 + C_2\ S_2 + C_3\ S_3 + C_4\ S_4 \tag{D.4a}$$

$$F_2 = -\ C_2\ S_1 + C_1\ S_2 - C_4\ S_3 + C_3\ S_4 \tag{D.4b}$$

$$F_3 = -\ C_3\ S_1 - C_4\ S_2 + C_1\ S_3 + C_2\ S_4 \tag{D.4c}$$

$$F_4 = \quad C_4\ S_1 - C_3\ S_2 - C_2\ S_3 + C_1\ S_4. \tag{D.4d}$$

The solutions S_1, S_2, S_3, and S_4 refer to the first-order constants $\bar{A}_b$, $\bar{B}_b$, $\bar{C}_b$, and $\bar{D}_b$ respectively. The forcing functions are given by

$$F_1 = (\alpha/2)\ (x_a/BE_b)\ \sin(Z_a)\ \cos(x_a\ Z_a) \tag{D.5a}$$

$$F_2 = (\alpha/2)\ (V_a/V_b)\ (1/BQ1_b)\ \cos(Z_a)\ \cos(x_a\ Z_a) \tag{D.5b}$$

$$F_3 = (\alpha/2)\ (x_a/BE_b)\ \sin(Z_a)\ \sin(x_a\ Z_a) \tag{D.5c}$$

$$F_4 = (\alpha/2)\ (V_a/V_b)\ (1/BQ1_b)\ \cos(Z_a)\ \sin(x_a\ Z_a). \tag{D.5d}$$

The solutions to (D.4) are

$$S_1 = [F_1\ M_{11} + F_2\ M_{12} - F_3\ M_{13} - F_4\ M_{14}]/D \tag{D.6a}$$

$$S_2 = [-\ F_1\ M_{12} + F_2\ M_{11} + F_3\ M_{14} - F_4\ M_{13}]/D \tag{D.6b}$$

$$S_3 = [F_1\ M_{13} + F_2\ M_{14} + F_3\ M_{11} + F_4\ M_{12}]/D \tag{D.6c}$$

$$S_4 = [-\ F_1\ M_{14} + F_2\ M_{13} - F_3\ M_{12} + F_4\ M_{11}]/D. \tag{D.6d}$$

Since there are only four unique constants, all the minors found in (D.2) can be expressed as one of four possible minors. The solutions to the four minors present in (D.6) are

$$M_{11} = C_1 (C_1^2 + C_2^2 + C_3^2 - C_4^2) + 2 C_2 C_3 C_4 \quad \text{(D.7a)}$$

$$M_{12} = - C_2 (C_1^2 + C_2^2 - C_3^2 + C_4^2) - 2 C_1 C_3 C_4 \quad \text{(D.7b)}$$

$$M_{13} = C_3 (C_1^2 - C_2^2 + C_3^2 + C_4^2) + 2 C_1 C_2 C_4 \quad \text{(D.7c)}$$

$$M_{14} = - C_4 (- C_1^2 + C_2^2 + C_3^2 + C_4^2) - 2 C_1 C_2 C_3. \quad \text{(D.7d)}$$

The second important result of this work is the fact that the general solutions, (D.6) and (D.7), also hold for both the second-order and third-order systems of equations. Naturally, the values of $C_1 - C_4$ and $F_1 - F_4$ are different for each order of equations.

For the second-order system of equations the solutions S_1, S_2, S_3, and S_4 are identified with the second-order constants $\bar{I}$, $\bar{J}$, $\bar{L}$, and $\bar{M}$ respectively. The other terms are

$$C_1 = \sin(BQ2_b\ Z_a) \sin(2\ BE_b\ Z_a) \quad \text{(D.8a)}$$

$$C_2 = \cos(BQ2_b\ Z_a) \sin(2\ BE_b\ Z_a) \quad \text{(D.8b)}$$

$$C_3 = \sin(BQ2_b\ Z_a) \cos(2\ BE_b\ Z_a) \quad \text{(D.8c)}$$

$$C_4 = \cos(BQ2_b\ Z_a) \cos(2\ BE_b\ Z_a), \quad \text{(D.8d)}$$

while the forcing functions are given by

$$F_1 = [Y_{1a}(Z_a) \cos(2\, x_a\, Z_a) - Y_{2a}(Z_a) \sin(2\, x_a\, Z_a)]/(2\, BE_b)$$

$$- Y_{1b}(Z_a) \cos(2\, BE_b\, Z_a) - Y_{2b}(Z_a) \sin(2\, BE_b\, Z_a) \quad \text{(D.9a)}$$

$$F_2 = [Y_{3b}(Z_a) \sin(2\, BE_b\, Z_a) + Y_{4b}(Z_a) \cos(2\, BE_b\, Z_a)]/BQ2_b$$

$$+ (\alpha/4)^2 (V_a/V_b) [Y_{3a}(Z_a) \sin(2\, x_a\, Z_a) + Y_{4a}(Z_a)$$

$$\cdot \cos(2\, x_a\, Z_a)]/BQ2_b \quad \text{(D.9b)}$$

$$F_3 = [Y_{1a}(Z_a) \sin(2\, x_a\, Z_a) + Y_{2a}(Z_a) \cos(2\, x_a\, Z_a)]/(2\, BE_b)$$

$$- Y_{1b}(Z_a) \sin(2\, BE_b\, Z_a) + Y_{2b}(Z_a) \cos(2\, BE_b\, Z_a) \quad \text{(D.9c)}$$

$$F_4 = - [Y_{3b}(Z_a) \cos(2\, BE_b\, Z_a) - Y_{4b}(Z_a) \sin(2\, BE_b\, Z_a)]/BQ2_b$$

$$- (\alpha/4)^2 (V_a/V_b) [Y_{3a}(Z_a) \cos(2\, x_a\, Z_a) - Y_{4a}(Z_a)$$

$$\cdot \sin(2\, x_a\, Z_a)]/BQ2_b. \quad \text{(D.9d)}$$

For the third-order solutions the constants C_1 - C_4 are identical with the first-order values given by (D.3). The solutions S_1, S_2, S_3, and S_4 are identified with the third-order constants $\bar{P}_b$, $\bar{Q}_b$, $\bar{R}_b$, and $\bar{S}_b$ respectively. The third-order forcing functions are

$$\begin{aligned} F_1 = &- Y_{5b} (Z_a) \cos(BE_b\, Z_a) - Y_{6b} (Z_a) \sin(BE_b\, Z_a) + [Y_{5a} (Z_a) \\ &\cdot \cos(x_a\, Z_a) + Y_{6a} (Z_a) \sin(x_a\, Z_a)]/BE_b \end{aligned} \qquad \text{(D.10a)}$$

$$\begin{aligned} F_2 = &(V_a/V_b)\ [Y_{7a} (Z_a) \sin(x_a\, Z_a) + Y_{8a} (Z_a) \cos(x_a\, Z_a)]/BQ1_b \\ &- [Y_{7b} (Z_a) \sin(BE_b\, Z_a) + Y_{8b} (Z_a) \cos(BE_b\, Z_a)]/BQ1_b \end{aligned} \qquad \text{(D.10b)}$$

$$\begin{aligned} F_3 = &[Y_{5a} (Z_a) \sin(x_a\, Z_a) - Y_{6a} (Z_a) \cos(x_a\, Z_a)]/BE_b \\ &- Y_{5b} (Z_a) \sin(BE_b\, Z_a) + Y_{6b} (Z_a) \cos(BE_b\, Z_a) \end{aligned} \qquad \text{(D.10c)}$$

$$\begin{aligned} F_4 = &- (V_a/V_b)\ [Y_{7a} (Z_a) \cos(x_a\, Z_a) - Y_{8a} (Z_a) \sin(x_a\, Z_a)]/BQ1_b \\ &+ [Y_{7b} (Z_a) \cos(BE_b\, Z_a) - Y_{8b} (Z_a) \sin(BE_b\, Z_a)]/BQ1_b . \end{aligned} \qquad \text{(D.10d)}$$

LIST OF REFERENCES

1. W.C. Hahn, "Small Signal Theory of Velocity Modulated Electron Beams," Gen. Elec. Rev., Vol. 42, pp. 258-270; June, 1939.

2. S. Ramo, 'The Electronic-Wave Theory of Velocity Modulated Tubes," Proc. IRE, Vol. 27, pp. 757-763; December, 1939.

3. P.K. Tien and L.M. Field, "Space-Charge Waves in an Accelerated Electron Stream for Amplification of Microwave Signals," Proc. IRE, Vol. 40, pp. 688-695; June, 1952.

4. C.K. Birdsall and J.R. Whinnery, "Waves in an Electron Stream with General Admittance Walls," Jour. Appl. Phys., Vol. 24, pp. 314-323; March, 1953.

5. C.K. Birdsall, "Rippled Wall and Rippled Stream Amplifiers," Proc. IRE, Vol. 42, pp. 1628-1636; November, 1954.

6. T.G. Mihran, "Scalloped Beam Amplification," Trans. IRE, PGED, Vol. 3, pp. 32-39; January, 1956.

7. R.W. Peter, S. Bloom, and J.A. Ruetz, "Space-Charge-Wave Amplification Along an Electron Beam by Periodic Change of the Beam Impedance," RCA Review, Vol. 15, pp. 113-120; March, 1954.

8. S. Bloom and R.W. Peter, 'Transmission-Line Analog of a Modulated Electron Beam," RCA Review, Vol. 15, pp. 95-112; March, 1954.

9. A.H.W. Beck, Space Charge Waves and Slow Electromagnetic Waves, Pergamon Press, New York, N.Y., pp. 99-141; 1958.

10. W.W. Harman, Fundamentals of Electronic Motion, McGraw- Hill Book Co., New York, N.Y., pp. 204-241; 1953.

11. R.G.E. Hutter, Beam and Wave Electronics in Microwave Tubes, D. Van Nostrand Co., Princeton, New Jersey, pp. 159-179; 1960.

12. G.M. Branch and T.G. Mihran, "Plasma Frequency Reduction Factors in Electron Beams," Trans. IRE, PGED, Vol. 2, pp. 3-6; April, 1955.

13. T.G. Mihran, 'The Effect of Space Charge on Bunching in a Two-Cavity Klystron," Trans. IRE, PGED, Vol. 6, pp. 54-64; January, 1959.

14. D.L. Webster, "Cathode Ray Bunching," Jour. Appl. Phys., Vol. 10, pp. 501-508, July, 1939.

15. P.K. Tien, L.R. Walker, and V.M. Wolontis, "A Large Signal Theory of Traveling-Wave Amplifiers," Proc. IRE, Vol. 43, pp. 260-277; March, 1955.

16. P.K. Tien, "A Large Signal Theory of Traveling-Wave Amplifiers Including the Effects of Space Charge and Finite Coupling Between the Beam and the Circuit," Bell Sys. Tech. J., Vol. 35, pp. 349-360; March, 1956.

17. S.E. Webber, "Ballistic Analysis of a Two Cavity Finite Beam Klystron," Trans. IRE, PGED, Vol. 5, pp. 98-108; April, 1958.

18. S.E. Webber, "Large Signal Bunching of Electron Beams by Standing-Wave and Traveling-Wave Systems," Trans. IRE, PGED, Vol. 6, pp. 365-372; October, 1959.

19. J.E. Rowe, "A Large Signal Analysis of the Traveling-Wave Amplifier: Theory and General Results," Trans. IRE, PGED, Vol. 3, pp. 39-56; January, 1956.

20. T.G. Mihran, "Harmonic Current Growth in Velocity-Modulated Electron Beams," Jour. Appl. Phys., Vol. 30, pp. 1346-1350; September, 1959.

21. F. Paschke, "On the Nonlinear Behavior of Electron-Beam Devices," RCA Review, Vol. 18, pp. 221-242; June, 1957.

22. S. Olving, "Nonlinear Space-Charge-Wave Theory of the Radially Finite Electron Beam," Res. Rep. EE 497, Cornell University; June, 1961.

23. F. Paschke, "Generation of Second Harmonic in a Velocity-Modulated Electron Beam of Finite Diameter," RCA Review, Vol. 19, pp. 617-627; December, 1958.

24. F. Paschke,"Nonlinear Theory of a Velocity-Modulated Electron Beam with Finite Diameter," RCA Review, Vol. 21, pp. 53-74; March, 1960.

25. F. Paschke, "New Results on Frequency Multiplication and Nonlinear Phase Distortion in Klystrons and T.W.T.'s," RCA Review, Vol. 22, pp. 162-184; March, 1961.

26. P. Engler, "Phase Relationships in a Nonlinear Velocity-Modulated Electron Beam," Res. Rep. EE 494, Cornell University; January, 1961.

27. S. Olving, "On the Nonlinear Theory of the Plane Klystron Tube," Res. Rep. EE 500, Cornell University; June, 1961.

28. P.R. McIsaac, "Nonlinear Space-Charge-Wave Analysis," Res. Rep. EE 513, Cornell University; September, 1961.

29. D.L. Bobroff, "Independent Space Variables for Small-Signal Electron Beam Analysis," Trans. IRE, PGED, Vol. 6, pp. 68-78; January, 1959.

30. J.R. Pierce and W.G. Shepherd, "Reflex Oscillators," Bell Sys. Tech, J., Vol. 26, pp. 629-639; July, 1947.

BIOGRAPHY

Ronald Carl Houts was born on September 22, 1937, in Chicago, Illinois. In September, 1951 he moved to Florida, and graduated from Auburndale High School in June, 1955. In September, 1955, he entered the University of Florida, and received the degree of Bachelor of Electrical Engineering with honors in June, 1959. The author was awarded a National Defense Act Fellowship for graduate study. He entered the Graduate School of the University of Florida in June, 1959, and received the degree Master of Science in Engineering in August, 1960. From September, 1960 until the present time he has pursued his work toward the degree Doctor of Philosophy at the University of Florida. For the past two years he has been employed as a teaching assistant by the Department of Electrical Engineering.

Ronald Carl Houts is married to the former Marilyn Leggett and is the father of a son, Ronald Scott. He is a member of the Institute of Electrical and Electronics Engineers, Tau Beta Pi, Sigma Tau, Phi Kappa Phi, and Phi Eta Sigma.

This dissertation was prepared under the direction of the chairman of the candidate's supervisory committee and has been approved by all members of that committee. It was submitted to the Dean of the College of Engineering and to the Graduate Council, and was approved as partial fulfillment of the requirements for the degree of Doctor of Philosophy.

August 10, 1963

Thomas L Martin Jr.
Dean, College of Engineering

Dean, Graduate School

Supervisory Committee:

W. W. Peterson
Chairman

J. D. Sutherland
Co-chairman

W. H. Chen

E. E. Muschlitz, Jr.

R. G. Blake